IDENTIFICATION OF OCEAN BOTTOM SEDIMENTS THROUGH MEASUREMENTS OF COHERENCE OF ACOUSTIC ECHOES

ROBERT RICHARD MacISAAC


CENTRE FOR NFLD. STUDIES
MAY 8 1979
MEMORIAL UNIVERSITY
OF NEWFOUNDLAND

NOTICE

The quality of this microfiche is heavily dependent upon the quality of the original thesis submitted for microfilming. Every effort has been made to ensure the highest quality of reproduction possible.

If pages are missing, contact the university which granted the degree.

Some pages may have indistinct print especially if the original pages were typed with a poor typewriter ribbon or if the university sent us a poor photocopy.

Previously copyrighted materials (journal articles, published tests, etc.) are not filmed.

Reproduction in full or in part of this film is governed by the Canadian Copyright Act, R.S.C. 1970, c. C-30. Please read the authorization forms which accompany this thesis.

THIS DISSERTATION
HAS BEEN MICROFILMED
EXACTLY AS RECEIVED

AVIS

La qualité de cette microfiche dépend grandement de la qualité de la thèse soumise au microfilmage. Nous avons tout fait pour assurer une qualité supérieure de reproduction.

S'il manque des pages, veuillez communiquer avec l'université qui a conféré le grade.

La qualité d'impression de certaines pages peut laisser à désirer, surtout si les pages originales ont été dactylographiées à l'aide d'un ruban usé ou si l'université nous a fait parvenir une photocopie de mauvaise qualité.

Les documents qui font déjà l'objet d'un droit d'auteur (articles de revue, examens publiés, etc.) ne sont pas microfilmés.

La reproduction, même partielle, de ce microfilm est soumise à la Loi canadienne sur le droit d'auteur, SRC 1970, c. C-30. Veuillez prendre connaissance des formules d'autorisation qui accompagnent cette thèse.

LA THÈSE A ÉTÉ
MICROFILMÉE TELLE QUE
NOUS L'AVONS REÇUE

IDENTIFICATION OF OCEAN BOTTOM SEDIMENTS

THROUGH

MEASUREMENTS OF COHERENCE OF ACOUSTIC ECHOES

by

© Robert Richard MacIsaac, B.Eng.

A Thesis submitted in partial fulfillment
of the requirements for the degree of
Master of Engineering

Faculty of Engineering
Memorial University of Newfoundland

October, 1977

St. John's Newfoundland

ABSTRACT

With the increased interest in the exploitation of offshore resources, it is evident that a need exists for a rapid, reliable and automatic method of determing the composition and properties of the ocean floor. Such information aids in the design and siting of offshore structures and pipelines, provides an inventory of the mineral resources for economic development and planning and improves our understanding of the geophysical structure of the sea bed.

In order to perform this work, data is required from a reliable, depth invariant echo sounder. In a joint cruise with the Bedford Institute of Oceanography (BIO) 500 km of echoes have been collected over varying sediment types using the Huntec broadband (10 khz) Deep Tow System.

In order to study methods of sediment classification, an approach based on filter theory is adopted and combined with an application of pattern recognition techniques. Using the data base obtained on the BIO cruise, results are presented on the quantatitive measurement of the coherent (reflected) energy versus total received energy in acoustic echoes from the seabed for four sediment types. Two metrics of the coherence of the received signals are developed. The first is a measure of the normalized cross-correlation coefficient between adjacent acoustic samples. When evaluated along the ship's track, 77% correct sediment classification is obtained with this procedure. The second is an estimate of the relative amount of coherent energy in the acoustic return

from the water-sediment interface when compared to the total energy received. A correct classification of 56% results from the use of this method.

When both metrics are combined in a two dimensional vector plane, complete isolation of regions in the plane is observed. These regions are identified with sediment type; for the acoustic data available, 100% correct sediment classification in the plane for the four sediment types is obtained.

ACKNOWLEDGEMENTS

The author wishes to thank, and is highly indebted to, his supervisor, Dr. A.D. Dunsiger, for his guidance and constant encouragement and help in all stages of this project, and in constructively critizing the original manuscript.

The work was supported by National Research Council of Canada, Operating Grant Number A9332 and by the Faculty of Engineering, Memorial University of Newfoundland.

This project would not have been possible without the efforts and assistance of the Atlantic Geoscience Center (Bedford Institute of Oceanography) and of Huntec ('70) Ltd. in providing sea trial time, equipment access and data support. The assistance of Dr. D.I. Ross and Dr. L.H. King of AGC/BIO, and Dr. P.G. Simpkin, Mr. R. Hutchins and Mr. D.R. Parrott of Huntec is deeply appreciated. They have given freely of their time and expertise in this field and have allowed access to their extensive seabed research program.

In conclusion, the author wishes to acknowledge the financial support provided by the Centre for Cold Ocean Resources Engineering (C-CORE) during the period from September 1975 until August 1977 through the C-CORE Fellowship program. He also wishes to thank Miss Julie Burnes for her continued personal support without which this work would not have been accomplished, and to Miss Jean Eveleigh for her patience in typing this manuscript.

TABLE OF CONTENTS

LIST OF TABLES

LIST OF FIGURES

LIST OF SYMBOLS

A	- Amplitude of pressure wave
B	- Signal bandwidth
c	- Velocity of sound in water
C_a	- Acoustic energy absorption coefficient
d	- Water column depth below transducer
E	- Energy
E_c	- Coherent signal energy
E_n	- Noise energy
E_T	- Received signal energy in time T
$E\Delta$	- Normalized energy in the first return
$E\Delta_T$	- Classification threshold for $E\Delta$ estimate
ε_ρ^2	- Mean square error of $\hat{\rho}_{i,\, i+1}$ estimate
h	- rms surface roughness
$h(t)$	- Time invarient impulse response
$h(t,\tau)$	- Time dependent impulse response
$H(\omega)$	- Time invarient transfer function
$H(\omega,\tau)$	- Time dependent transfer function
j	- $\sqrt{-1}$
k	- Wave number, $2\pi/\lambda$
$\widetilde{n(t)}$	- Received noise
P	- Power
P_c	- Coherent signal power
P_n	- Noise power

r	- First Fresnel zone radius
$r(t)$	- Received signal without noise
R_s	- General space dependence
$R(o)$	- Peak value of auto-correlation
$R(\tau)$	- Correlation function
t	- Time
t_w	- Multiple free time window
T	- Received signal time duration
$[x(t)]$	- Set of bottom reflected signals
Δt	- Time duration of transmitted signal
$\zeta(R_s T_s)$	- Space and time dependent bottom profile
θ	- Angle of incidence
λ	- Wavelength, $2\pi c/\omega$
ρ	- Density
ρ_T	- Classification threshold for $\bar{\rho}_{i,\, i+1}$ estimate
$\rho_{i,\, i+1}$	- Normalized cross-correlation coefficient
$\rho_{i,\, i+1}(\tau)$	- Normalized cross-correlation function
τ	- Correlation time delay
ω	- Angular frequency

CHAPTER 1

INTRODUCTION

With the current interest in the exploitation of offshore resources, it is evident that a need exists for rapid, reliable and automatic method of determining the composition and properties of the ocean floor. Such information aids in the design and siting of offshore structures and pipelines, provides an inventory of the mineral resources for economic development and planning and improves our understanding of the geophysical structure of the seabed.

Acoustic sources provide a rapid, non-intrusive method of remotely sensing the ocean floor. The use of a high resolution system permits the examination of small areas of the sea floor at frequent spatial intervals. Generally the echo returns require ground truthing by conventional methods such as core and grab samples, but with proper interpretation acoustic techniques can supply averaged information over large bottom swaths.

Many authors, over the past years, have shown that a relationship exists between sediment physical properties and acoustic reflection coefficient. Akal (1972, 1974), Bell and Porter (1973, 1974, 1975), Breslau (1964, 1967), Faas (1969), Hamilton (1970b, 1971a, 1974a), Li and Smith (1966, 1969) and McLeroy (1972), are a few who have empirically related observed values of Rayleigh reflection coefficient to sediment porosity, density and mean grain size. Many of these authors also have observed the relationship between these same physical parameters

and compressional sound wave velocity through a sediment. They include Akal (1972, 1974), Anderson (1974), Bell and Porter (1974), Hamilton (1970a), and Westneat and Porter (1975). The conclusions of these authors indicate that ocean bottom sediments can be classified by their porosities or densities, as estimated from measurements of reflection coefficients or of sound velocities.

In recent years, attempts to derive an optimum solution for the wave equation for sound propagation and acoustic response in a liquid overlying a viscoelastic half space have been proposed. New sediment models have been put forth, using linear viscoelasticity assumption with complex Lamé parameters. Hamilton (1971a, b, 1974b, 1975) has shown that, under ideal conditions, all elastic constants for a sediment can be estimated from a measurement of sediment porosity, sound velocity and the bulk modulus of the sediment. His assumptions are that the sediment is a porous, gas free, uncemented, mineral structure, fully saturated with water, and is macroscopically isotropic; the applied stresses are compressive or shear of low amplitude, and the acoustic wavelengths used are much greater than the grain size.

Magnuson (1972a, b, 1973, 1975) and Katsekas (1973) used a model similar to Hamilton's, and formulated the response in the acoustic field as a Green's function in integral form. Newman (1973) and Magnuson (1973) used these results in computer analysis of the Green's function for various sediment types with positive results, particularly in distinguishing sediments with identical acoustic impedances but with different ratios of impedance parameters.

Several authors have treated the sea surface (Fortuin, 1973) and the sea bottom (Baggeroer et al, 1973) as a filter consisting of a deterministic and a random pair. A similar model was used by Clay and Leong (1974) in deep ocean at seismic frequencies. By modeling the bottom roughness as a stochastic variable, large scale roughness features were observed in deep oceans and an expression for the scattering function was formulated. The end result was a statistical description of the seafloor.

Pace (1974) suggested that pattern recognition techniques could be used with acoustic returns to classify sediments. In a laboratory environment, with artificial sediments, using a broadband signal, the sediments were correctly placed in one of three classes with a probability of over 60%. More recently, Dodds (as reported in Simpkin et al, 1976) suggests that a pattern recognition approach with four variables can be used to correctly classify real ocean bottom sediments. His choice of variables are the time of arrival of the acoustic pulse at the bottom, and the total energy in three time windows of variable length centered at the time of peak amplitude reception.

Knott et al (1977) suggest the use of the cumulation of reflected energy with travel time to measure and compare the relative magnitudes of reflected energy returned from sedimentary bottoms, and to estimate the time rate of cumulative energy. They suggest that the time rate of reflectance changes with geological structure.

In this thesis, an attempt is made to use the combination filter approach of Fortuin (1973), Baggoerer et al (1973), and Clay and Leong

(1974) together with a simple pattern recognition application similar to that used by Pace (1974) to classify sediments. Preliminary results of this concept were shown in MacIsaac and Dunsiger (1977). Using shallow seismic frequencies (nominally in the band from 1 khz to 10 khz), the effects of bottom roughness on signal coherence are examined. It is believed that estimates of signal coherence provide more clues by which correct sediment classification may be accomplished. The results are based on acoustic data collected over the western part of the Scotian Shelf and in the eastern part of the Gulf of Maine in June 1976 aboard CCS Hudson (Figure 1).

A boomer-type broadband sound source is used at normal incidence to transmit acoustic energy into the water column as shown in Figure 2. Reflected signals from the sea bottom and stratified sub-bottom are received by hydrophones attached to the towed body containing the sound source. These signals are amplified and recorded in analog form on an instrumentation recorder. In all, approximately fifty hours of recordings were made of acoustic returns from soft sediments, representing in the order of 240,000 acoustic echoes.

Because of the impracticality of investigating each echo individually, a data base consisting of nine sections of these recordings was made. The nine sections represent data obtained over all bottom types encountered at sea in the Gulf of Maine, ranging from bedrock to soft silts and clays. The acoustic records obtained were at times highly contaminated by noise generated in the towed body. It was decided, therefore, to select four sediments from this base for which data with an apparent high signal-

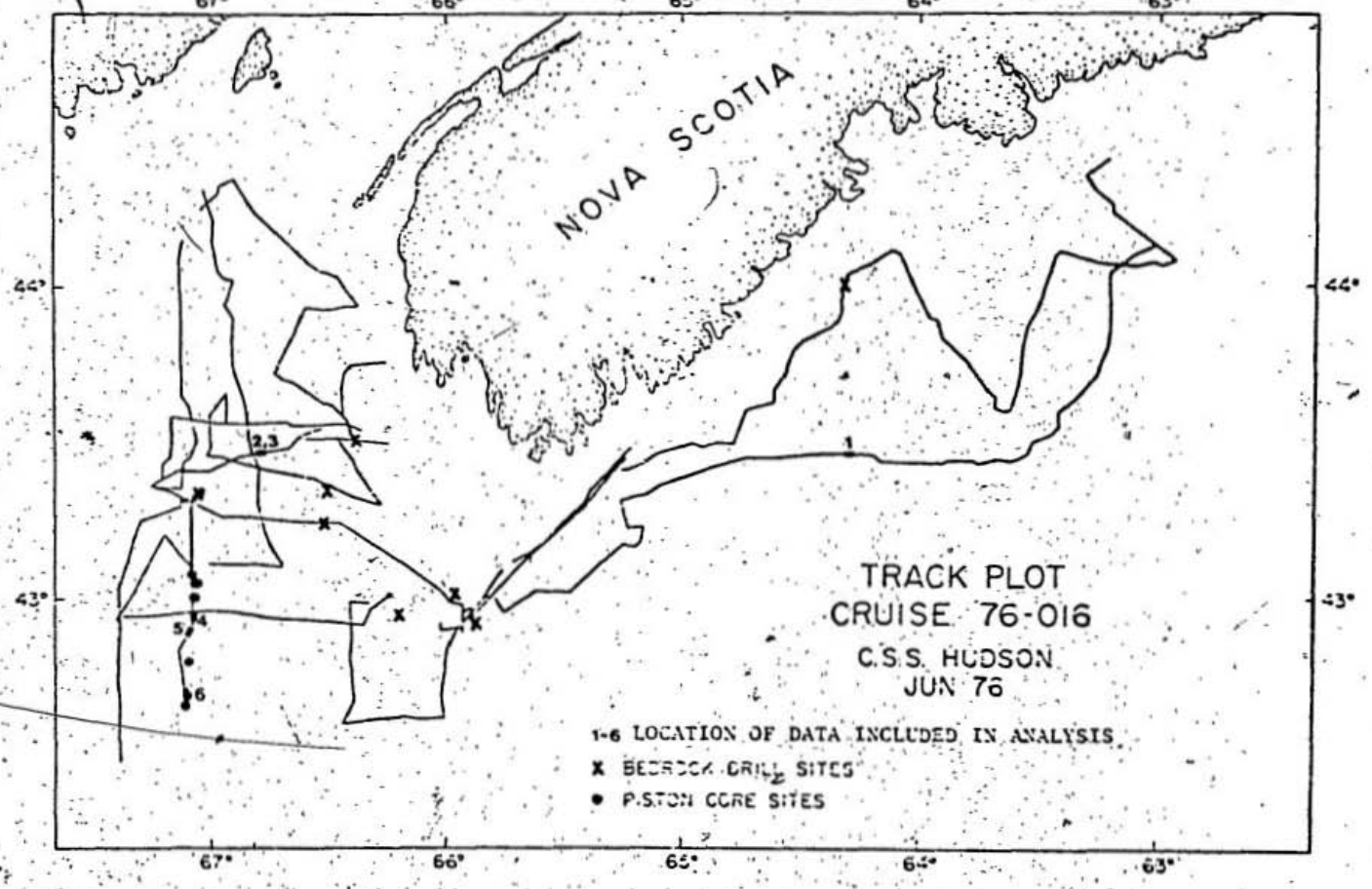

Figure 1 Operational Area and Cruise Track Plot

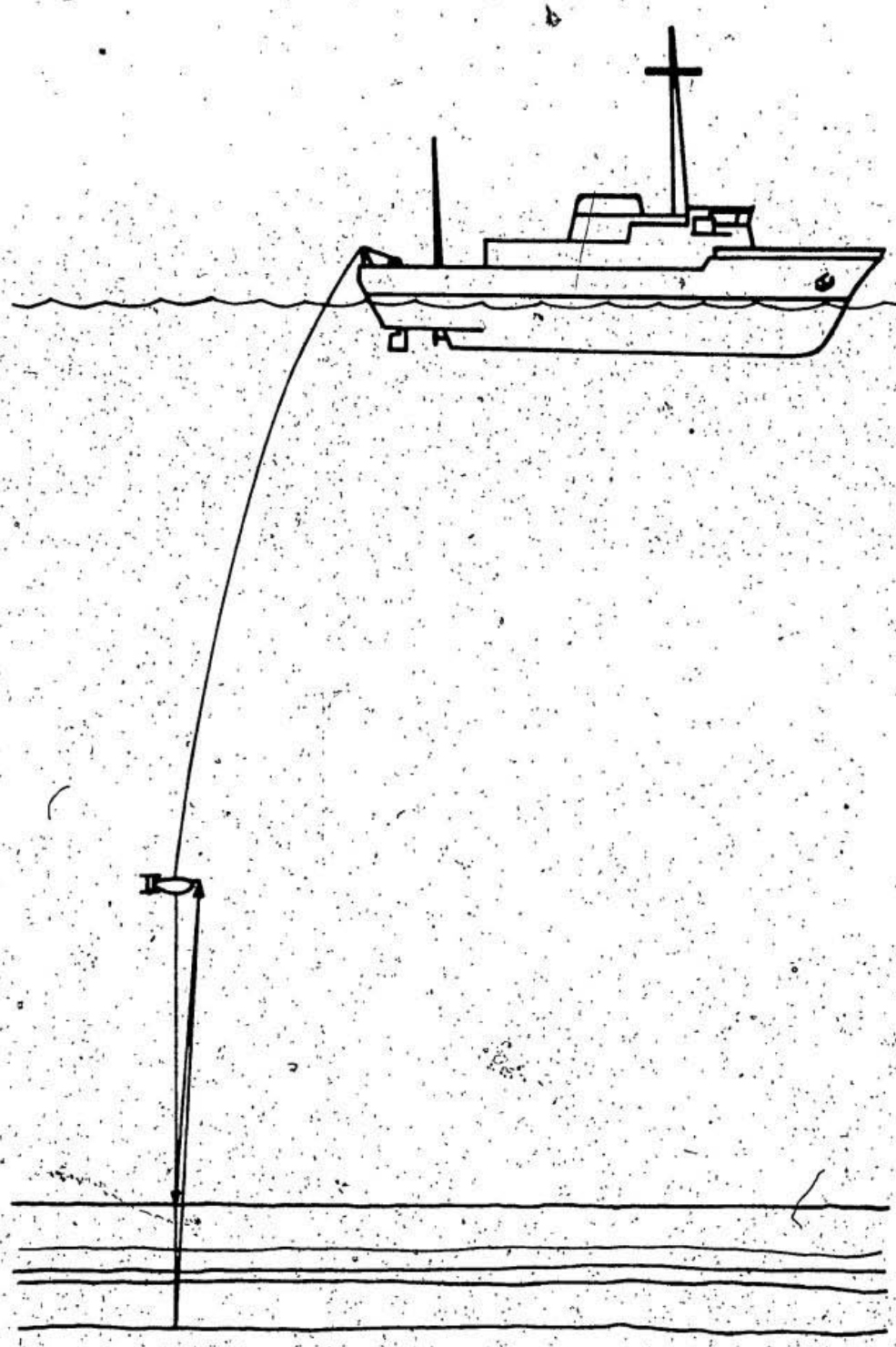

Figure 2 Huntec System in Operation

to-noise ratio was available, and to concentrate efforts on separating these by digital signal processing. The four sediments selected are (using the nomenclature in Drapeau and King, 1972):

1. Emerald Silt
2. Sambro Sand-Gravel
3. La Have Clay
4. Scotia Shelf Drift (Glacial Till)

The six locations shown in Figure 1 include two for each of Emerald Silt and Sambro Sand-Gravel, and one for each of LaHave Clay and Scotia Shelf Drift. Acoustic reflection coefficient measurements have proven very useful in estimating bottom sediment types through the empirical relationship between reflection coefficient and sediment porosity. It is suggested that these measurements can be augmented by estimates of the relative amount of coherent energy contained in the returned acoustic signals.

The acoustic returns from the sediment types listed above are subjected to two methods of analysis. By calculating the normalized cross-correlation coefficents between pairs of acoustic returns, the running average of the normalized event to event correlation is obtained, along with the corresponding standard deviation. A measure of the energy in the returned signals, on an event to event basis, is also obtained by squaring and integrating the return; a running average and standard deviation for normalized cumulative energy is produced.

The results of calculating the running mean of the normalized correlation coefficients indicate that a sediment can be correctly

placed in one of the four sediment classes approximately 70 percent of the time. The calculation of the normalized cumulative energy running mean shows that, even though two of the sediments above cannot be resolved using this measure alone, when combined with the normalized correlation coefficient, a higher correct-classification percentage can be obtained. The results of combining the two methods of estimating the degree of coherence in a set of received echoes indicate that complete separation of sediments into four classes is possible with the available acoustic data.

CHAPTER 2

DESCRIPTION OF EQUIPMENT

2.1 Introduction

Since the scientific purpose of the cruise was to map the surficial geology of the Gulf of Maine and Bay of Fundy part of the Scotian Shelf, CSS Hudson was equipped with the Huntec Deep Tow Seismic (DTS)System, along with precision chart recorders, side scan sonar and analog instrumentation recorders. A block diagram of the data gathering system is shown in Figure 3. A Hewlett-Packard 5451B Fourier Analysis System was in operation at the university. When the data tapes were returned to the university after the cruise, digitization was accomplished with this system, and a library of acoustic returns obtained over a number of different sediment types was started.

2.2 The Huntec DTS System

The Huntec DTS System (Hutchins, et al, 1976) employs a towed body containing an electro-dynamic (boomer) source. This source produces a high energy, repeatable pulse signature. The towed body contains two single element hydrophones. One is mounted directly beneath the transmitting transducer; the other is mounted in the nose of the towed body.

The transmitting plate is 60 centimeters in diameter and produces an impulsive, broadband pressure pulse. The pulse shape, as seen in Figure 4, varies with aspect angle. Figure 5 shows the dependence of

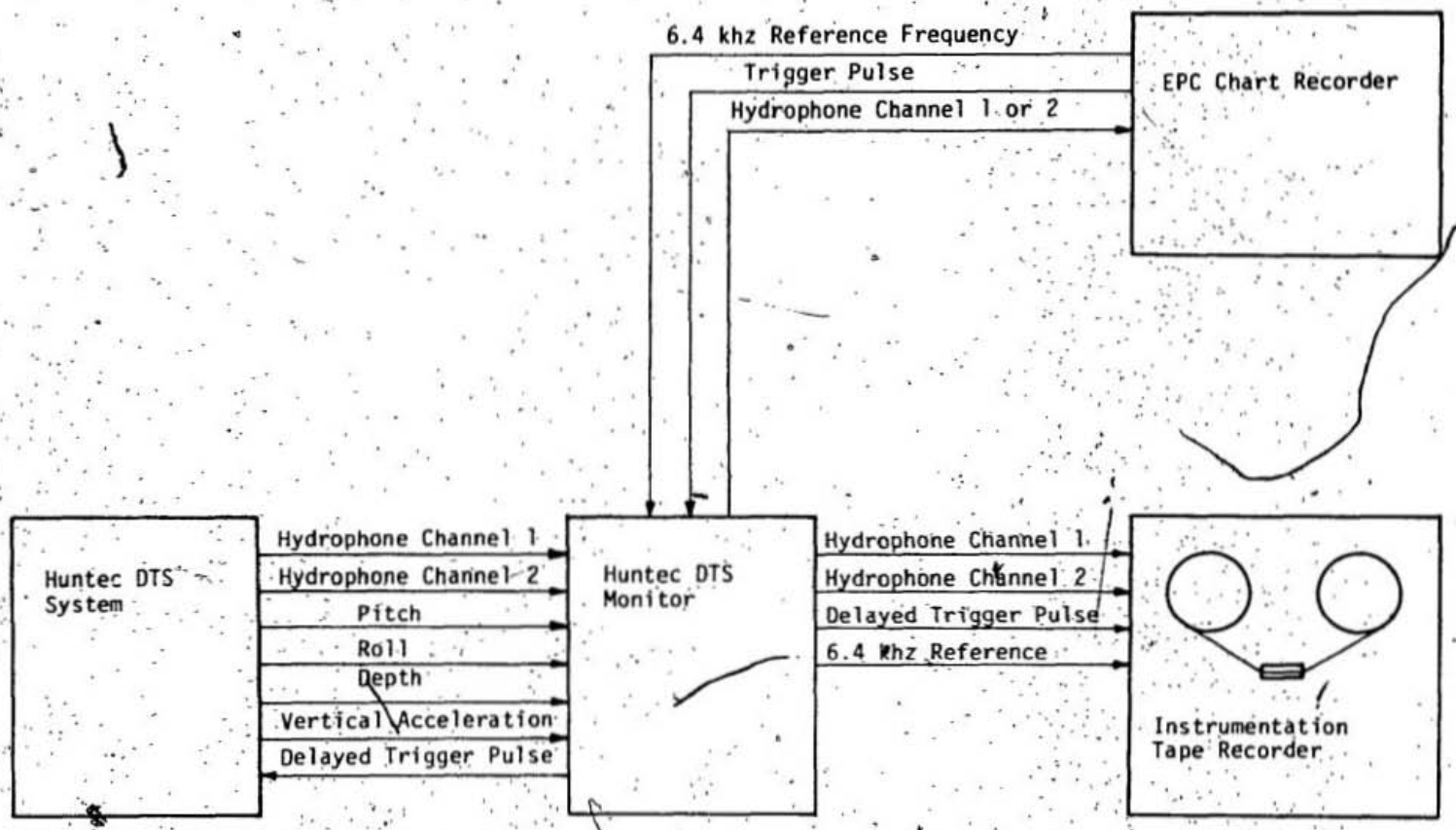

Figure 3. Acoustic Data Recording Block Diagram

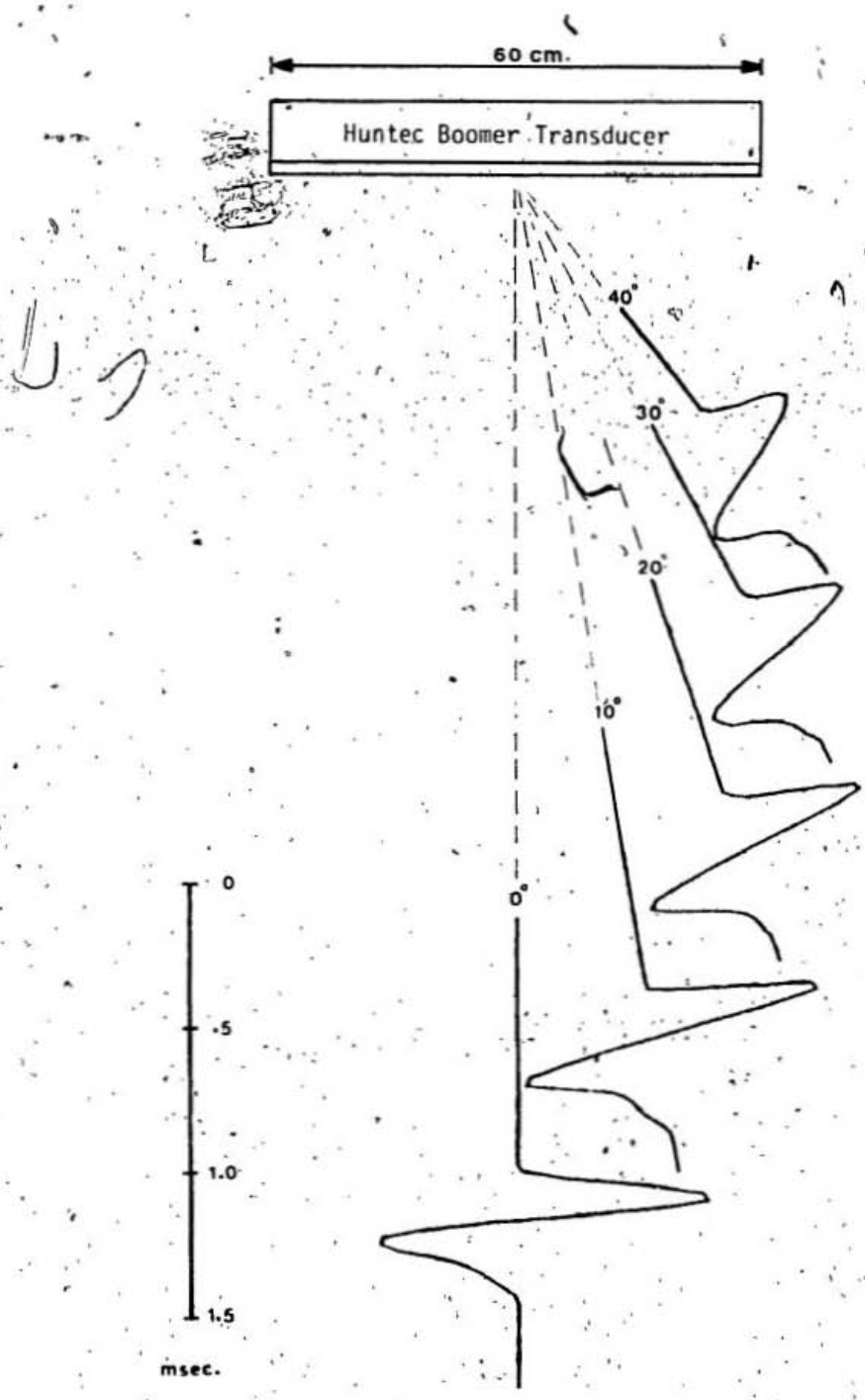

Figure 4 Huntec Source Signature as a Function of Aspect

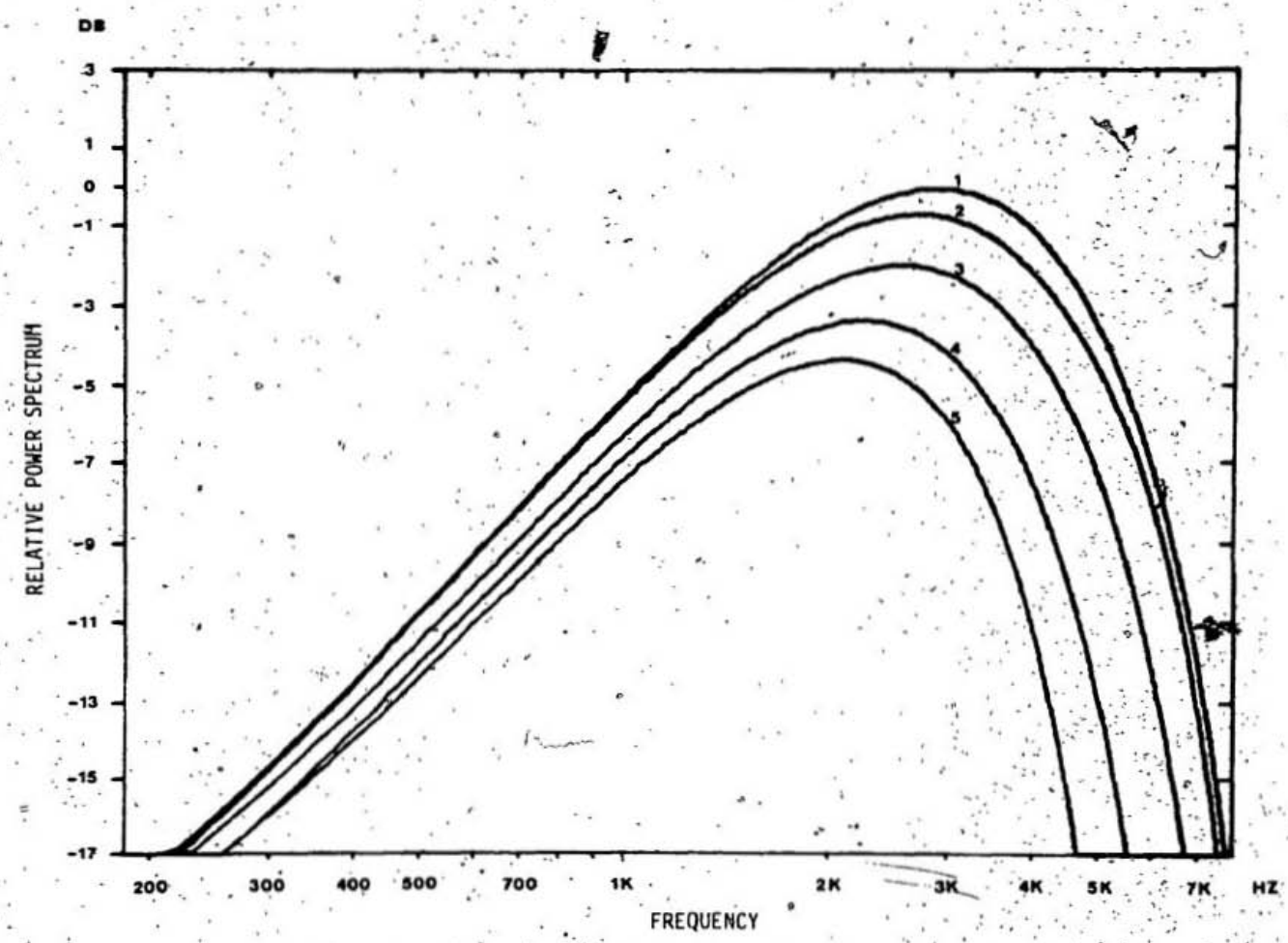

Figure 5. Huntec Source Spectrum as a Function of Aspect

the frequency spectrum with aspect angle. The 3db bandwidth extends from 1.5 kHz to 4.5 kHz. The pulse signature shown in Figure 4 was obtained from a recording of calibration tests supplied by HUNTEC ('70) Ltd. The power spectrum in Figure 5 was calculated from this pulse.

The DTS System was operated at 6 kilovolts, discharging 30 microfarads of capacitance through the boomer coil, for an energy input of 540 joules. The period between successive firings was 0.75 seconds.

The nominal sub-bottom penetration capability of the DTS system is of the order of 50 meters, dependent on sediment type. The towed body is normally trailed at greater than one half the total water column depth. This results in a time window about the bottom and sub-bottom returns which is free from surface and multiple reflections. This multiple-free time window is:

$$t_w = \frac{2(d_2 - d_1)}{c} \qquad 1.$$

where, d_2 is the length of the water column above the towed body,

d_1 is the length of the water column below the towed body,

c is the velocity of sound in water.

The seismic source is pressure compensated so that the acoustic pressure is constant with the depth to 300 meters. The towed body contains roll, pitch, vertical acceleration and depth sensors. A single, armoured, faired multiconductor cable is used to tow the body, supply power to the sound source and electronics, and transmit the hydrophone and altitude sensor outputs to the surface.

The pitch and roll sensors are used to monitor the attitude of the towed body. The vertical acceleration and depth transducers are used to

generate a time delay. This time delay is used to automatically adjust the firing time of the sound source, such that it fires at a constant depth relative to the mean water surface level. The result of this procedure is a correction for the displacement of the towed body caused by ship's heave and a true profile of the seabed.

During the duration of the cruise, the decoupling of the received hydrophones from the towed body was found to be insufficient. Hence the mechanical vibration of the structural members of the towed body was reflected in the recorded data. This ringing of the receiving hydrophones is a major source of interference in the receiving system and requires filtering of the raw data prior to further processing.

2.3 Analog Recording Systems

The HP 3960 4 channel instrumentation tape recorder is operated at a tape speed of 3 3/4 in/sec. At this speed, the recording passband extends from 50 Hz to 15 kHz and the signal to noise ratio is 38 db. The measured peak to peak flutter was less than 0.4%. The 2400 foot magnetic tape used (3M 296) provides a continuous recording of 2 hours before a change of tape is required. All magnetic tapes are de-magnetized prior to recording.

An EPC graphic recorder is used to produce chart records of bottom profiles. A crystal controlled 6.4 kHz signal generated in the graphic recorder is used to generate drive signals for this recorder. The 6.4 kHz signal is recorded on track 1 of the analog magnetic tape so that proper synchronization is attainable upon tape playback.

2.4 The HP 5415B Fourier Analyzer

The HP 5451B Fourier Analyzer is a dedicated computer system, optimized for the rapid spectral analysis of time series data. It contains a mini computer (CPU) which performs spectral analysis via the Cooley-Tukey Fast Fourier Transform (FFT) algorithm, and controls a host of peripherals. These peripheral devices include:

1. 4 channel analog to digital (A-D) converter (digitizer)
2. 1 magnetic digital tape drive (for data and program storage)
3. 1 magnetic disc drive (for data storage)
4. 1 channel digital to analog (D-A) converter
5. 1 graphic display unit and hard copier
6. 1 standard oscillographic display unit

The analog recorded data was digitized using the Fourier Analyzer at a 50 kHz rate. As seen in Figure 5 on page 12, the spectrum drops after 4.5 kHz, the upper 3 db point for the on-axis spectrum. It is concluded from the sampling theorem and Figure 5 that the 50 kHz sampling rate is adequate and aliasing is not a problem.

The digitized data base sections were recorded immediately on digital magnetic tape in blocks of 4096 sampled points. This corresponds to a sampled record length of 81.92 msec. and a depth of 61.5 meters at water equivalent sound velocity. Sampling of each record was initiated by delaying the trigger pulse recorded on track 4 of the analog magnetic tape by a measured amount such that the A-D converter in the Fourier System was triggered just prior to the arrival of the return from the water sediment interface. Figure 6 shows, in schematic

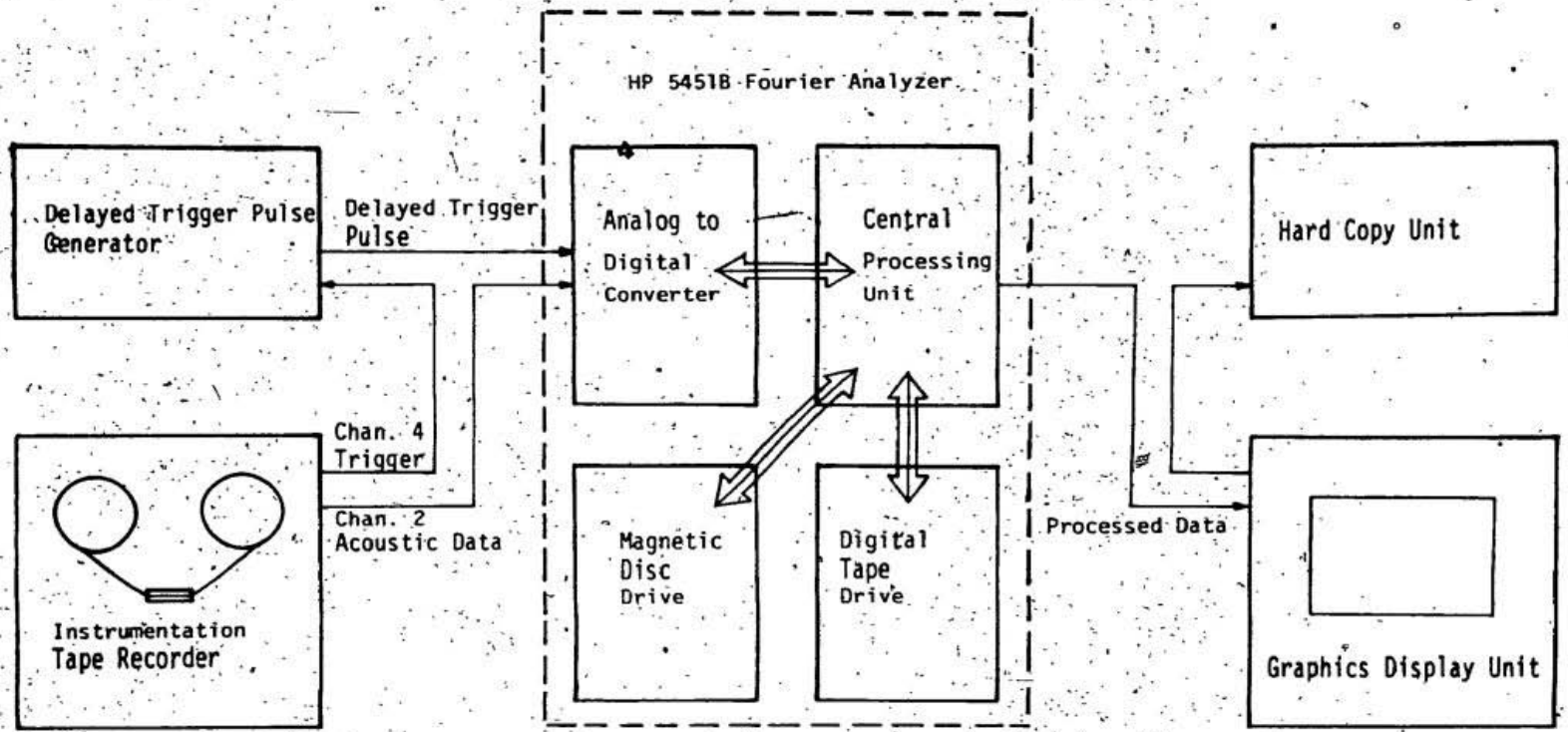

Figure 6 Data Digitization Equipment Block Diagram

form, the digitization procedure. The timing sequence of this procedure is seen in Figure 7.

2.5 Sediment Descriptions

In this thesis, examples of four different sediment types are investigated. They are (Drapeau and King, 1972):

i. Emerald silt; a finer grained, muddy sediment which is generally silty and locally sandy. Angular gravel is also present locally. It has a smooth relatively soft surface and has a high degree of acoustic transparency.

ii. Sambro sand-gravel facies; a medium to fine grained, poorly sorted sediment with high gravel content, and considered to be a modified till. It has a relatively smooth surface and is only moderately acoustically transparent.

iii. La Have Clay. This term is used to describe fine grained deposits that cover basins and depressions. The unit generally overlies Emerald Silt and Till. It has a smooth, soft surface and high degree of acoustic transparency. It is a loosely compacted silty clay.

iv. Scotia Shelf Drift (Glacial till); a cohesive, poorly sorted sediment generally containing angular fragments in pebble, cobble and boulder range. It is dominantly sandy but contains abundant silt and clay. The top surface of the till is characteristically rough and undulating, and parallels more or less the underlying

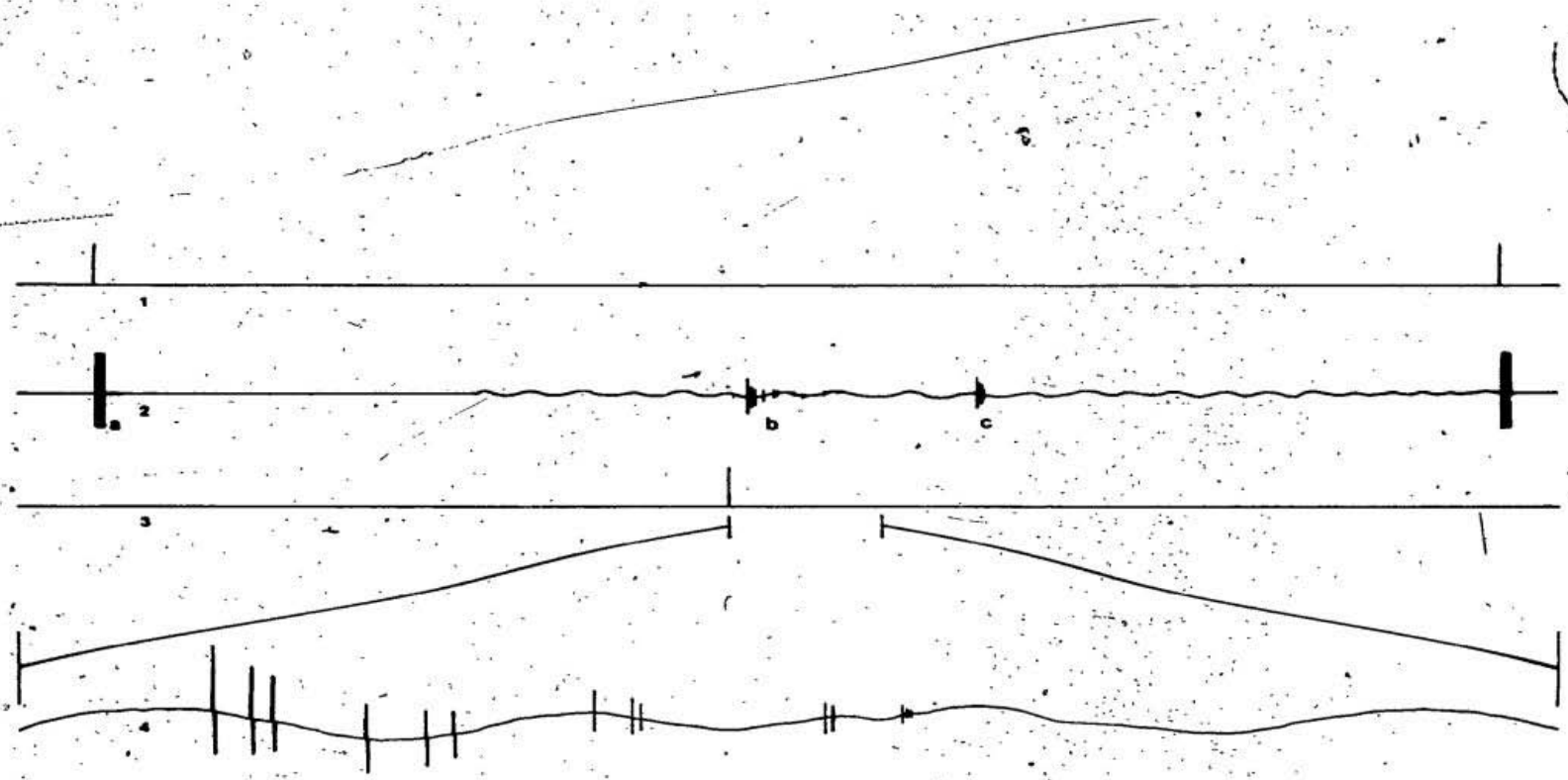

1. Huntec trigger pulse recorded on magnetic tape track #4
   PRR = 4 pulses/3 sec.

2. Signals on Huntec receiving channel recorded on track #3
   (a) Calibration tone
   (b) Bottom reflected signals
   (c) Surface reflected multiple

3. Trigger pulse to begin digitization; obtained by digitally delaying 1

4. Expanded view of bottom reflected signals in 82.92 msec. time window

Figure 7 Data Digitization Timing Diagram

surface of the bed rock.

Figures 8, 9, 10 and 11 show portions of chart records obtained over the bottoms described above.

The acoustic data used in this thesis was obtained at the following locations:

i. Emerald Silt - Longitude 42°39'N Latitude 67°08'W
Longitude 42°47'N Latitude 67°05'W

ii. Sambro Sand - Longitude 43°28'N Latitude 66°48'W
Longitude 43°29'N Latitude 66°43'W

iii. La Have Clay - Longitude 43°28'N Latitude 64°18'W

iv. Scotia Shelf Drift - Longitude 42°45'N Latitude 67°05'W

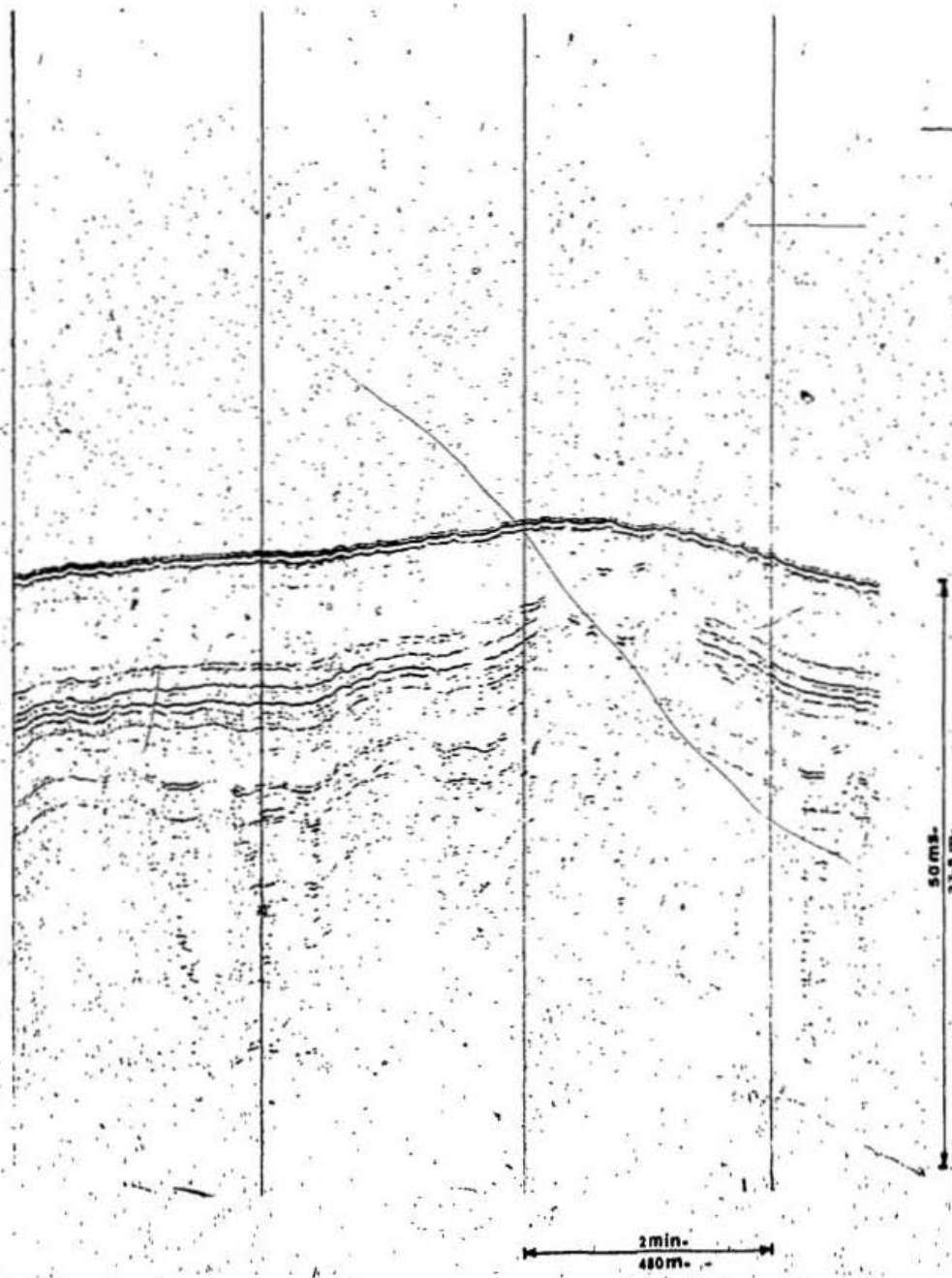

Figure 8 Portion of Chart Record for Emerald Silt Bottom

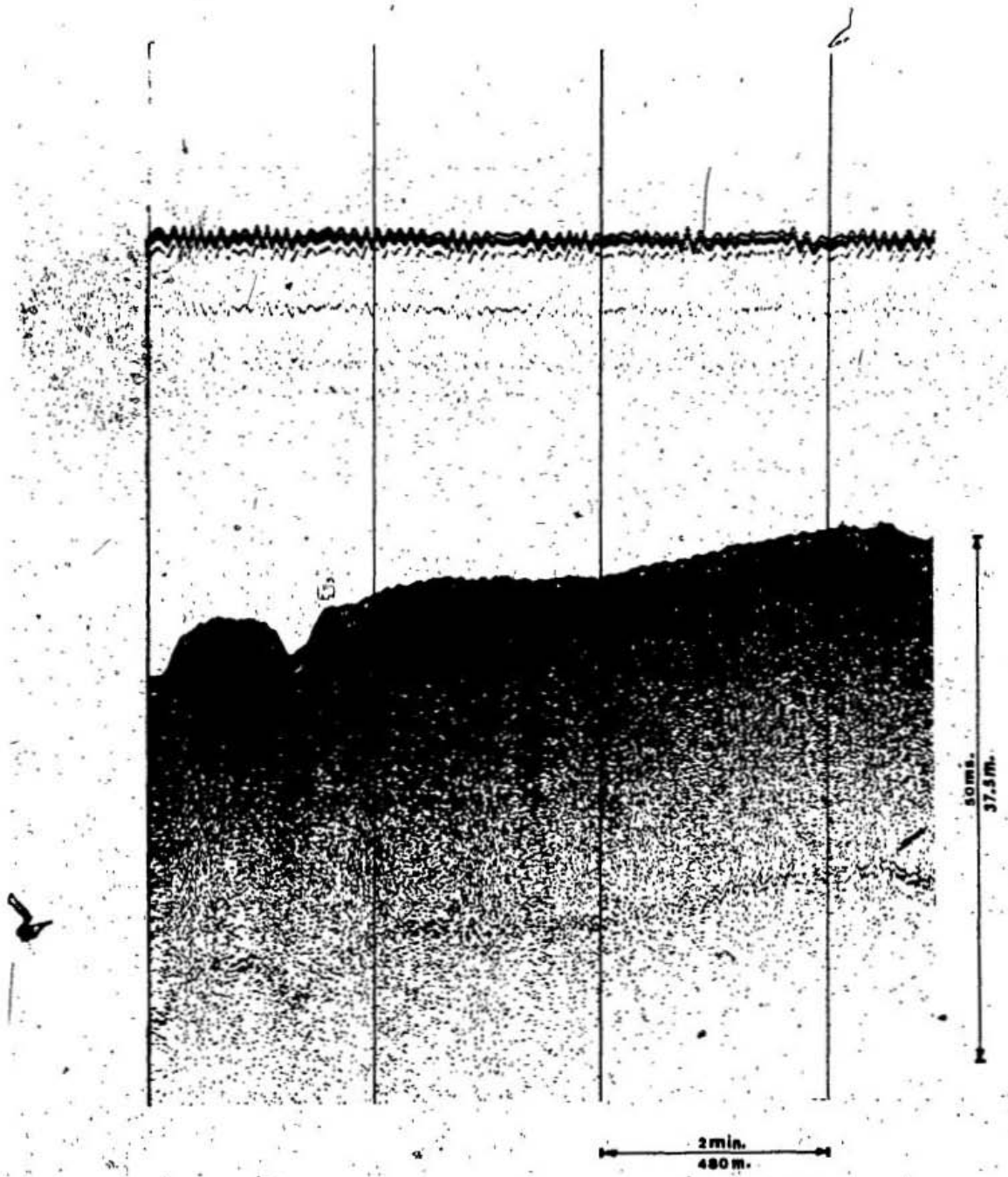

Figure 9 Portion of Chart Record for Sambro Sand Bottom

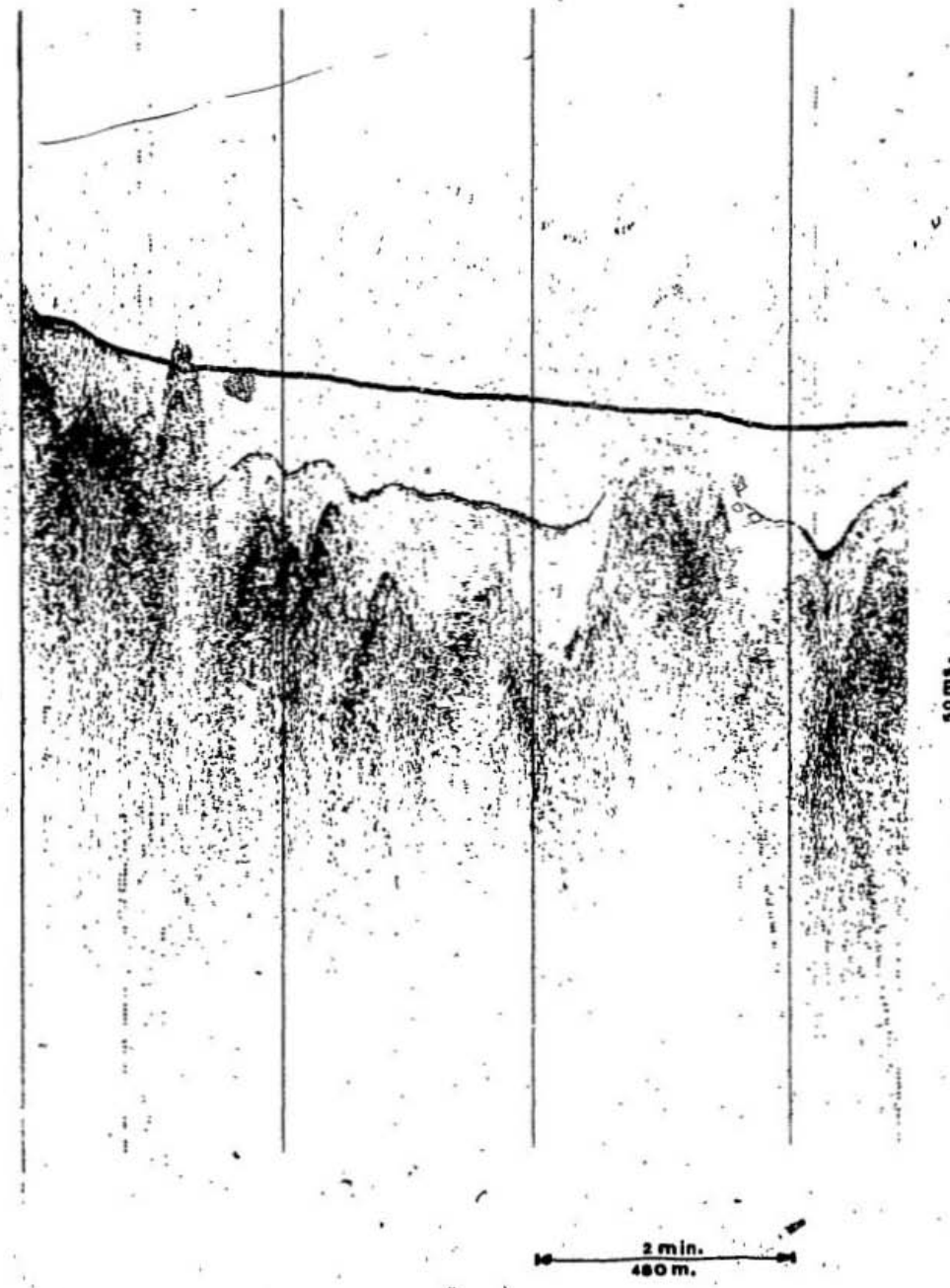

Figure 10 Portion of Chart Record for La Have Clay Bottom

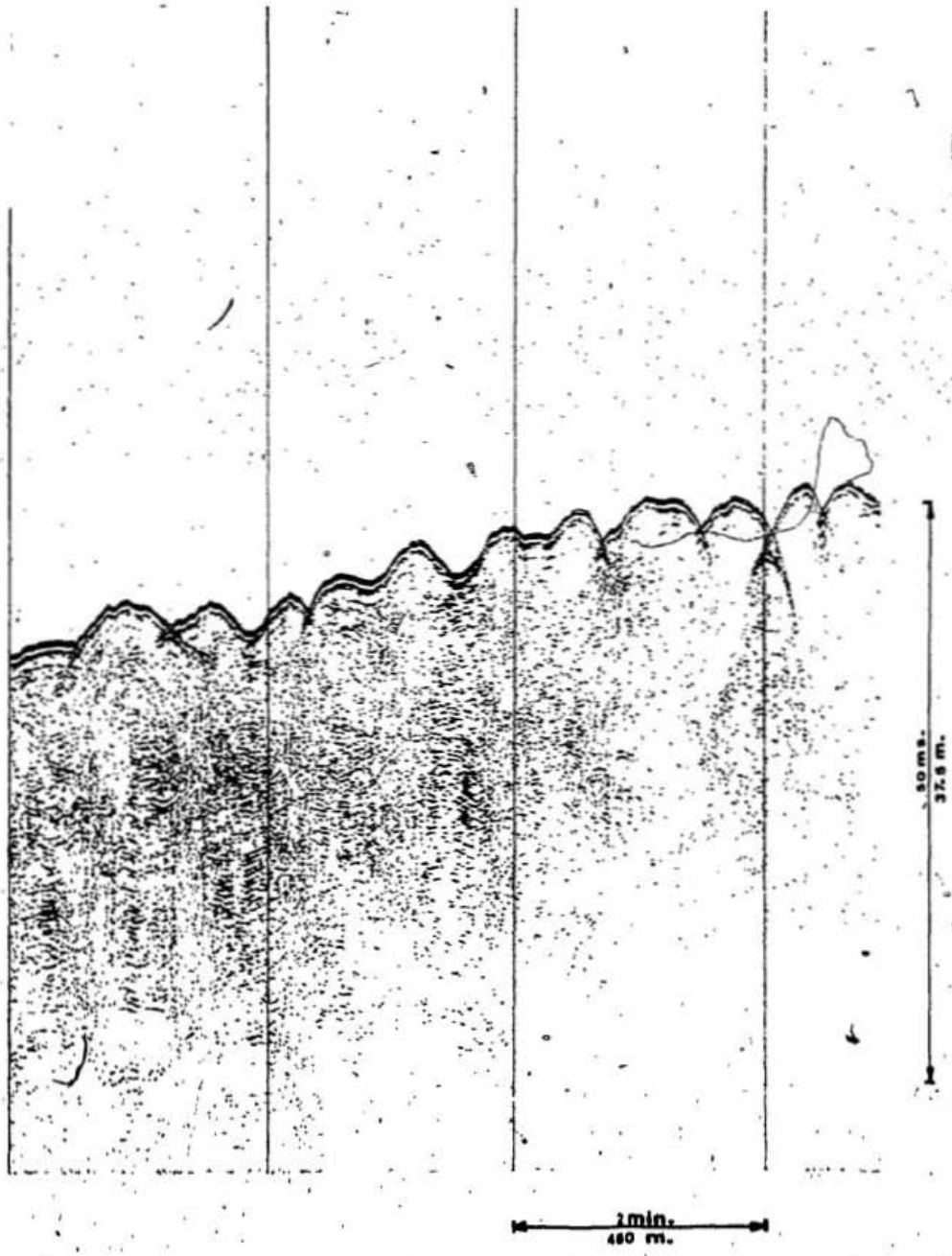

Figure 11. Portion of Chart Record for Scotia Shelf Drift Bottom

CHAPTER 3

SEDIMENT MODEL

3.1 Introduction

In the Huntec Deep-Tow System, the source and receiver are mounted on the same towed body. Therefore, during operation, the source and receiver can be considered to occupy the same point in space - i.e. it is a monostatic system. The equivalent water path to be considered in calculating transmission loss is twice the distance of the towed body to the bottom.

If a source of sound is located in a homogeneous, unbounded, lossless medium, the power generated by the source is radiated equally in all directions. It is equally distributed over the surface of any imaginary sphere with the sound source in its center. The ocean in the Continental Shelf regions of the earth is not homogeneous, lossless, nor unbounded. However, the physical character of the ocean does not change significantly in the water depths being considered. Urick (1975) concluded that when propagation measurements are made at sea, spherical spreading, together with frequency dependent absorption, provides a reasonable fit to measured data under a wide variety of conditions. The water column is certainly bounded, but for the acoustic path lengths involved (i.e. the water-sediment interface being in the far field with respect to the towed body) the error introduced by assuming an unbounded medium is negligible.

If a plane pressure wave is incident at a grazing angle, θ_1, upon

the boundary between two fluids of densities, ρ_1, and ρ_2 and of sound velocities c_1 and c_2, the ratio of the pressures of the reflected wave to the incident wave is given by:

$$\frac{A_r}{A_i} = \frac{\rho_2 c_2 \sin\theta_1 - \rho_1 c_1 \sin\theta_2}{\rho_2 c_2 \sin\theta_1 + \rho_1 c_1 \sin\theta_2} \qquad 2.$$

In the case of normal incidence, as with the Huntec system, the relationship reduces to:

$$\frac{A_r}{A_i} = \frac{\rho_2 c_2 - \rho_1 c_1}{\rho_2 c_2 + \rho_1 c_1} \qquad 3.$$

The plane wave approximation may be used since the interface is in the far field with respect to the towed body (Officer, 1958).

All ocean bottoms are both reflectors and scatterers of sound, and act to redistribute in the ocean a portion of the sound incident upon it. Clay and Leong (1974) have shown that completely rough bottoms return acoustic energy by a scattering mechanism while smooth bottoms reflect the acoustic energy in a coherent manner as seen in Figure 12. Intermediate values of roughness return properties of reflected and scattered energy. The assumptions for the application of this theory are as follows:

i. the interface is an average plane surface; and,

ii. its roughness has the same statistical description in one area as in any other area.

In actual fact, an ocean bottom is quite variable and its slope and roughness change radically from one place to another. However, since

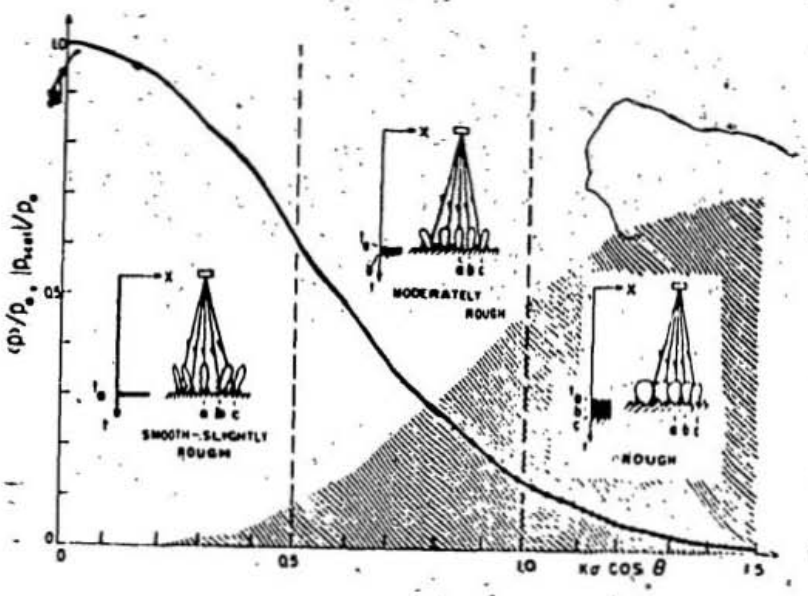

K = wave number of incident radiation
σ = rms roughness of the surface
θ = incident angle of incident radiation

The expected mean signal as a function of Kσ cos θ. The solid curve, $\langle p \rangle / p_0$, is the form Eq. 2.1 and the shaded area shows a crude estimate of the incoherently scattered signals, $\langle p^2 \text{ scattered} \rangle^{1/2} / p_0$ from rough surfaces. The three sketches show the echo soundings and ray paths from bottoms having different roughnesses. The beam patterns at a, b, and c indicate the directivity of the scattered signals. For the smooth to slightly rough bottom, sound at a reflects back to the transducer (shown by a small rectangle), with paths at b and c reflect in other directions. For the moderately rough bottom, sound is scattered back from a and b to the transducer. For the rough bottom the scattering pattern is still broader and sound is scattered to the transducer from a, b, and c.

(From Clay and Leong, 1974)

Figure 12 Relative Reflected and Scattered Energy vs Bottom Roughness Parameter, Kσ cos θ

an acoustic system insonifies a relatively small area of the bottom, the roughness is measured relative to the average plane in the insonified area. Bottom features outside the illuminated area are not observed. By making a number of measurements in an area, an average roughness of bottom elevations can be estimated.

The terms "rough" and "smooth" must be defined in relation to the wavelengths of the incident energy used. Rough bottoms contain scatterers whose dimensions are of the same orders of magnitude as the wavelengths used. Smooth bottoms contain scatterers whose dimensions are very much smaller than the wavelengths used.

The propagation medium between a transmitter and receiver may be considered as a filter that operates a transformation on the transmitted signal. In the case of an acoustic signal in a viscous medium, this transformation may be assumed linear except in the case of very high amplitude signals (Laval, 1973). The transformation can be defined by its impulse response $h(t)$ or by its transfer function $H(\omega)$ which is the Fourier Transform of $h(t)$.

For a plane surface, the transformation is a simple one. Ocean bottom sediments, however, are not represented by plane surfaces, since they are generally rough and/or stratified. Signals returned from such bottoms travel via different paths between transmitter and receiver, with each path corresponding to a different time of arrival. An ocean bottom then can be modelled as a time varying filter. This is discussed in Section 3.2 and in Laval (1973).

Drapeau and King (1972) have associated sediment types with bottom

roughness characteristics. They describe a range from flat and smooth for mud bottoms (silts and clays) to a rough hummocky surface, unsuitable for most bottom fishing operations, for glacial till (a mixture of mud, sand, gravel and boulders).

The coherent reflected energy from a smooth bottom yields an initial echo pulse from the sediment which is closely related in shape to the transmitted pulse. The echo returns from a completely rough bottom result in time elongation of the transmission duration with no clearly discernable initial replica pulse. Intermediate values of roughness result in echos which contain both a reduced coherent portion and an elongated tail referred to as reverberation. A measurement of the amount of coherent return from an ocean floor gives a measure of sediment roughness. This roughness may then be associated with a particular sediment type. The classification of sediment type by means of coherence measurements is based on the supposition that hard bottoms are generally rough while soft sediments are generally smooth.

In terms of filter theory, then, a hard, rough bottom can be represented as a fast, time varying transfer function, while a soft, smooth bottom can be associated with a slow, time varying transfer function.

3.2 Sediment Model Description

Since signal paths between acoustic source and receiver through the water and a sediment structure are different and assumed to be linear, each may be considered as a filtering function. The filtering functions

of the medium represent effects of a number of different physical factors. The effective filter may be considered as a linear combination of a number of simple filters associated with the different physical effects that may change the signal along each path.

These simple filters can be divided into two categories as seen in Figure 13.

i. Deterministic Filters: For a sedimentary bottom, these include coherent reflection from a flat, layered bottom; spherical spreading losses in the water column; frequency dependent absorption in the water column.

ii. Stochastic Filters: These include scattering from a rough sediment surface and scattering from inhomogenities within the sediment volume.

The deterministic filter transfer functions are well known and documented and their effects on the received signal can be calculated.

The random filter transfer functions can only be described in a statistical manner; estimates of their effects can be made.

Both the deterministic filter and the random filter are time (or space) dependent, since the bottom is acoustically sampled along a defined track, and not continuously at one particular point in space. The filters may then be represented by their time dependent transfer functions $H_d(\omega,T)$ for the deterministic filter and $H_r(\omega,T)$ for the random filter.

The total filtering effect for the medium can therefore be represented as the transfer function $H(\omega,T) = H_d(\omega,T) + H_r(\omega,T)$. If the

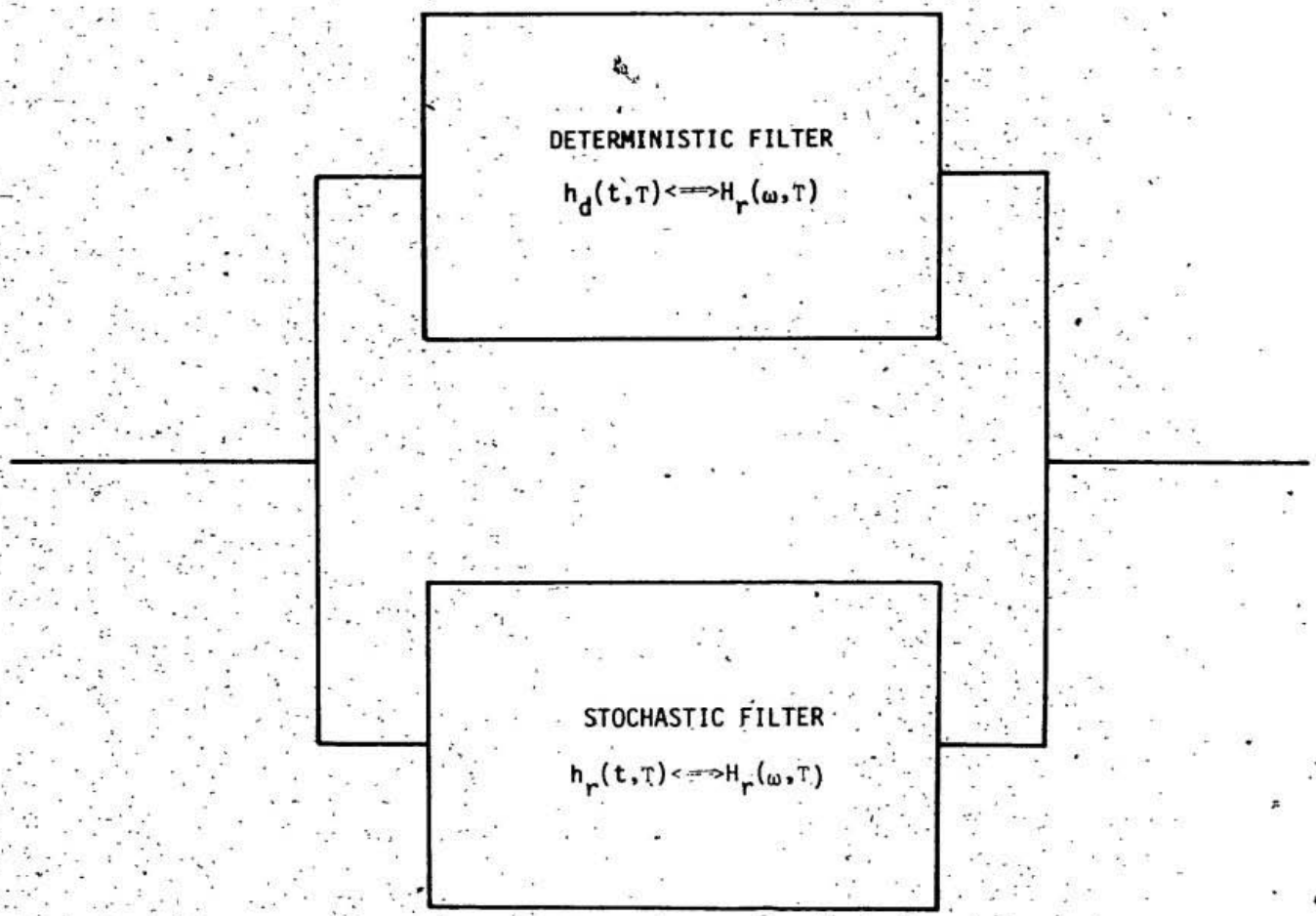

Figure 13 Composite Filter Representation of a Sedimentary Bottom

assumption is made that the bottom roughness elevation encountered is an ergodic process in space and is stationary, and that the surface roughness has Gaussian statistics, the deterministic filter function reduces to $H_d(\omega;T) = H_d(\omega)$. Fortuin (1972) has shown that for a surface described by Gaussian Statistics, the deterministic filter transfer function is given by:

$$H_d(\omega) = -\frac{1}{2d} \exp\,(2jkd - 2k^2h^2\cos^2\theta) \qquad 4.$$

where d is the distance from the towed body to the water sediment interface

h is the rms surface roughness

θ is the grazing angle of the incident radiation; for the case of normal incidence, $\cos\theta = 1$

k is the wave number of the incident radiation.

Then,

$$H_d(\omega) = -\frac{1}{2d} \exp\,(2jkd - 2k^2h^2) \qquad 5.$$

Fortuin (1972) has also shown that the random filter transfer function is time (space) dependent, and is given by the expression:

$$H_r(\omega,T) = -\frac{\exp\,(2jkd)}{2d}\,[\exp\,\{-2jk\cos\theta\,\zeta\,(R_s, T_s)\} - \exp\,\{-2k^2h^2\cos^2\theta\}] \qquad 6.$$

where d, k, h and θ are as before and $\zeta(R_s, T_s)$ is the bottom profile as a function of space and time. At normal incidence:

$$H_r(\omega;T) = -\frac{\exp\,(2jkd)}{2d}\,[\exp\,\{-2jk\zeta\,(R_s, T_s)\} - \exp\,\{-2k^2h^2\}] \qquad 7.$$

The total filter transfer function may be written as the addition of equations 5 and 7.

$$H(\omega,\tau) = -\frac{1}{2d} \exp\left[2jkd - 2jk\zeta\,(R_s, \tau_s)\right] \qquad 8.$$

Frequency dependent absorption in the water column can be incorporated in the total transfer function for the filter as another added term:

$$H_a(\omega) = \exp\left(-2\omega^2 dC_a\right) \qquad 9.$$

where C_a is an absorption coefficient.

Over the path lengths and source frequency spectrum involved, H_a can be neglected (Fortuin, 1973; Urick, 1976).

In this thesis, an experimental approach is taken to obtain a measure of the time varying impulse response of a number of sediments, $h(t,\tau)$, where $h(t,\tau)$ is defined as the Fourier transform of $H(\omega,\tau)$ in equation 8. The methods used in making these measurements are described in Chapter 4 and 5.

CHAPTER 4

NORMALIZED CROSS-CORRELATION COEFFICIENT MEASUREMENT

4.1 Introduction

An incident wavefront produced by the DTS system is nearly spherical at the sea floor; the interaction of the wavefront with the sea floor can be considered a phenomena in the Fresnel diffraction region of physical optics.

The Huygens principle is the basis for scattering theory. The incident wavefront illuminates the scattering interface and each scattering element on the interface is a source of wavelets. The travel time, or phase, of the signal returned by each scattering element is proportional to twice the distance from the source to the scattering element.

If the Huntec DTS System is represented as a point source and receiver occupying the same space at a height d above the sea-bed, the radius of the first Fresnel zone is given by:

$$r = \sqrt{\frac{\lambda d}{2} + \frac{\lambda^2}{16}} \qquad 10.$$

where λ is the wavelength of the energy generated; and

d is the distance from the source to the interface.

Because the Huntec DTS system produces significant energy over a broad band (1.5 khz to 4.5 khz), Fresnel zone dimensions vary with

the spectrum. Figure 14 shows the variation in the first Fresnel zone radius as a function of depth to the sea-bed and frequency. At mid-band (i.e. the frequency at which the energy produced is maximum) and for a 50 meter depth below the towed body, the radius of the first Fresnel zone is 3.54 meters.

The question of statistical independence of spatial samples at a ship's speed of 2.67 meters per second arises. The distance traversed at this speed between samples taken every 3/4 second is 2 meters.

Consider two point scatterers, a and b, at opposite locations at the edges of the first Fresnel zone along the ship's track as in Figure 15. The path lengths to each scatterer are equal when a sample is taken at point c. The contributions from each scatterer are in phase. Let a second sample be taken at a point 2 meters removed from the first, at point d. Now, the path lengths are unequal; the returns from the two scatterers are received with a time displacement. The returns received are more than half a wavelength apart; they are out of phase and therefore uncorrelated.

As the distance between the towed body and the bottom decreases, the first Fresnel radius decreases and de-correlation is maintained. Only if the source to bottom depth is increased will the returns from these scatterers be in phase and hence non-independent samples. Figure 16 shows the acoustic paths length differences as a function of distance between scatterers and water depth below the transducers.

The Fresnel zone consideration is important because if the bottom is flat over the first Fresnel zone, the reflected signal will be large,

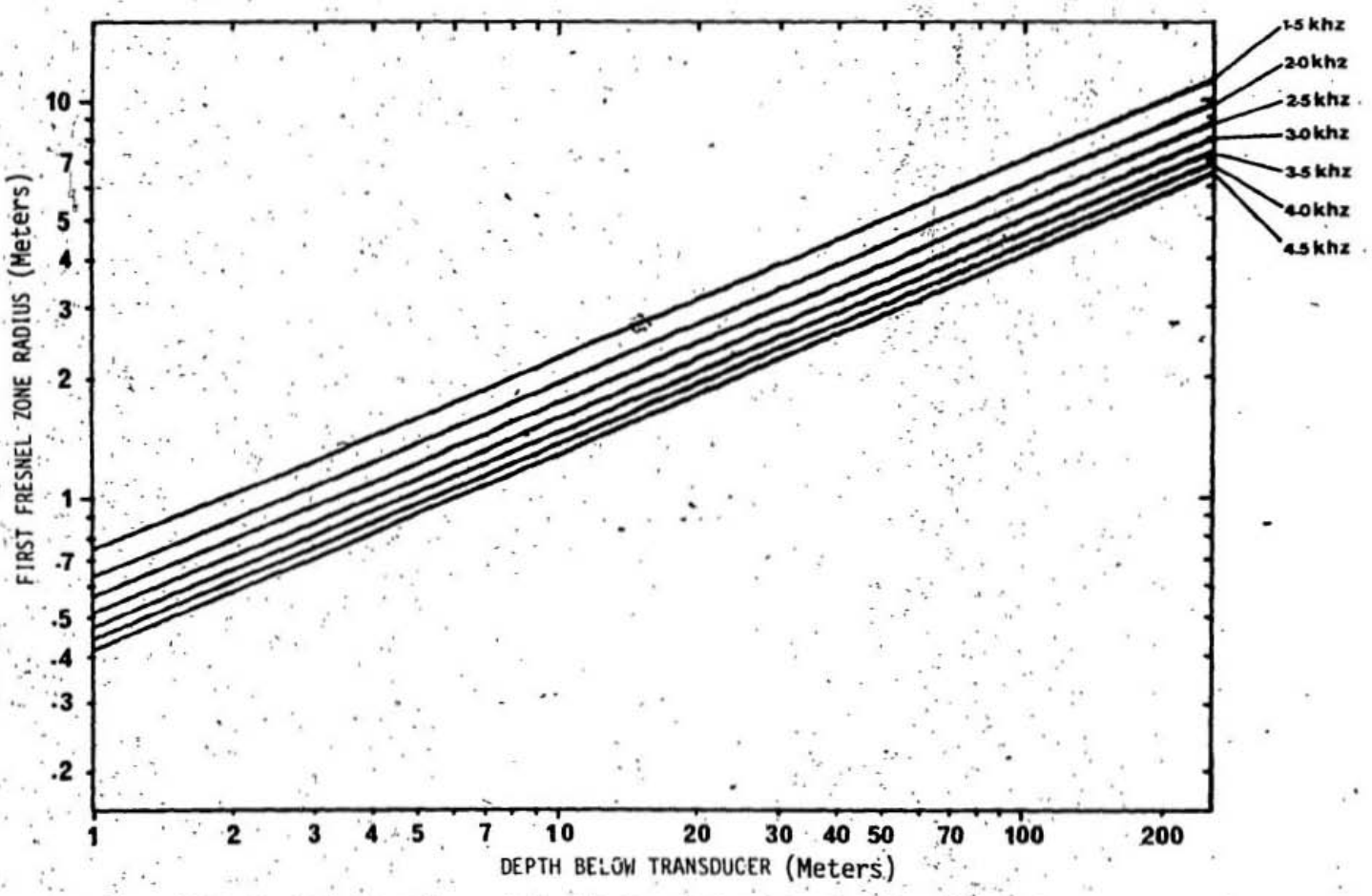

Figure 14 First Fresnel Zone Radius vs Water Depth Below Transducer as a Function of Frequency

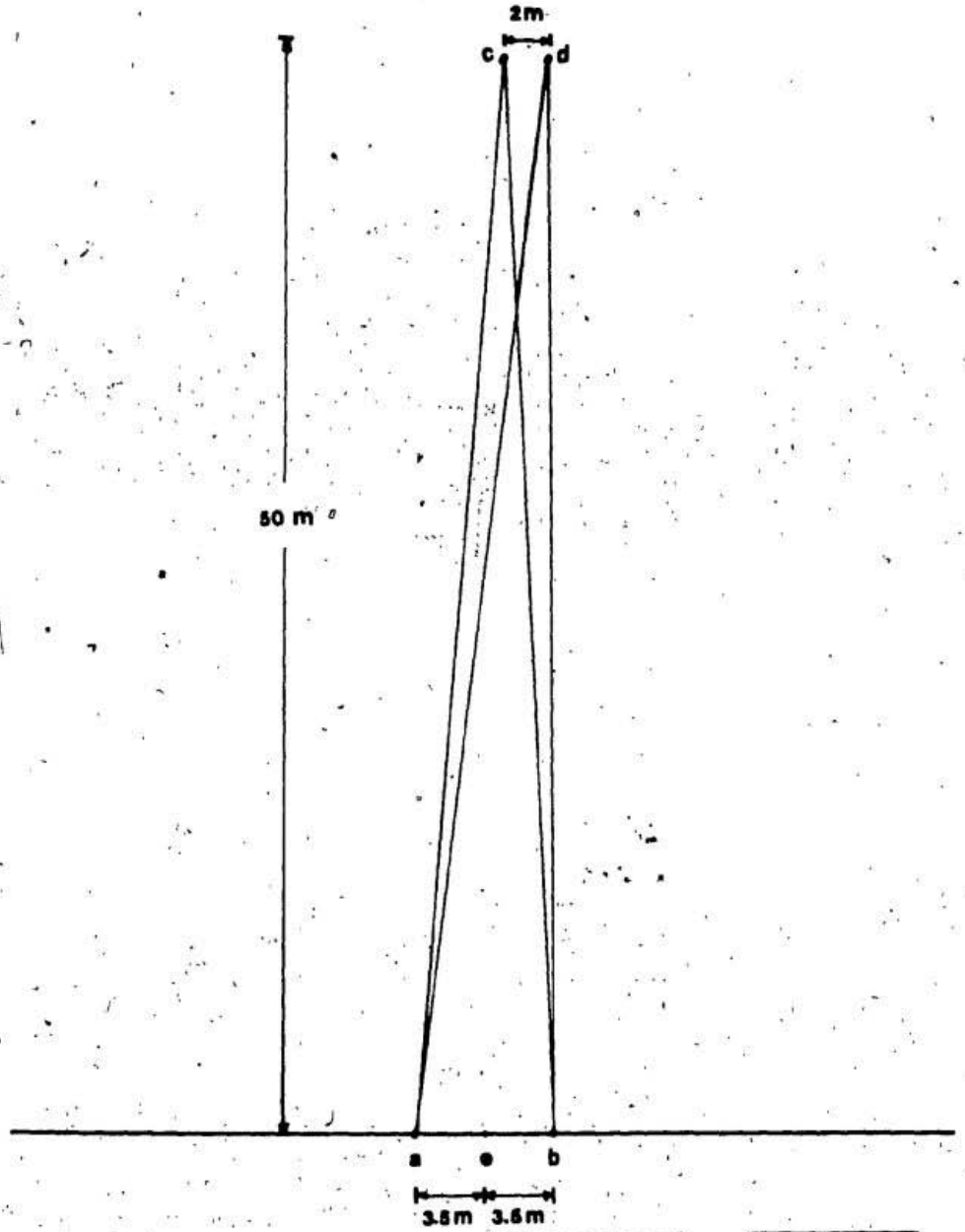

$$\text{Acoustic Path Length Difference} = 2[\sqrt{ce^2 + (ae+cd)^2} - \sqrt{ce^2 + (ae-cd)^2}]$$

$$= 2[\sqrt{50^2+5.5^2} - \sqrt{50^2+1.5^2}] = 0.56 \text{ m.}$$

Figure 15 Acoustic Path Length Differences Between Two Point Scatterers at Opposite Edges of the first Fresnel Zone

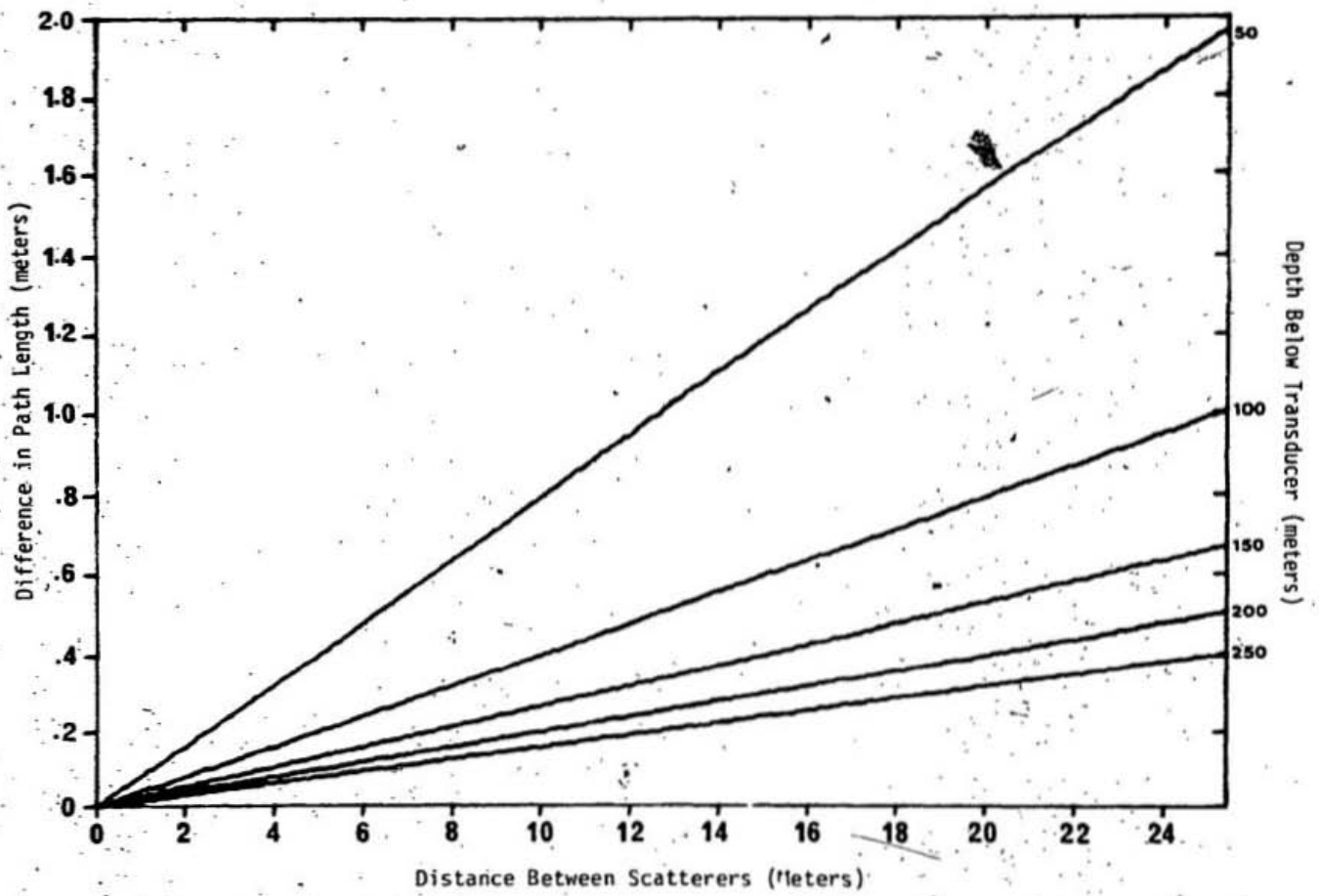

Figure 16 Acoustic Path Length Differences vs Distance Between Scatterers as a Function of Water Depth Below Transducer

regardless of how rough the bottom is elsewhere (Clay and Leong, 1974). A rough surface causes the phases of the contributions within a single zone to differ. If the number of scatterers, n, in the first zone is small, and the reflections from these scatterers are in phase, the scattered signal is proportional to the number of scatterers. If, however, the bottom is very rough, with a large number of scatterers, the scattered signal components will have random phase. The components in this case will add as the signal squared.

For the Fresnel zone approach, it is obvious that the dimensions of the roughness must be much less than the dimension of the first Fresnel zone. This situation does exist with the DTS System as it was used. The sediment with the largest grain size is Scotia Shelf Drift as described in Section 2.5.

4.2 Measurement of Normalized Cross-Correlation Coefficient

The measure of coherence used is the maximum value of the normalized cross-covariance function between two successive echoes. Since the energy produced by the sound source and intercepted by the sedimentary bottom is impulsive, the bottom returned signal is the impulse response of the sediment scaled by the spherical spreading losses along the path. The impulse response is denoted as $h(t,\tau)$ where τ is the space-time dependent variable of the filter. Then a measure of the cross-correlation function between two successive returns from a sediment is a measure of the degree of coherence of $h(t,\tau)$ over time t with fixed τ. τ is fixed by the ping to ping interval of 0.75 seconds.

If a series of echo returns from a bottom is represented by the set

$$[x(t)] = x_1(t),\ x_2(t) \ldots\ldots,\ x_i(t),\ x_{i+1}(t) \ldots,$$

the function referred to as the normalized cross-correlation function is defined by:

$$\rho_{i,\ i+1}(\tau) = \frac{R_{i,\ i+1}(\tau)}{[R_i(0)\ R_{i+1}(0)]^{1/2}} \qquad 11.$$

where $R_{i,\ i+1}(\tau)$ is the cross-correlation function between the ith and (i+1)th echo

$$R_{i,\ i+1}(\tau) = \frac{1}{T}\int_0^T x_i(t)\ x_{i+1}(t+\tau)\ dt \qquad 12.$$

$$0 \leq t < T$$

and $[R_i(0)\ R_{i+1}(0)]^{1/2}$ is the normalizing factor.

$$[R_i(0)\ R_{i+0}\ (0)]^{1/2} = \left[\frac{1}{T^2}\int_0^T x_i^2(t)\ dt \int_0^T x_{i+1}^2\ (t)\ dt\right]^{1/2} \qquad 13.$$

$R_i(0)$ is an estimate of the power in the echo $x_i(t)$. The maximum value of the normalized cross-correlation function is designated the correlation coefficient.

$$\rho_{i,\ i+1} = \text{Max.}\ [\rho_{i,\ i+1}(\tau)] \qquad 14.$$

where $|\rho_{i,\ i+1}| \leq 1$

Smooth, flat bottoms yield high values of correlation coefficients while rough bottoms, due to the random nature of the echo returns,

produce low coherence values.

Individual correlation coefficients were determined for the four sediment types being investigated over a total track of 7 kilometers. The running average and standard deviation of $\rho_{i,\ i+1}$ over 50 successive ping pairs was evaluated. At a towing speed of 6 knots, this corresponds to an averaging distance of 100 meters. Figures 17a, b, c and d show the running mean values of $\rho_{i,\ i+1}$ for each sediment type considered as a function of track length. Figures 18a, b, c and d show the corresponding standard deviation for each sediment type as a function of track length. From observation of Figures 17a, b, c and d, it is evident that a separation of sediment types is possible, some of the time. Emerald silt has a high value of correlation coefficient in the region of 0.8. Sambro sand-gravel follows, and the correlation coefficient value is generally below 0.8. La Have Clay shows a correlation coefficient value in the region of 0.6, while the Glacial Till varies generally between 0.4 to 0.6.

A close observation of Figures 18a, b, c and d, the plots of the standard deviation of $\rho_{i,\ i+1}$ for each sediment yields additional information about the process. If the plot of the running mean of $\rho_{i,\ i+1}$ for any of the four sediments is compared to the plot of the standard deviation, it is seen that as the mean value decreases in value, the standard deviation tends to increase. This phenomena is simply explained since a decrease in cross-correlation coefficient is indicative of a increase in incoherent or scattered energy. This increase in scattered energy, a stochastic variable, is reflected by the increase in

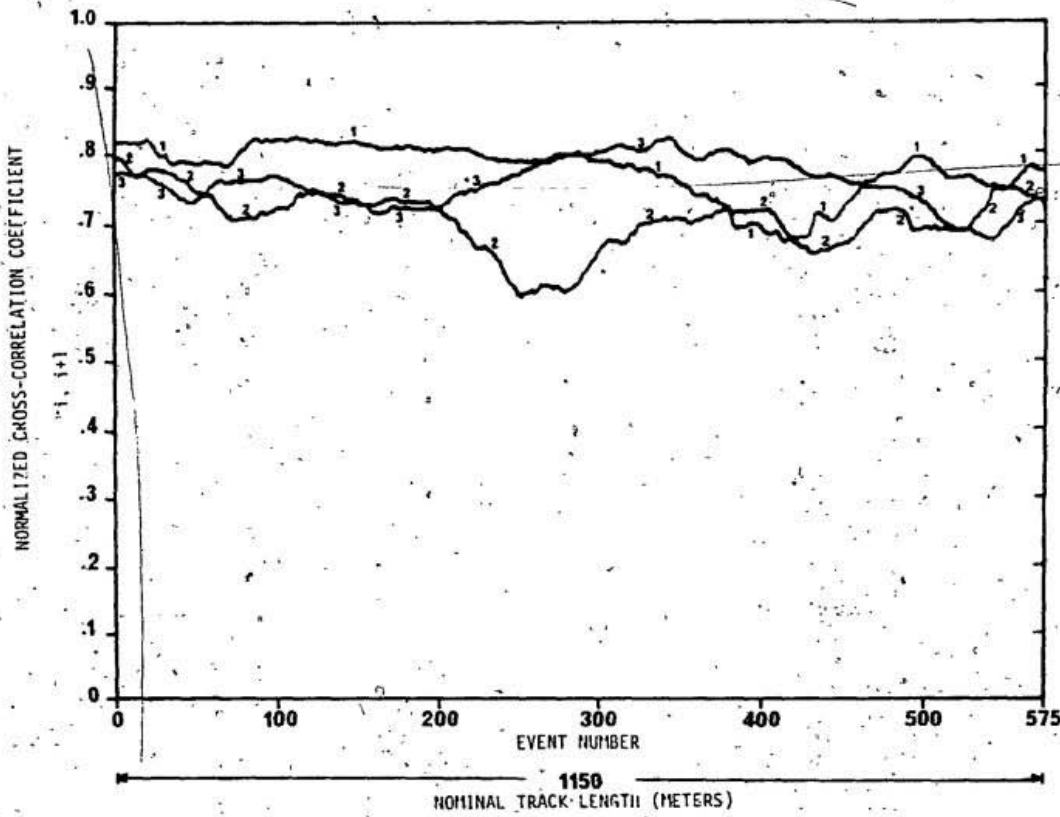

Figure 17a $r_{i,\,i+1}$ vs Track Length - Emerald Silt

1. Longitude 42°47' Latitude 67°05'
2. Longitude 42°47' Latitude 67°05'
3. Longitude 42°39' Latitude 67°08'

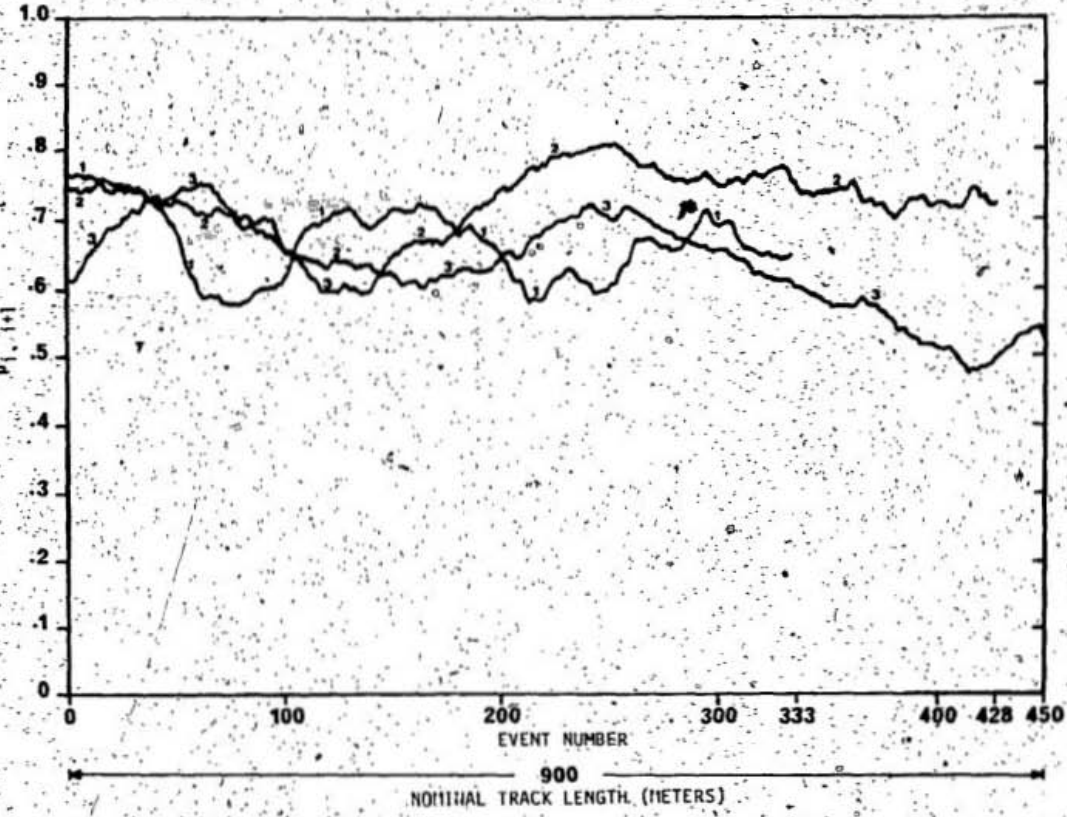

Figure 17b $\rho_{i,\,i+1}$ vs Track Length - Sambro Sand

1. Longitude 43°28' Latitude 66°48'
2. Longitude 43°28' Latitude 66°48'
3. Longitude 43°29' Latitude 66°43'

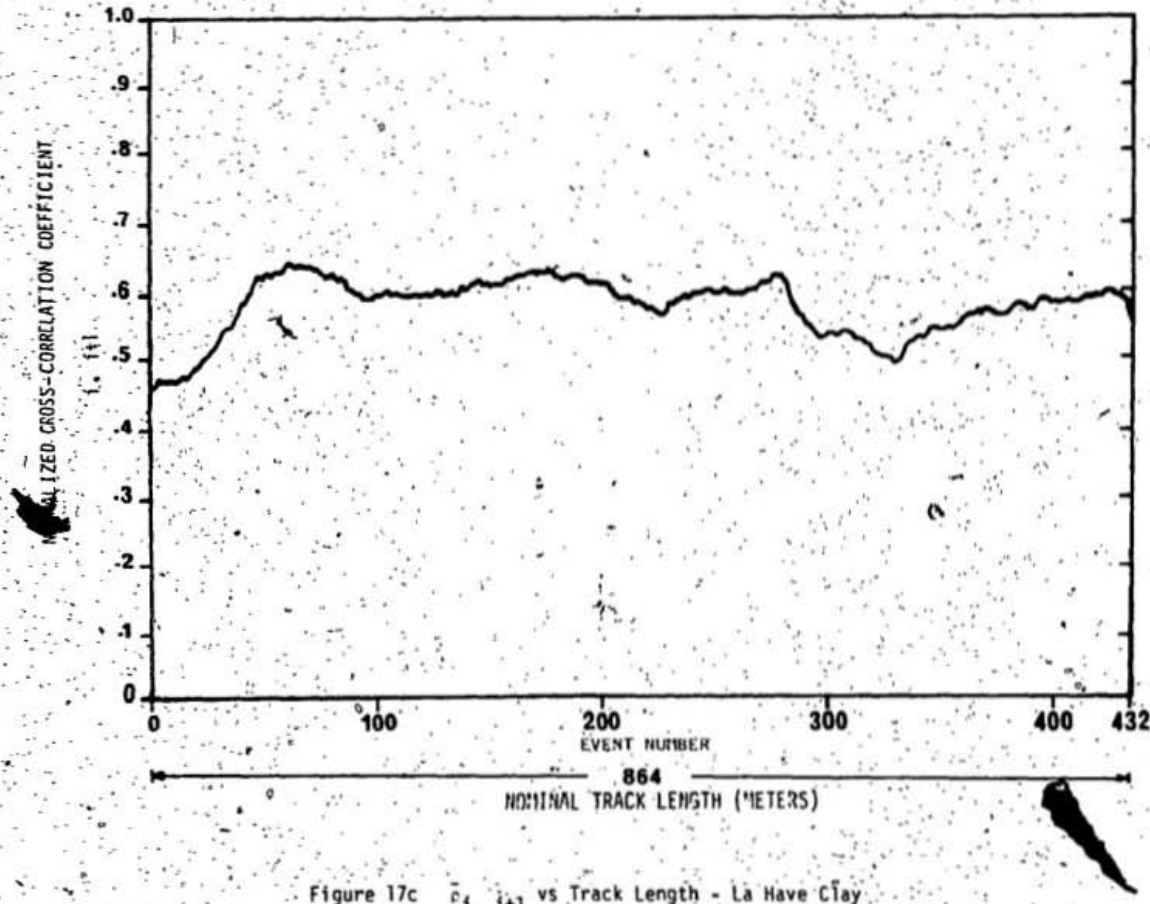

Figure 17c $r_{i,\,i+1}$ vs Track Length - La Have Clay

Longitude 43°28' Latitude 64°18'

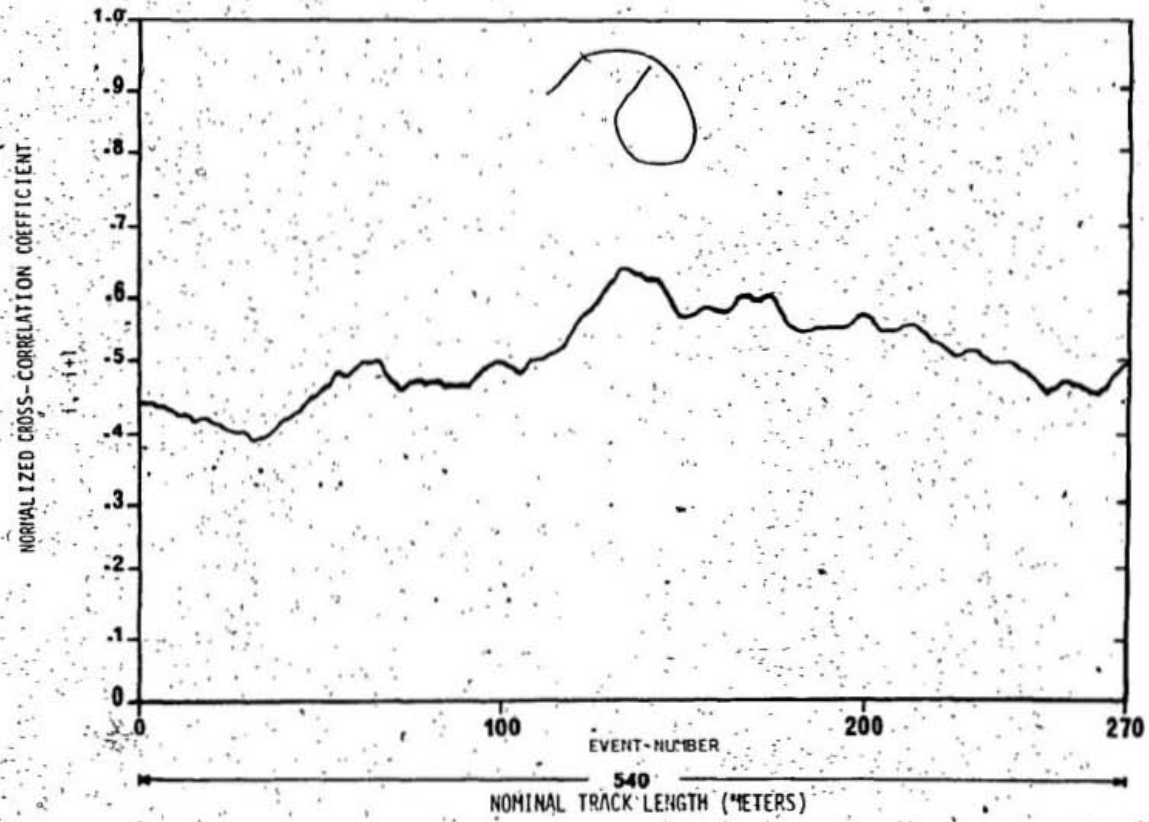

Figure 17d $r_{i,\,(+)}$ Track Length - Scotia Shelf Drift

Longitude 42°45' Latitude 67°05'

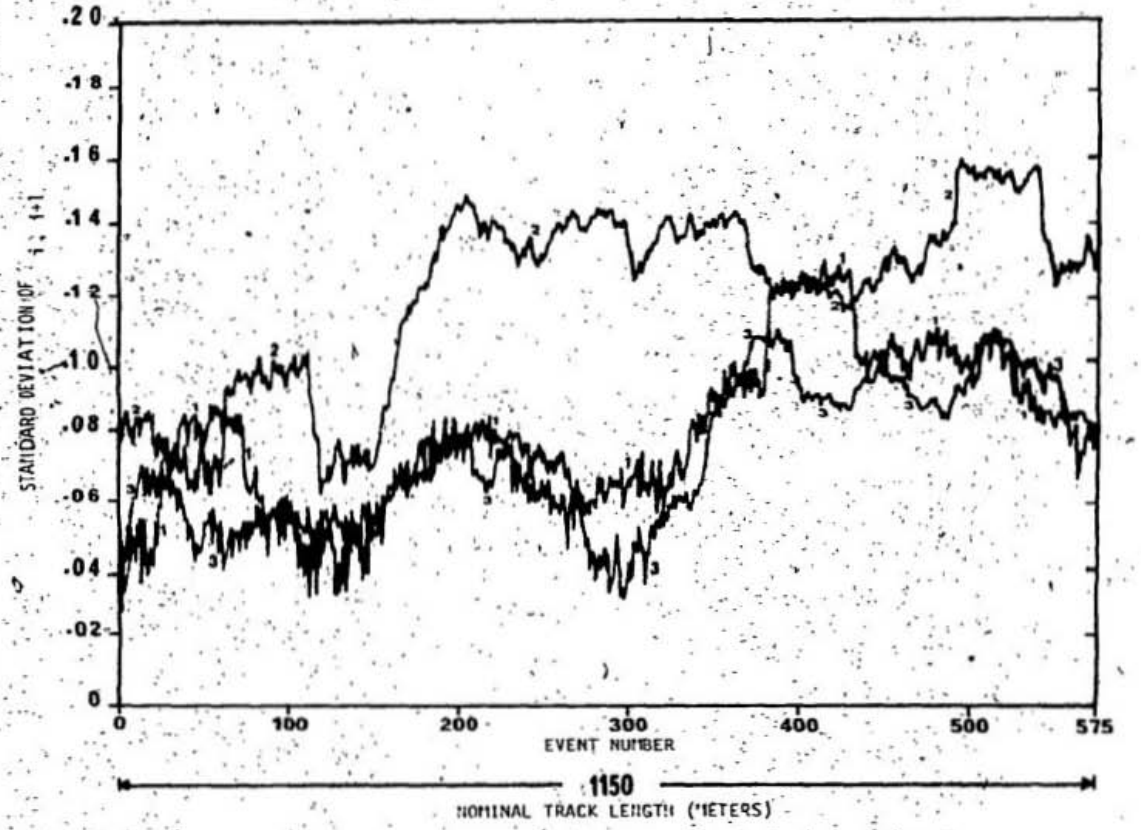

Figure 18a Standard Deviation of $\sigma_{i,\,i+1}$ vs Track Length - Emerald Silt

1. Longitude 42°47' Latitude 67°05'
2. Longitude 42°47' Latitude 67°05'
3. Longitude 42°39' Latitude 67°08'

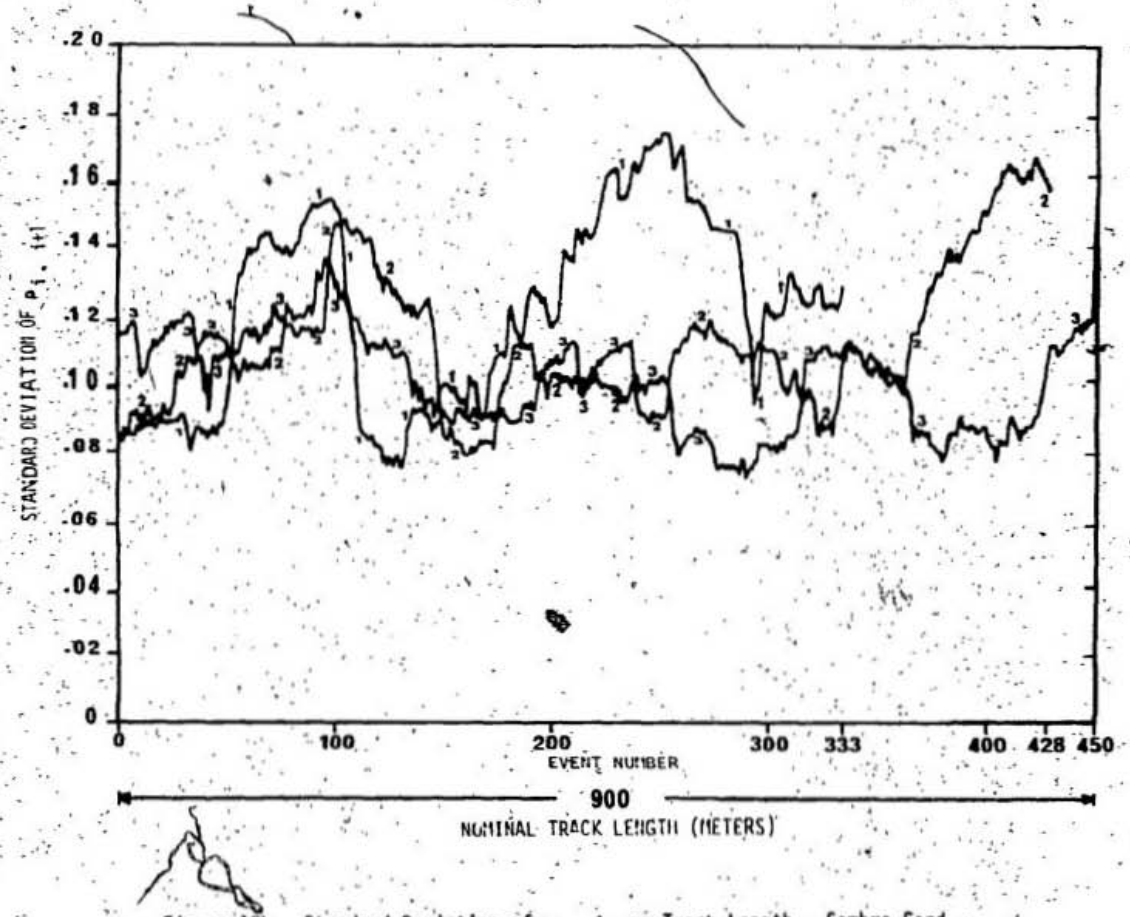

Figure 18b Standard Deviation of $\rho_{i,\ i+1}$ vs Track Length - Sambro Sand

1. Longitude 43°28' Latitude 66°48'
2. Longitude 43°28' Latitude 66°48'
3. Longitude 43°29' Latitude 66°43'

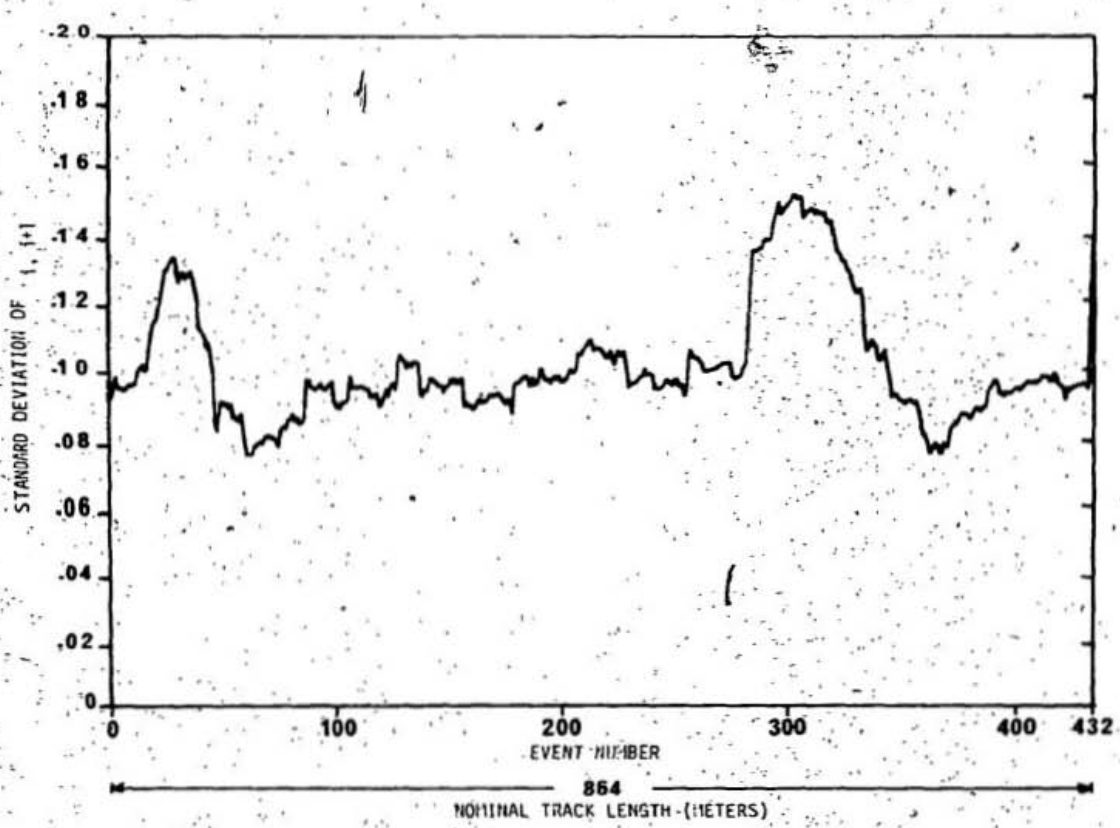

Figure 18c Standard Deviation of $\sigma_{i,\ i+1}$ vs Track Length - La Have Clay

Longitude 43°28' Latitude 64°18'

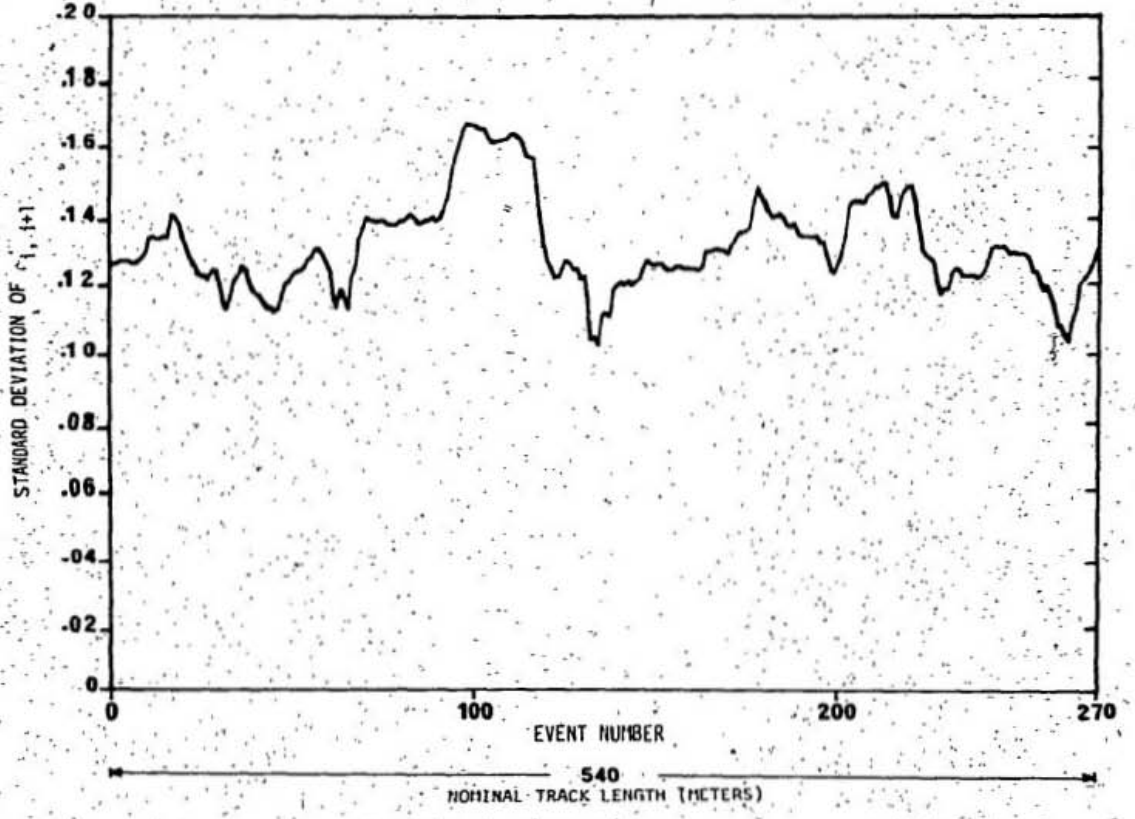

Figure 18d Standard Deviation of $\sigma_{i,\,i+1}$ vs Track Length - Scotia Shelf Drift

Longitude 42°45' Latitude 67°05'

the standard deviation of the measurement. Then, departures of the standard deviation plot from its average value indicate, in a rough manner, the degree of inconsistancy of the particular sediment, if any effects in the measuring system that would cause decorrelation are eliminated. The effects of signal to noise ratio on the measurement is discussed in Appendix 1.

In detection problems, low values of normalized cross-correlation coefficients are generally regarded with some degree of scepticism; in other words, two signals are considered as being correlated if the value of $\rho_{i,\ i+1}$ obtained is high, typically greater than 0.7.

For a band limited, zero mean Gaussian process, Bendat and Piersol (1971) have shown that the normalized mean squared error in a cross-correlation estimate is given by:

$$E_{\rho}^{2} \approx \frac{1}{2BT} \left(1 + \frac{1}{\rho_{i,\ i+1}^{2}}\right) \qquad 15.$$

where B is the signal bandwidth, ≈ 3KHz

T is the length of correlation window, ≈ 40ms

$\rho_{i,\ i+1}$ is the normalized cross-correlation coefficient.

Thus, for the sediment named Scotia Shelf Drift (Glacial Till), for which there is often no discernable coherent echo, an estimate of the merit of the measured normalized cross correlation coefficient can be made. If the acoustic returns from till contain only reverberant (incoherent) energy the process can be considered a band limited, zero mean process. The assumption that a rough bottom has Gaussian amplitude statistics and therefore scatters acoustic signals in a random manner has

been made in Section 3.2.

Then, because of the large BT products involved, evaluation of equation 15 indicates that the mean square error in the cross-correlation estimate is low. Therefore, there is a relatively high degree of confidence in the normalized cross-correlation estimate, even when the numerical value of this estimate is low.

By selecting correlation coefficient thresholds, it is possible to optimize the separation of the sediment types. Thresholds chosen for this data are:

1. Emerald Silt, $0.725 < \rho_T < 1.0$
2. Sambro Sand, Gravel, $0.625 < \rho_T < 0.725$
3. La Have Clay, $0.575 < \rho_T < 0.625$
4. Scotia Shelf Drift, $0.3 < \rho_T < 0.575$

where ρ_T is the coherence threshold.

A scatter matrix for all the data analyzed for each sediment type is shown in Table 1. This table compares the sediment falling within the threshold range to the classification base given in Section 2.5. Using this base as a reference, the percentage of correct classifications is found on the diagonal of the matrix. The overall correct classification based solely on the running average of the coherence coefficient is 77%.

Since LaHave Clay is a very smooth, fine grained sediment, the result that Sambro Sand has a higher value of $\bar{\rho}_{i,\, i+1}$, by comparison, seems surprising. However, it must be remembered that LaHave Clay is known to fill depressions in other sediments, as stated in Section 2.5. The lower value of $\bar{\rho}_{i,\, i+1}$, then is a result of echoes from a scattering layer underlying the LaHave Clay. This scattering layer can be observed in Figure 10.

Table 1 Normalized Cross-correlation Scatter Matrix

Classification threshold, ρ_T, are at the following levels:

1. Emerald Silt, $0.725 < \rho_T < 1.0$
2. Sambro Sand, Gravel, $0.625 < \rho_T < 0.725$
3. La Have Clay, $0.575 < \rho_T < 0.625$
4. Scotia Shelf Drift, $0.3 < \rho_T < 0.575$

Values shown are percentages.

Cross-correlation Coefficient Classification	Reference Base (Drapeau and King and Fader et al)			
	Emerald Silt	Sambro Sand	La Have Clay	Scotia Shelf Drift
Emerald Silt	70	28	--	--
Sambro Sand	27	53	--	--
La Have Clay	3	18	84	--
Scotia Shelf Drift	--	1	16	100
Number of Events	1725	1076	432	270
Track Length (km)	3.5	2.2	0.9	0.5

CHAPTER 5

CUMULATIVE ENERGY FUNCTION AND E_Δ MEASUREMENT

5.1 Introduction

From Figures 17a, b, c and d (pages 41 through 44), it is observed that the usual descending order of coherence coefficients is silt, sand, clay, till. However, there are regions where these curves overlap and one sediment may be misidentified as being another type. For example: Sand is a relatively homogeneous sediment with a small grain size. In a very flat area of sandy bottom, a high average value of $\rho_{i,\ i+1}$ can be recorded; the value in this case can exceed the threshold used for identifying silt and the sediment can be misinterpreted as being silt. In other words, there is a need to differentiate between smooth, homogeneous media, and smooth, finely layered media.

The energy in a returned signal is found by squaring and integrating the signal; the final value of the integral is the contained energy. The energy in the signal can be divided into a coherent portion and an incoherent portion. The coherent energy is returned from coherent interfaces; the incoherent energy received is the result of random scattering at an interface plus any noise that is added to the signal along the transmission path.

As a second estimation of the relative amount of coherent energy contained in a return, the normalized value of energy in the return from the water-sediment interface (the first return) is used. As described in the Section 4.1, a returned signal from a sedimentary bottom is a

scaled measure of its impulse response, $h(t,T)$. The normalized energy in the first return is, then, a measure of degree of coherence of $h(t,T)$ contributed by the water-sediment interface. The relationship between $\rho_{i,\,i+1}$ and the energy in the first return is shown in Appendix 2.

5.2 NCE and EΔ Measurement

The Normalized Cumulative Energy Function (NCE) is formed by squaring and integrating an echo return; the value of the integral at the point after the coherent return has passed is normalized by the final value of the integral.

$$NCE = \frac{1}{E_T} \int_0^t x_i^2(t)\,dt \qquad \begin{matrix} t<T \\ t>t \end{matrix} \qquad 16.$$

$$= 1$$

where NCE is the normalized cumulative energy function and E_T is the total energy in the window T.

$$E_T = \int_0^T x_i^2(t)\,dt \qquad 17.$$

The NCE function for Emerald Silt (Figure 19a) shows a rapid increase in energy which corresponds to the return from the water-silt interface. The stratification in the silt is reflected in the plot by the corresponding increases in returned energy as time increases. As the returns decrease in amplitude towards the noise level, the slope of the plot decreases near the end of the trace.

The NCE function for Sambro Sand (Figure 19b) shows an initial

high intensity return from the water-sand interface, with little internal reverberation, as is expected from a homogeneous medium. The trace slope decreases as the return signal amplitude approaches the system noise level.

The NCE function for La Have Clay is shown in Figure 19c. There is a rapid increase in energy from the water-clay interface, followed by the low level reverberation from the homogeneous clay structure. However, there is then an increase in the returned energy in the latter half of the observation time window. This is due to high amplitude returns from a highly stratified Emerald Silt structure which underlies the La Have Clay deposit. The presence of a second sediment underlying the sediment of interest necessitates special consideration in processing the data.

Figure 19d shows the NCE function for Scotia Shelf Drift. For this rough sediment, the initial increase in returned energy is immediately followed by a relatively high level of reverberation due to both surface and internal volume scattering. As the level of reverberation approaches the system noise level, the slope of the plot decreases near the end of the trace.

As indicated above, the case of one sediment overlying another within the observation window requires special processing considerations. Since the La Have Clay is a highly transparent sediment, the underlying Emerald Silt, in this instance, reflects nearly as much energy as does the clay. This is seen in Figure 19c. Since the concern in this section is to estimate the relative energy returned from the interface between

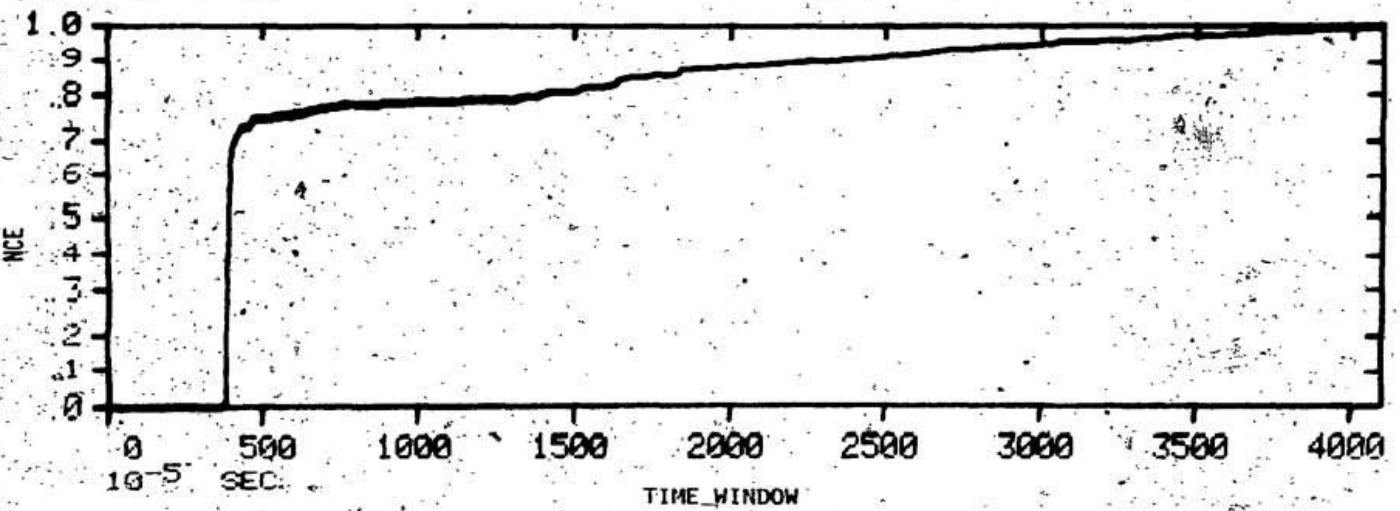

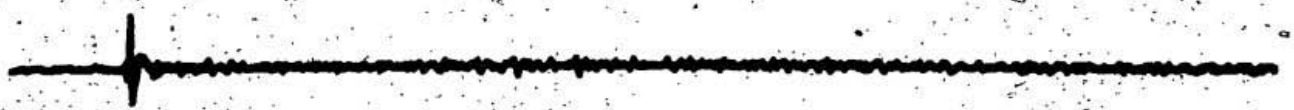

UNSCALED BOTTOM ECHO

Figure 19a Typical Bottom Return and NCE for Emerald Silt

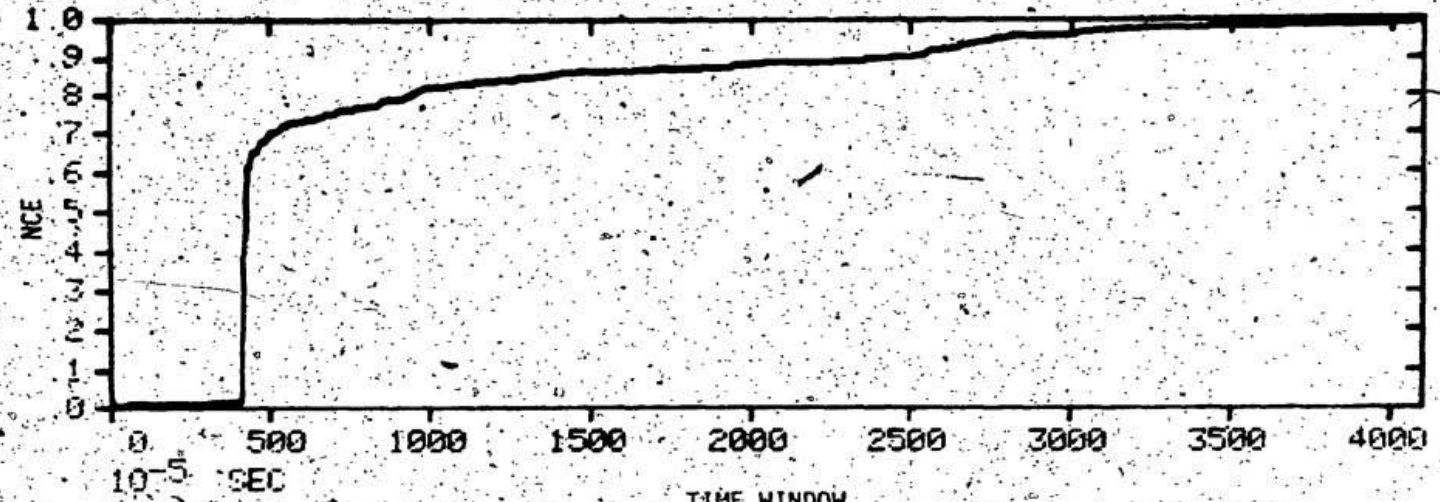

UNSCALED BOTTOM ECHO

Figure 19b Typical Bottom Return and NCE for Sambro Sand

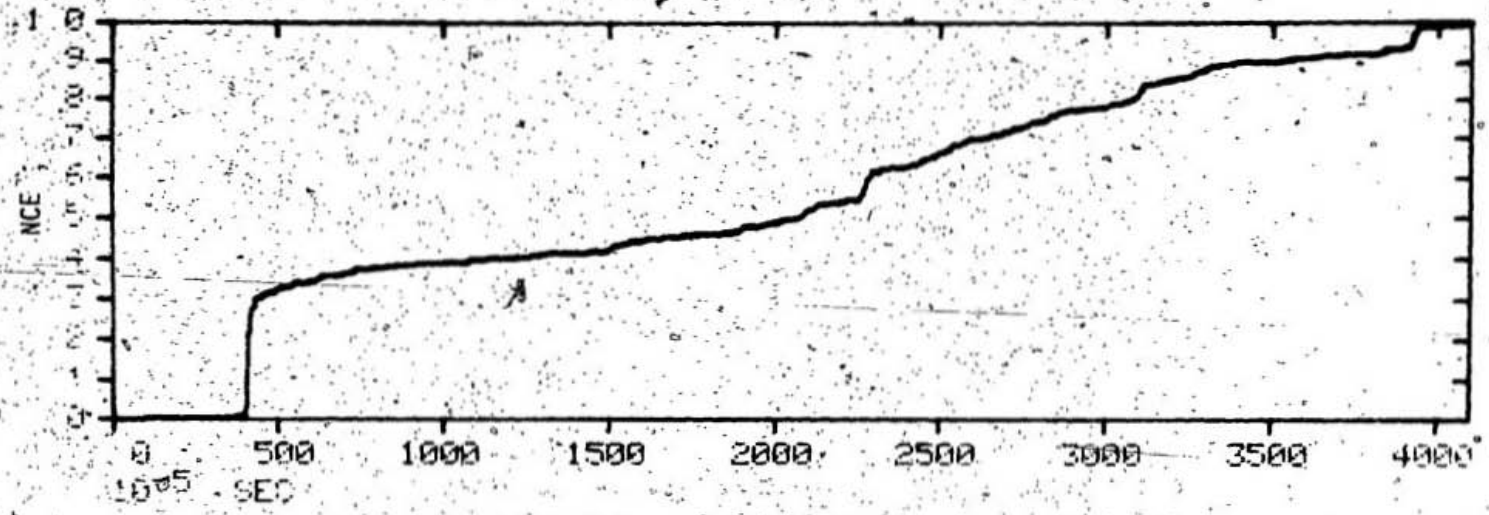

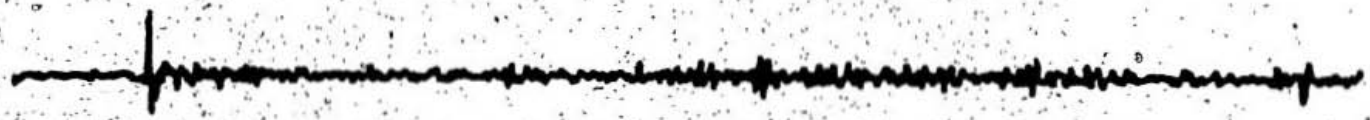

UNSCALED BOTTOM ECHO

Figure 19c Typical Bottom Return and NCE for La Have Clay

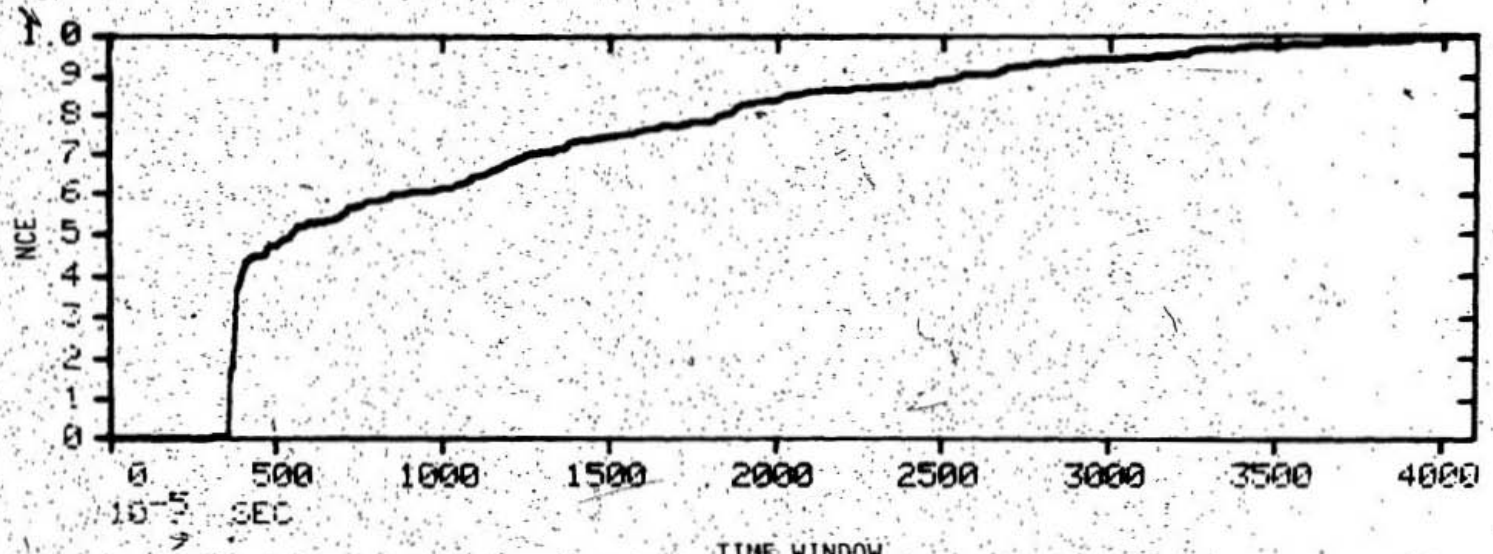

Figure 19d Typical Bottom Return and NCE for Scotia Shelf Drift

the water column and the sediment and since a large amount of energy is returned from a second sediment interface with the first, the effects of the energy returned from the second sediment should be eliminated. This is done by reducing the size of the observation window.

For the sediments named Emerald Silt, Sambro Sand and Scotia Shelf Drift, the window size for evaluation of the energy contained in the first return is 40.96 milliseconds, or a maximum sediment depth at water equivalent sound velocity of about 30 meters. For La Have Clay, the window size is reduced to 10.24 milliseconds, or a maximum depth of clay of about 7.5 meters. This reduction in window size is sufficient to eliminate reflections from the underlying Emerald Silt in the available data. However the window size should be adjusted for other data, if the depth of the La Have Clay in a basin increases or decreases appreciably. This problem is discussed in more detail in Appendix 3.

Since coherent reflections yield essentially a replica echo of the transmitted pulse, then by determining NCE over a time window Δt equal to the length of the transmitted pulse, an estimate of the amount of coherent energy in the initial reflected portion of the echo is obtained. This value of the NCE function is designated by $E\Delta$. $E\Delta$ only approximates the coherent energy in the first return since the portion of the echo within Δt also contains some incoherent energy (reverberent noise) to an amount which is difficult to estimate without using replica filters. A similar problem is discussed for sea surface coherence measurements by Wijmans (1973).

By using the Fourier Analyzer to perform the squaring, integrating,

normalizing, $E\Delta$ can be calculated by alignment of the NCE function to the 10% level of the total energy in the window. $E\Delta$ is found on the NCE function at displacement Δt = 0.32 msec. from the 10% alignment point.

For rough ocean bottoms, low values of $E\Delta$ would be expected. For smooth bottoms, $E\Delta$ can be either large or small dependent on whether the particular sedimentary layer is homogeneous or highly stratified. Individual values of $E\Delta$ were determined along for the four sediment types under investigation over a total track of 5.2 kilometers. The effects of signal to noise ratio on $E\Delta$ are discussed in Appendix 4.

An example of the $\bar{E}\Delta$ functions for the four sediments being discussed is seen in Figures 20a, b, c and d, while Figures 21a, b, c and d shows the standard deviation of $E\Delta$ as a function of track length. As with the case of the estimates of $\bar{\rho}_{i,\ i+1}$, the running average and standard deviation of $E\Delta$ over 50 successive ping pairs was evaluated.

It is seen in Figures 20b and c that the sediments termed Sambro Sand-Gravel and La Have Clay are difficult to separate on the basis of $\bar{E}\Delta$ alone. The values of $\bar{E}\Delta$ for Emerald Silt in Figure 20a takes an intermediate position above that for Glacial Till, in Figure 20d which has the lowest proportion of energy of the four in the Δt window. The sand and clay are relatively homogeneous sediments with smooth surface profiles, and are expected to show a high value for $\bar{E}\Delta$. However, as shown in Chapter 4 they can be separated on the basis of their coherence coefficient. The silt is usually a highly stratified soft sediment. Hence the $\bar{E}\Delta$ values are lower because of contributions from the layering. For silt, however, the coherence coefficient, $\bar{\rho}_{i,\ i+1}$, is high

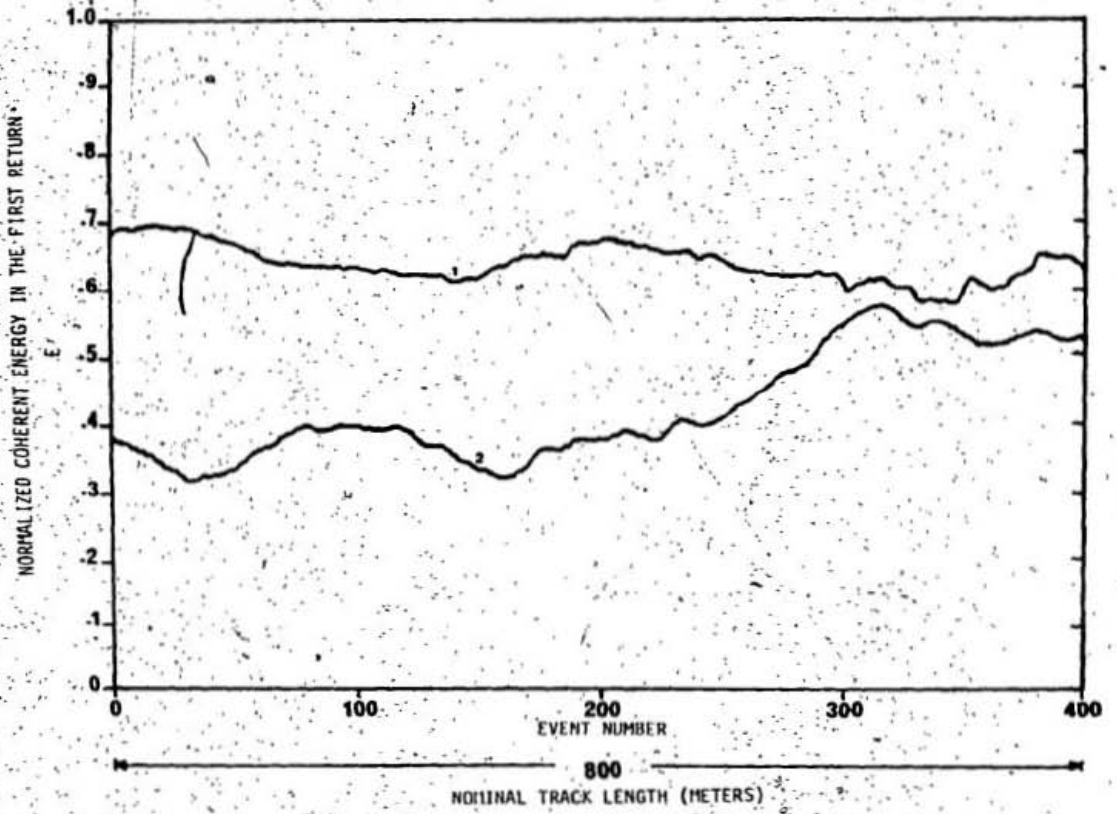

Figure 20a E' Track Length - Emerald Silt

1. Longitude 42°47' Latitude 67°05'
2. Longitude 42°39' Latitude 67°08'

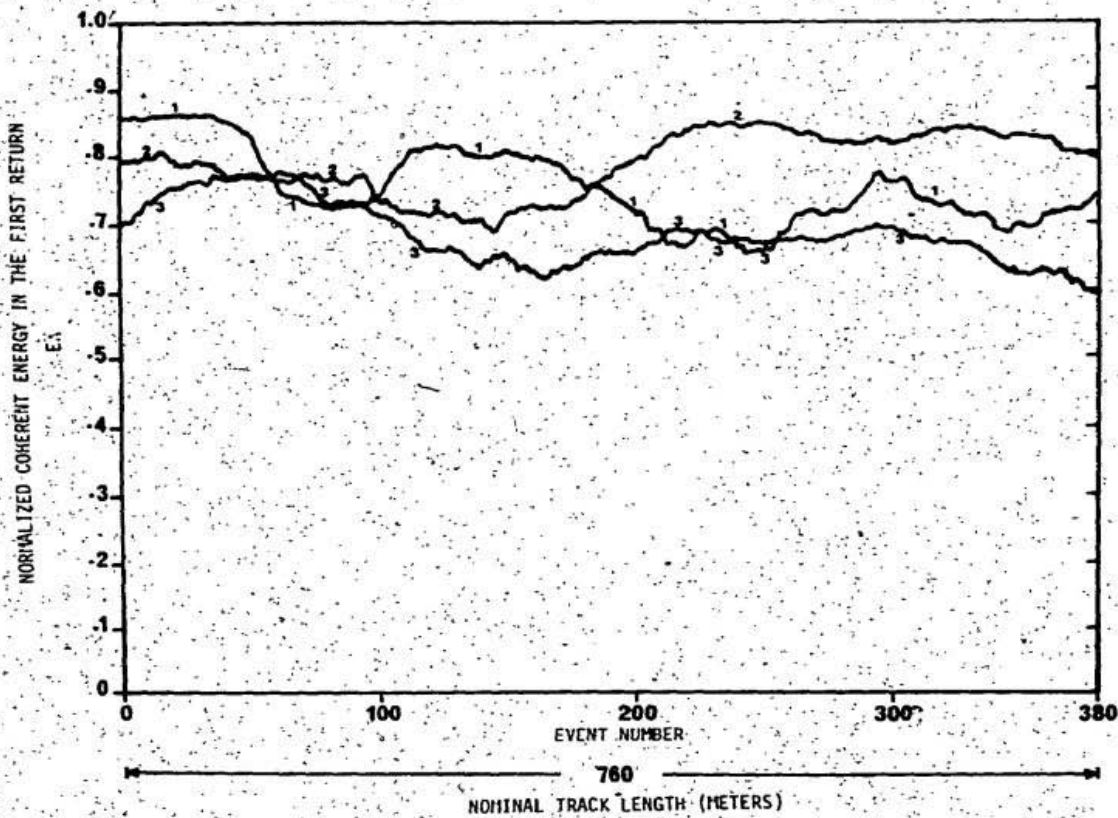

Figure 20b E_Δ Track Length - Sambro Sand

1. Longitude 43°28' Latitude 66°48'
2. Longitude 43°28' Latitude 66°48'
3. Longitude 43°29' Latitude 66°43'

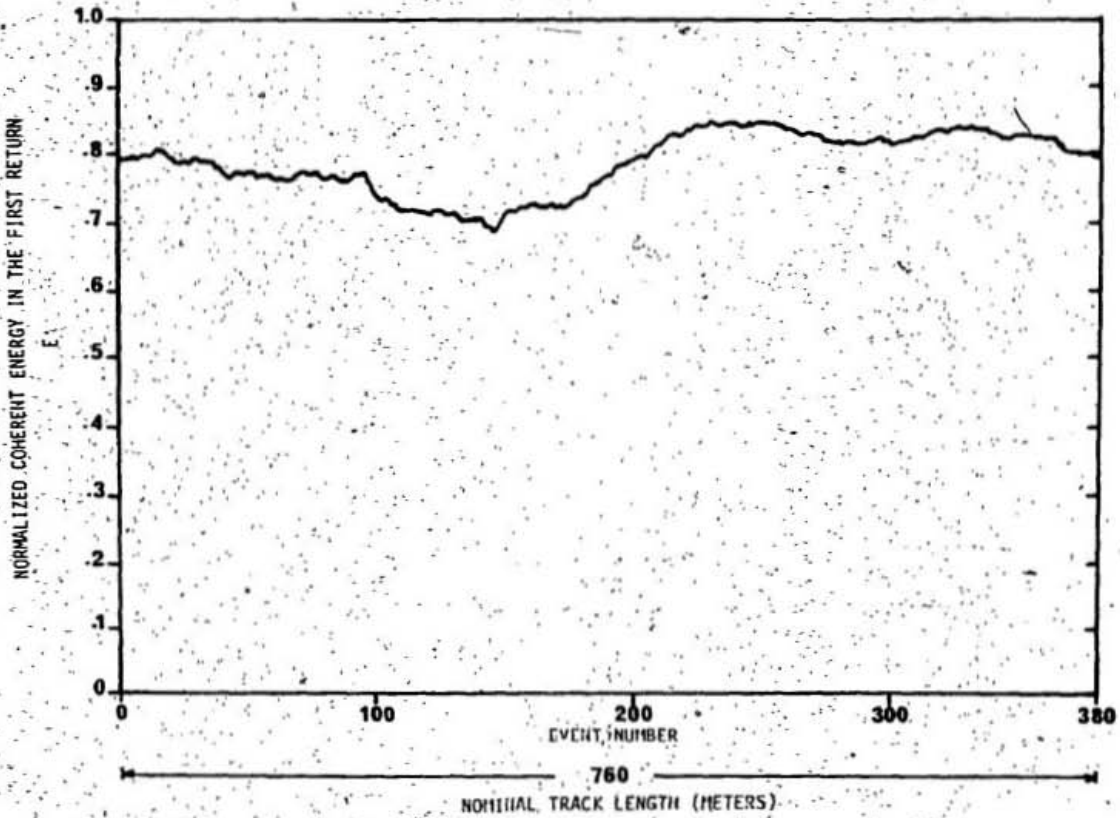

Figure 20c E1 Track Length - La Have Clay

Longitude 43°28' Latitude 64°18'

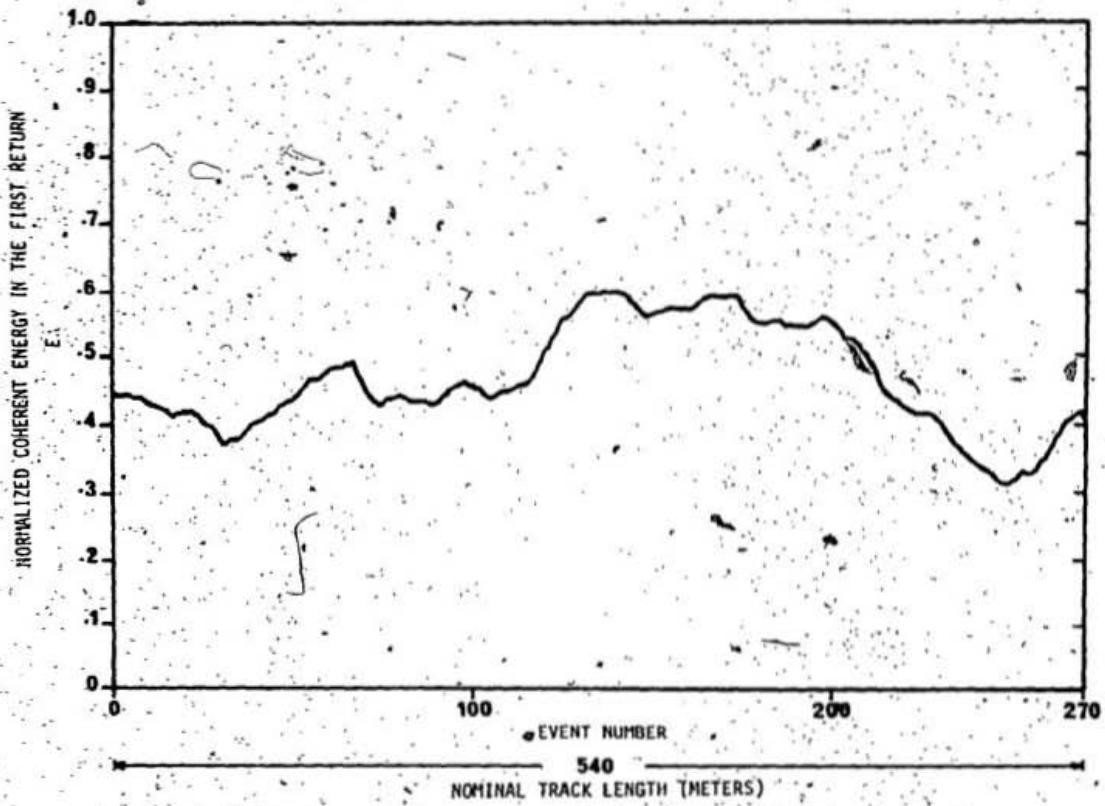

Figure 20d E_0 Track Length - Scotia Shelf Drift
Longitude 42°45' Latitude 67°05'

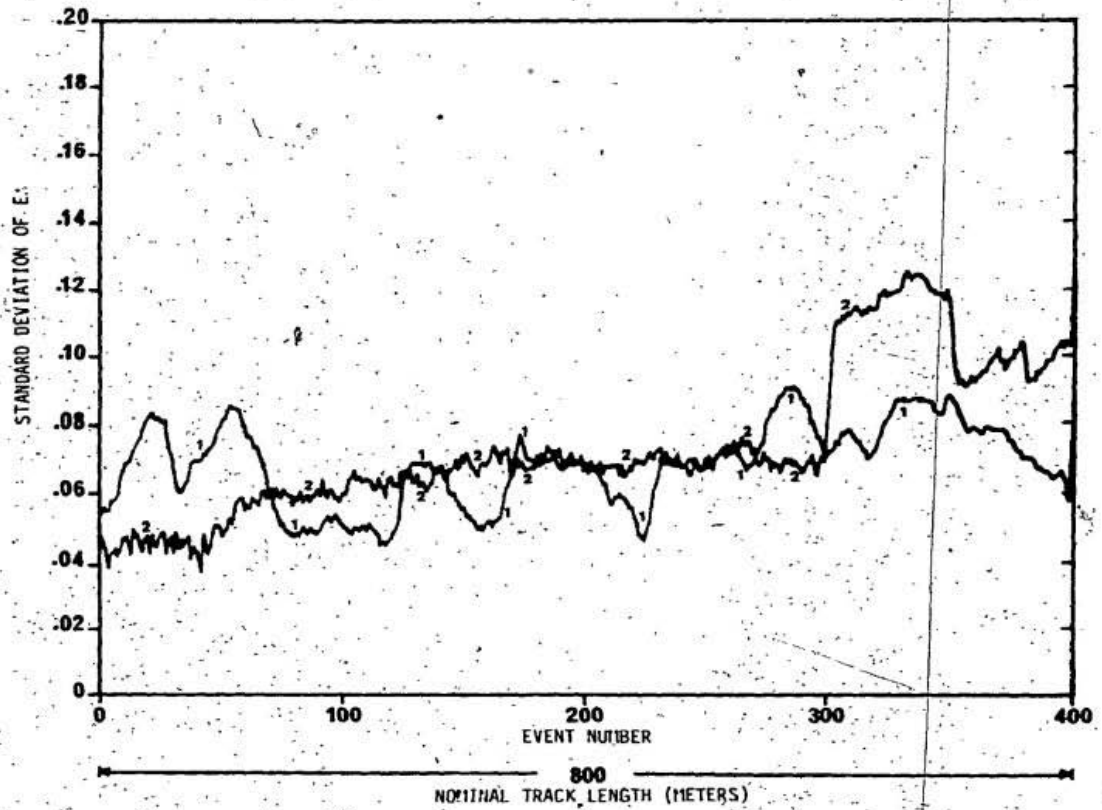

Figure 21a. Standard Deviation of Eᵢ vs Track Length - Emerald Silt

1. Longitude 42°47' Latitude 67°05'
2. Longitude 42°39' Latitude 67°08'

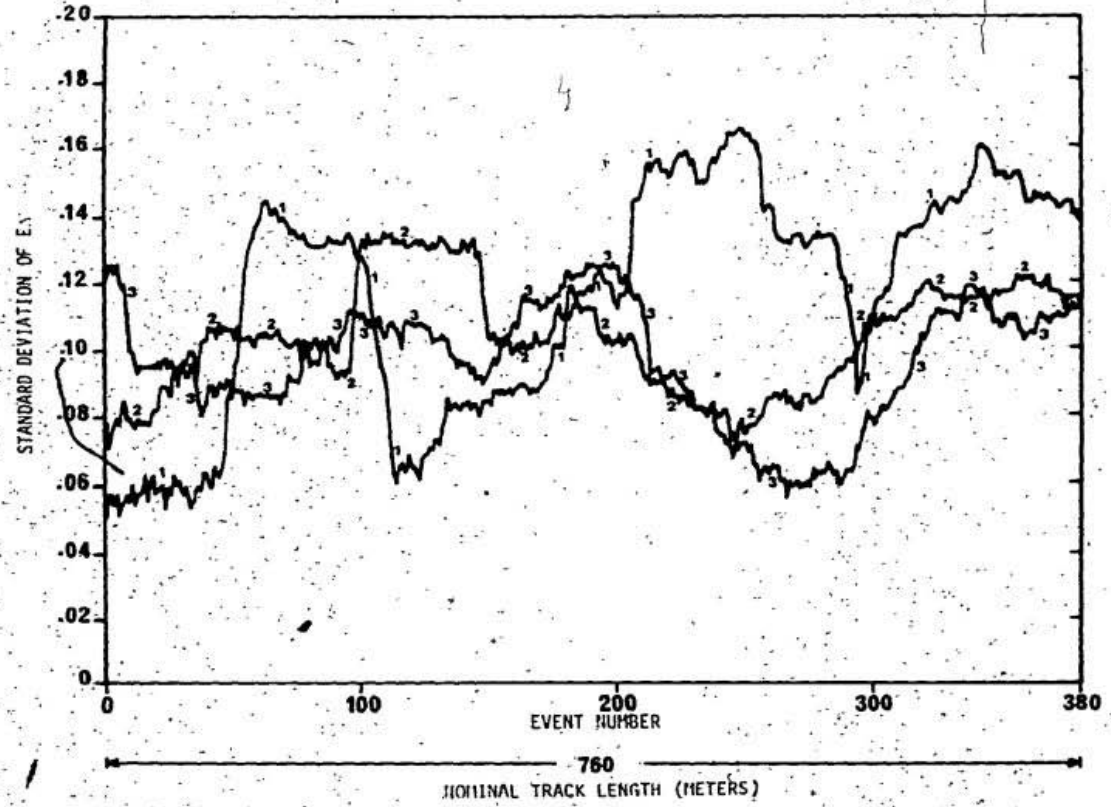

Figure 21b Standard Deviation of Eᐃ vs Track Length - Sambro Sand

1. Longitude 43°28' Latitude 66°48'
2. Longitude 43°28' Latitude 66°48'
3. Longitude 43°29' Latitude 66°43'

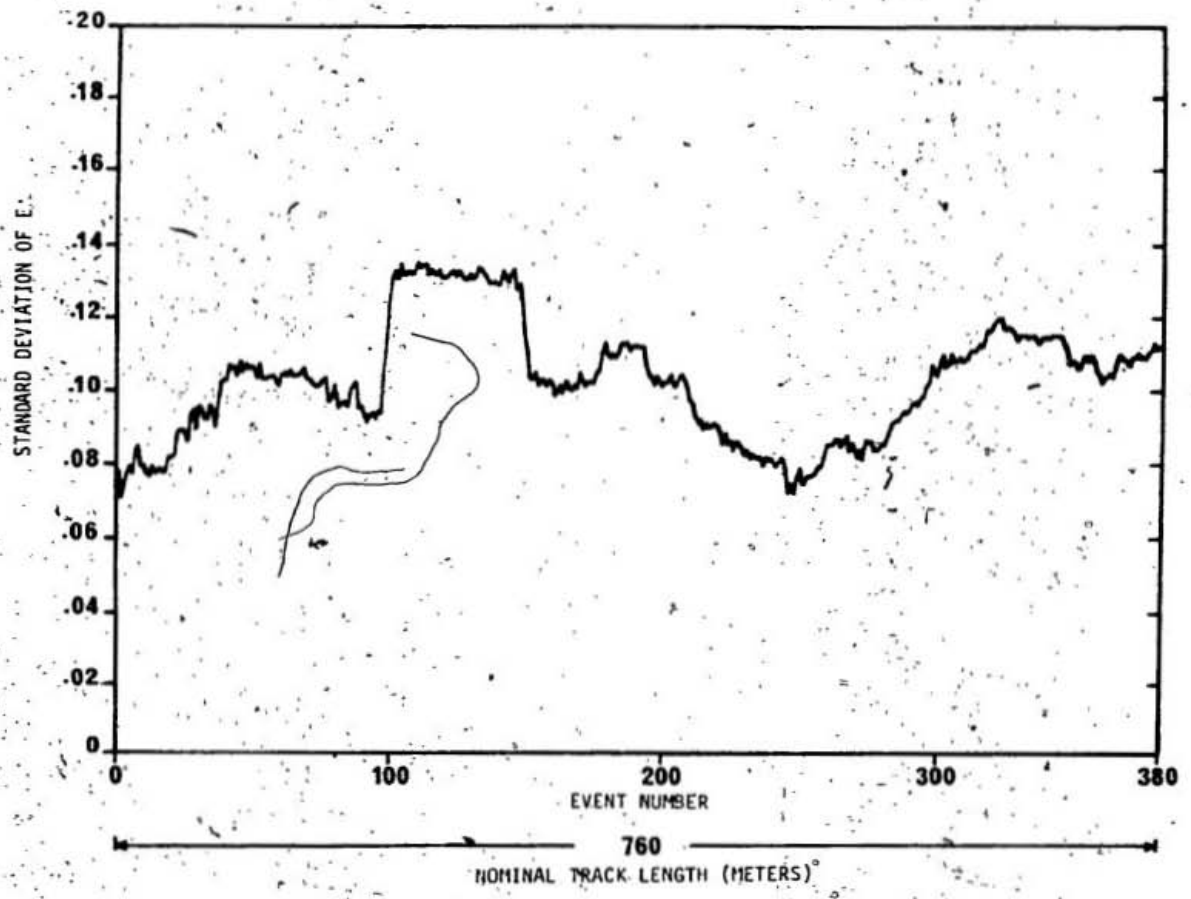

Figure 21c Standard Deviation of E: vs Track Length - La Have Clay

Longitude 43°28' Latitude 64°18'

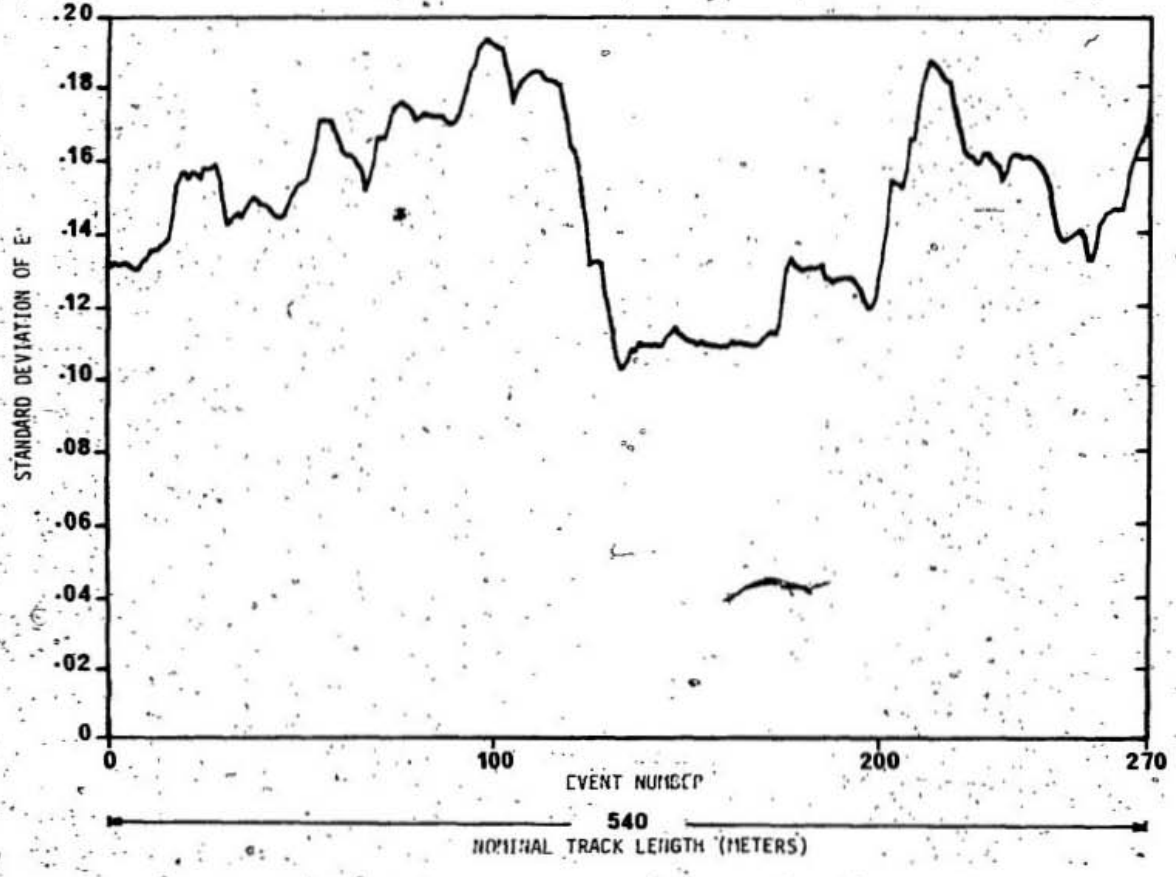

Figure 21d Standard Deviation of E: vs Track Length - Scotia Shelf Drift

Longitude 42°45' Latitude 67°05'

because the stratification in the sediment is coherent over the distance traversed between acoustic sample. Till, which is characteristically rough, contains many scattering sources, and the echo returns show high reverberation levels. The values of $\bar{E\Delta}$ and $\bar{\rho}_{i,\,i+1}$ for till are both low and highly variable.

A similar decision process may be carried out for the measurements of $\bar{E\Delta}$ as was performed for the measurements of $\bar{\rho}_{i,\,i+1}$ in Chapter 4. By selecting $E\Delta_T$ thresholds, it is possible to optimize the separation of sediment types with this metric. The thresholds chosen for this data are:

1. La Have Clay, $0.8 < E\Delta_T < 1.0$
2. Sambro Sand, Gravel, $0.7 < E\Delta_T < 0.8$
3. Emerald Silt, $0.5 < E\Delta_T < 0.7$
4. Scotia Shelf Drift, $0.3 < E\Delta_T < 0.5$

where $E\Delta_T$ is the threshold for normalized energy in the first return.

A scatter matrix for all the data analyzed for each sediment type is shown in Table 2. This table compares the sediment falling within the threshold range to the classification base given in Section 2.5. Using this base as a reference, the percentage of correct classification based solely on the running average of the $\bar{E\Delta}$ measurement is 56%.

As with the case of the cross-correlation measurement, an observation of the standard deviation of $E\Delta$ shown in Figures 21a, b, c and d is made. A comparison of the plot of the running mean of $E\Delta$ with the plot of the standard deviation for any of the four sediments described indicates that the standard deviation tends to increase as the mean

value decreases. This observation was made in Chapter 4 for the measurement of $\bar{\rho}_{i,\ i+1}$, and since the measure of $\bar{E}_{\Delta}$ is another measure of coherent energy, the same argument and explanation apply in this case. If de-correlation effects of the measurement system are eliminated, the departures of the standard deviation plot of E_{Δ} indicate, to some degree, the inconsistancy of the sediment being investigated.

Table 2 Normalized Coherent Energy Coefficient Scatter Matrix

Classification Thresholds, $E\Delta_T$, are at the following levels:

1. La Have Clay, $0.8 < E\Delta_T < 1.0$
2. Sambro Sand, Gravel, $0.7 < E\Delta_T < 0.8$
3. Emerald Silt, $0.5 < E\Delta_T < 0.7$
4. Scotia Shelf Drift, $0.3 < E\Delta_T < 0.5$

Values shown are percentages.

Coherent Energy Coefficient Classification	Reference Base (Drapeau and King and Fader et al)			
	La Have Clay	Sambro Sand	Emerald Silt	Scotia Shelf Drift
La Have Clay	46	21	--	--
Sambro Sand	53	49	--	--
Emerald Silt	1	30	64	33
Scotia Shelf Drift	--	--	36	67
Number of Events	380	1,140	800	270
Track Length (km)	0.8	2.3	1.6	0.5

CHAPTER 6

RESULTS OF COMBINED OBSERVATION OF $\rho_{i,\,i+1}$ AND $E\Delta$

6.1 Introduction

It has been shown in Chapters 4 and 5 that by considering the system as a time varying filter, measurements of coherent acoustic energy can be used individually to differentiate, to a degree, some sedimentary ocean bottom structures. Specifically, the measure of $\bar{\rho}_{i,\,i+1}$, the mean value of normalized cross-correlation coefficient between adjacent acoustic samples, and of $\bar{E}\Delta$, the mean value of normalized energy contained in the first return, appear to provide complementary information. This observation is the result of comparing Figures 17a, b, c and d, the plots of $\bar{\rho}_{i,\,i+1}$ vs track length for each sediment type with Figures 20a, b, c and d, the plots of $\bar{E}\Delta$ vs track length for each sediment type.

By combining both measures of relative coherent energy received, the apparent complementary nature of each may be used to advantage. This combination procedure can be considered the part of a pattern recognition process. A pattern is made up of features of a number of measureable aspects of an object. The values of the measurements are considered as components of a vector. If n-observations are made, the pattern becomes an n-dimensional vector and can be located as a point in an n-dimensional space. The objective of pattern recognition is to place an observed pattern vector into a class of objects with the greatest probability that the correct class is chosen. Implicit in this procedure is a "learning" stage. A "learning" set of pattern vectors is a number which have been measured under known class conditions.

Applying this to the problem of sediment classification, a simple two dimensional pattern vector can be found, consisting of the measurements of $\bar{\rho}_{i,\,i+1}$ and $\bar{E}\Delta$. These measurements were taken from data obtained over known sedimentary areas. They, therefore, can be considered a set of "learning" pattern vectors.

6.2 Combined Observation of $\bar{\rho}_{i,\,i+1}$ and $\bar{E}\Delta$

A most convenient method of displaying two time or space dependent variables such that the effects of both variables are immediately obvious is through the use of the scatter diagram. This method permits the isolation of regions in the scatter space that may be assigned to a particular set of process dependent variables. An individual process itself then may be identified with a region in the space.

For the case of sediment classification, the two variables developed in this thesis are the mean values of $\rho_{i,\,i+1}$ and $E\Delta$ which have been defined in Chapters 4 and 5. The differences among rough, smooth finely layered, and smooth homogeneous sediments can be established by examining cojointly the coherence coefficient and $E\Delta$. For the rough sediments, both $\bar{\rho}_{i,\,i+1}$ and $E\Delta$ are low. For smooth finely layered sediments $\bar{\rho}_{i,\,i+1}$ is high while $E\Delta$ is low. For the smooth homogeneous sediments both $\bar{\rho}_{i,\,i+1}$ and $E\Delta$ are high.

A scatter diagram using these variables is shown in Figure 22. In this diagram, the $\bar{\rho}_{i,\,i+1}$ is plotted against $E\Delta$. The data analysis described in Chapter 5 for each sediment type was performed

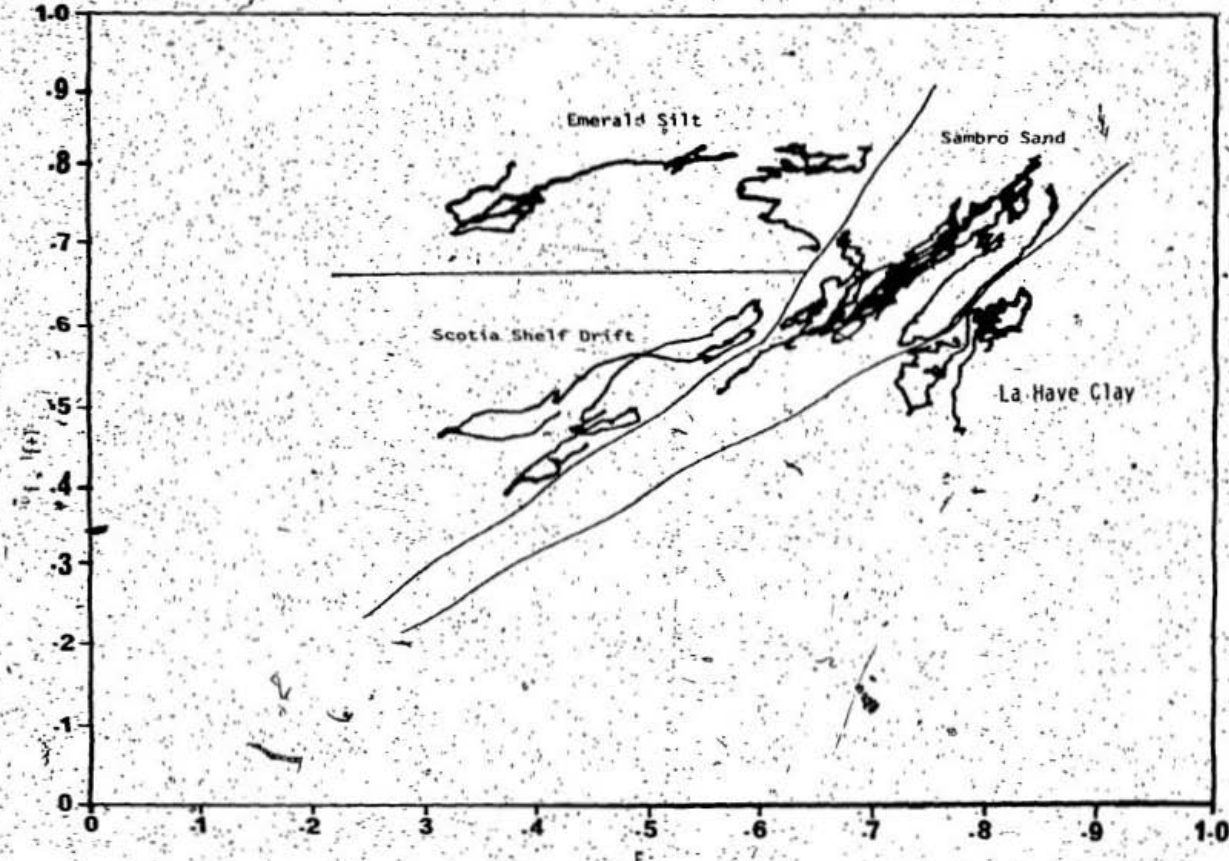

Figure 22: Scatter Diagram, E_i vs $\tau_{i, i+1}$

over a different track length than that in Chapter 4. The scatter diagram described above includes all sediment types for which coincident measurements of $\rho_{i,\,i+1}$ and $E\Delta$ were made. Regions in the plane are identified with the four sediment types considered in this study.

It is seen from Figure 22 that the regions assigned to each sediment type are separated without overlap. This observation, then, indicates that for the acoustic data available, the combined measurement of $\bar{\rho}_{i,\,i+1}$ and $\bar{E}\Delta$ is a reliable method of placing a sediment into one of four possible categories, i.e. Emerald Silt, Sambro Sand, La Have Clay or Scotia Shelf Drift.

CHAPTER 7

CONCLUSIONS AND FURTHER WORK

Using a model based on the relative roughness of marine sediments, it has been postulated that the fraction of coherent energy in an acoustic return from a sediment is indicative of the type of sediment being insonified. Two complementary measures of the coherent component in a return have been developed and implemented on a computer based time series analysis system. These are the measure of the average normalized cross-correlation coefficient between successive acoustic events, $\bar{\rho}_{i,\,i+1}$ and the measure of the average normalized energy contained in the return from the water-sediment interface, $E\Delta$. By setting appropriate thresholds, a sediment can be placed in one of the four categories outlined in Section 2.5, the sediment descriptions, by observing the value of $\bar{\rho}_{i,\,i+1}$. Evaluation of $E\Delta$ for the four sediment types results in a conflict in distinguishing sand from clay; however by setting thresholds on the $E\Delta$ measurement, some degree of success is obtained in placing a sediment into one of the four test categories.

The measurement of $E\Delta$ complements the measurement of $\bar{\rho}_{i,\,i+1}$. When $E\Delta$ is plotted against $\bar{\rho}_{i,\,i+1}$ for all sediment types investigated, the resulting scatter diagram shows regions in the plane that can be associated with sediment type. For the limited data base used, there is a high degree of isolation between these regions in the plane, indicating a confidence in the combined measurement of normalized cross-correlation coefficient, $\bar{\rho}_{i,\,i+1}$ and of

normalized energy in the first return, E_Δ. The combined metric appears very well suited as a method of classifying sediments.

In this thesis, no use has been made of the measurements of standard deviations of $\rho_{i,\ i+1}$ and E_Δ, even though the measurements contains significant information. It is suggested that further work in sediment classification at this university include a study in the further use of pattern recognition techniques. Variables which could be included in the space as pattern vectors include the four variables defined in this thesis; that is the mean and standard deviation of the normalized event-to-event cross-correlation coefficient, and the mean and standard deviation of the normalized energy in the first return. Other measurement variables thought suitable, but not included in this thesis are the mean and standard deviation of the Rayleigh reflection coefficient and measurements of the time of arrival of the acoustic pulse at the water-sediment interface. The calculation of the reflection coefficient is a simple matter, once the amplitudes of the transmitted and received signals are known, and the effects of spherical spreading of acoustic energy in the water column are taken into account.

The measurement of the time of arrival of the acoustic pulse at the bottom, relative to the height of the transducer above the bottom yields a profile of bottom topography. This information should prove useful in a pattern recognition approach, as suggested in Simpkin et al, 1976.

One other avenue of investigation that has not been addressed

in this thesis involves better use of the broad bandwidth of the acoustic source. The frequency domain coherence function, as defined in Bendat and Piersol (1971), shows the proportion of mean square value of a signal at the output of a process that is contributed by the input signal, as a function of frequency. The coherence function then should reflect any frequency dependence that exists in a sediment in the sound source bandwidth.

There is a need for more acoustic data, both from well sorted, homogeneous sedimentary bottoms and from poorly sorted, mixed sedimentary areas. There are more than four classes available in which to place sediments. These have not been investigated, since data was not available at the time of this work.

Finally, the methods and conclusions discussed in this thesis should not be blindly accepted as a procedure for sediment classification. However, the methods are based on classical signal processing techniques, and within the assumptions stated in the model, produce very acceptable results for the four classes used. It is suggested that the approach described should prove fruitful in a broader sphere of investigation, one in which all sediment types are included. Such an investigation would benefit from a combined approach with the use of broadband acoustics, piston corers and cone penetrometers to correlate and more clearly define the variables which determine the engineering properties of ocean bottom sediments.

BIBLIOGRAPHY AND LIST OF REFERENCES

Akal, T., The Relationship Between the Physical Properties of Underwater Sediments that Affect Bottom Reflection, Marine Geology, 13, p 251-266, 1972.

_____ Acoustical Characteristics of the Sea Floor: Experimental Techniques and Some Examples from the Mediterranean Sea, in Hampton, ed., Physics of Sound in Marine Sediments, p. 447-480, Plenum Publishing Corp., New York, N.Y., 1974.

Anderson, R.S., Statistical Correlation of Physical Properties and Sound Velocity in Sediments in Hampton, ed., Physics of Sound in Marine Sediments, p. 481-518, Plenum Publishing Corp., New York, N.Y., 1974.

Baggeroer, A.B., Knott, S.T., Koskins, H., Bunce, E.T., Digital Signal Processing of Oceanic Seismic Profiler Data, 1977, Reflectivity and Sediment Classification, Report No. WHOI-73-38, Woods Hole Oceanographic Institute, Woods Hole, Mass., 1973.

Bell, D.L., Porter, W.J. and Westneat, A.S., Progress in the use of Acoustics to Classify Marine Sediments, Ocean '73, Proc. Int. Conf. on Engineering in the Ocean Environment, held at Seattle, Washington, p. 354-359, 1973.

Bell, D.L. and Porter, W.J., Remote Sediment Classification Potential of Reflected Acoustic Signals in Hampton, ed. Physics of Sound in Marine Sediments, p 319-335, Plenum Publishing Corp., New York, N.Y., 1974.

Bendat, J.S. and Piersol, A.G., Random Data: Analysis and Measurement Procedures, Wiley-Interscience, New York, N.Y., 1971.

Breslau, L., Classification of Sea Floor Sediments with a Shipborne Acoustical System, Le Petrole et La Mer, Sect. 1, No. 132, 1964.

_____ The Normally-Incident Reflectivity of the Sea Floor at 12 Kc and Its Correlation with the Physical and Geological Properties of Naturally Occurring Sediments, Woods Hole Oceanographic Institution Reference 67-16, 1967.

Clay, C.S., Scattering and Reflection of Acoustic Waves at the Bottom and Surface of the Ocean, Final Report No. 74-1, University of Wisconsin, Geophysical and Polar Research Center, Department of Geology and Geophysics, Madison, Wisconsin, August, 1974, 49 pp.

Clay, C.S. and Leong, W.K., Acoustic Estimates of the Topography and Roughness Spectrum of the Sea Floor Southwest of Iberian Peninsula, in Hampton, ed., Physics of Sound in Marine Sediments, p. 373-446, Plenum Publishing Corp., New York, N.Y., 1974.

Caruthers, J.W., (ed.), Lectures on Marine Acoustics, Vol. 1 and 2, Sea Grant Publication, Texas A and M University, College Station, Texas, 1973.

Drapeau, G. and King, L.H., Surficial Geology of the Yarmouth-Browns Bank Map Area, joint publication of Marine Sciences Directorate, Dept. of the Environment and Dept. of Energy, Mines and Resources, Ottawa, Canada, 1972.

Faas, R.W., Analysis of the Relationship Between Acoustic Reflectivity and Sediment Porosity, Geophysics, Vol. 34, No. 4, p. 546-553, 1969.

Fader, G.B., King, L.H. and MacLean, B., Surficial Geology of the Eastern Gulf of Maine and the Bay of Fundy, a joint publication of the Canadian Hydrographic Service, Dept. of Fisheries and the Environment and the Geological Survey of Canada, Dept. of Energy, Mines and Resources, Ottawa, Canada, 1977.

Fortuin, L., The Sea Surface as a Random Filter for Underwater Sound Waves, Ph.D. Thesis, Uitgeverij Waltman, Delft, 1973.

Hamilton, E.L., Sound Velocity and Related Properties of Marine Sediments, North Pacific, J. Geophys. Res., 75, p 4423-4446, 1970a.

_____ Reflection Coefficients and Bottom Losses at Normal Incidence Computed from Pacific Sediment Properties, Geophysics, Vol. 35, p 995-1004, 1970b.

_____ Elastic Properties of Marine Sediments, J. Geophys. Res., Vol. 76, p 579-604, 1971a.

_____ Prediction of in situ Acoustic and Elastic Properties of Marine Sediments, Geophysics, Vol. 36, p 266-284, 1971b.

_____ Prediction of Deep Sea Sediment Properties: State of the Art, in Inderbitzen, ed., Deep Sea Sediments, Physical and Mechanical Properties, p 1-44, Plenum Publishing Corp, New York, N.Y., 1974a.

_____ Geoacoustic Models of the Sea Floor in Hampton, ed., Physics of Sound in Marine Sediments, p 181-221, Plenum Publishing Corp, New York, N.Y., 1974b.

———, Acoustic Properties of the Sea Floor: A Review, in Oceanic Acoustic Modeling, proceedings of a conference, part 4, 96 pp., Saclant ASW Research Centre, La Spezia, Italy, 1975.

Hampton, L., (ed.) Physics of Sound in Marine Sediments, Plenum Publishing Corp., New York, N.Y., 1974.

Hurdle, B.G., Flowers, K.D. and De Santo, J.A., Acoustic Scattering from Rough Surfaces, in Oceanic Acoustic Modeling, proceedings of a conference, part 4, 28 pp., Saclant ASW Research Centre, La Spezia, Italy, 1975.

Hutchins, R.W., Computer Simulation of a Transiently Excited Underwater Sound Projects, Ocean '74, Proc. Int. Conf. on Engineering in the Ocean Environment, Vol. 2, p 115-119, Halifax, N.S., 1974.

Hutchins, R.W., McKeown, D.L. and King, L.H., A Deep Tow High Resolution Seismic System for Continental Shelf Mapping, Geoscience Canada, p 95-100, Vol. 3, No. 2, May, 1976.

Katekas, J., The Normal Incidence Acoustic Response for a Liquid Overlying a Viscoelastic Halfspace, UNH-Raytheon Sea Grant Project Report UNH-SG-117, University of New Hampshire, 1973.

Kinsler, L.E. and Frey, A.R., Fundamentals of Acoustics, John Wiley and Sons, Inc., New York, N.Y., 1962.

Laval, R., Sound Propagation Effects on Signal Processing, in Signal Processing with particular reference to Underwater Acoustics, Loughborough University, Loughborough, England, Academic Press, London, 1973.

Li, W.N. and Taylor-Smith, D., Identification of Sea Floor Sediments using Underwater Acoustics, Geophysical Prospecting, Vol. 17, p 231-247, 1969.

MacIsaac, R.R. and Dunsiger, A.D., Ocean Sediment Properties Using Acoustic Sensing, POAC '77, Proceedings of the Fourth International Conference on Port and Ocean Engineering Under Arctic Conditions, Memorial University of Newfoundland, St. John's, Newfoundland, Sept., 1977, in press.

Magnuson, A.H., Sound Propagation in a Semi-infinite Liquid Overlying a Homogeneous Viscoelastic Halfspace, Ocean '72, Proc. Int. Conf. on Engineering in the Ocean Environment, held at Newport, Rhode Island, p 530-536, 1972a.

———, Sound Propagation in a Liquid Layer Overlying a Multilayered Vicsoelastic Halfspace, Ocean '72, Proc. Int. Conf. on Engineering in the Ocean Environment, held in Newport, Rhode Island, p 537-543, 1972b.

_____ Sound Propagation in a Liquid Overlying a Viscoelastic Halfspace, UNH - Raytheon Sea Grant Project Report UNH-SG-114, University of New Hampshire, 1973.

_____ Acoustic Response in a Liquid Overlying a Homogeneous Viscoelastic Halfspace, J. Acoustical Soc. Am., Vol. 57, No. 5, 1975.

McKeown, D.L., Evaluation of the Huntec ('70) Hydro Sonde Deep Tow Seismic System, Report Series BI-R-75-4, Bedford Institute of Oceanography, Dartmouth, N.S., 1975.

McKinney, C.M. and Anderson, C.D., Measurements of Backscattered Sound from the Ocean Bottom, J. Acoustical Soc. Am., Vol. 36, No. 1, 1964.

McLeroy, E.G., Measurement and Correlation of Acoustic Reflection and Sediment Properties off Panama City, Florida, Informal Report No. 112-72, Navel Coastal Systems Laboratory, Panama City, Florida, 1972.

Mitsikos, J.P., Use of Acoustic (Seismic) Waves for Deep Sea Bottom Layers Identification and Computation of their Physical and Engineering Properties, in Inderbitzen, ed., Deep Sea Sediments, Physical and Mechanical Properties, Plenum Publishing Corp., New York, N.Y., 1974.

Officer, C.B., Introduction to the Theory of Sound Transmission, McGraw-Hill Book Co. Inc., New York, N.Y., 1958.

Pace, N.G., Sediment Identification Using Acoustic Techniques, Bath University, Bath, U.K., 1974.

Papoulis, A., Probability Random Variables and Stochastic Processes, McGraw-Hill Book Company, New York, N.Y., 1965.

Porter, W.J. and Bell, D.L., Development of Quantitative Remote Acoustic Indices for Location and Mapping of Sea Floor Spoil Deposits, Paper 2288, Offshore Technology Conference, Houston, Texas, 1975.

Rayleigh, Lord J.W.S., Theory of Sound, Vol. 1 & 2, Dover Publications, Inc., New York, N.Y., 1945.

Simpkin, P.G., Geophysical Investigation of Marine Sediments Under In Situ Conditions, Ph.D. Thesis, University College of North Wales, 1975, unpublished.

Simpkin, P.G., Parrott, D.R., Hutchins, R. and Ross, D.I., Seabed '75 - Objectives and Achievements, Report Series BI-T-76-15, Bedford Institute of Oceanography, Dartmouth, N.S., 1976.

Shirley, D.L. and Anderson, A.L., Acoustic and Engineering Properties of Sediments, Report No. ARL-TR-75-58, Applied Research Laboratories, University of Texas at Austin, 1975.

Smith, D.T. and Li W.N., Echo Sounding and Sea Floor Sediments, Marine Geology 4, p 353-364, 1966.

Tolstoy, I. and Clay C.S., Ocean Acoustics: Theory and Experimentation Underwater Sound, McGraw-Hill, Inc., New York, N.Y., 1966.

Tucker, D.G. and Gazey, B.K., Applied Underwater Acoustics, Pergamon Press, Oxford, U.K., 1966.

Tyce, R.C., Real Time Processing and Display of Near Bottom Acoustic Reflectivity Measurements, Ocean '75, Proc. Int. Conf. on Engineering in the Ocean Environment, held at San Diego, California, p 30-34, 1975.

Urick, R.J., Principles of Underwater Sound, McGraw-Hill Co. Inc., New York, N.Y., 1975.

Wijmans, W., An Experimental Study of Forward Scattering and Reflection of Underwater Sound Waves from the Rough Sea Surface, SACLANTCEN Memorandum SM-26, Saclant ASW Research Centre, La Spezia, Italy, 1973.

Westneat, A.S. and Porter, W.C., Computation of Compressional Wave Velocity in Unconsolidated Sea Floor Sediments using Scaled Seismic Approaches, Ocean '75, Proc. Int. Conf. on Engineering in the Ocean Environment, held at San Diego, California, p 603-606, 1975.

Zhitkovskii, Y.Y., Measurement of the Acoustic Scattering Coefficient of the Ocean Bottom by means of a Short Pulse, Soviet Physics Acoustics, Vol. 12, No. 3, 1967.

Zhitkovskii, Y.Y. and Lysanov, Y.P., Reflection and Scattering of Sound from the Ocean Bottom, Soviet Physics-Acoustics, Vol. 13, No. 1, 1967.

APPENDIX 1

EFFECTS OF SNR ON THE NORMALIZED CROSS-CORRELATION COEFFICIENTS

The measurement of coherence and cumulative energy, is very much dependent on the signal to noise ratio (SNR). The returned signal, be it reflected, scattered, or a combination of the two, can be represented as:

$$x(t) = r(t) + n(t) \qquad 18.$$

where $x(t)$ is the received signal

$r(t)$ is the true signal without noise

$n(t)$ is the noise

The correlation of two adjacent returns with additive Gaussian noise can be represented by the integral:

$$R_{i,\,i+1}(\tau) = \frac{1}{T}\int_0^T [(r_i(t) + n_i(t))(r_{i+1}(t+\tau) + n_{i+1}(t+\tau))]dt \qquad 19.$$

which can be expanded into individual cross-correlation terms:

$$R_{i,\,i+1}(\tau) = R_{r_i,\,r_{i+1}}(\tau) + R_{n_i,\,n_{i+1}}(\tau) + R_{r_i,\,n_{i+1}}(\tau) + R_{n_i,\,r_{i+1}}(\tau) \qquad 20.$$

The first term in 20 is the desired cross-correlation of the adjacent returned acoustic signals. The second term is the cross-correlation of the noise accompanying the two acoustic signals. The noise has zero mean Gaussian statistics, therefore it is assumed to be uncor-

related, with a low numerical result for the calculation of $R_{n_i, n_{i+1}}$.

The third and fourth terms are the cross-correlations between one signal and the noise accompanying the other signal. The transmitted signal and the noise are assumed to be uncorrelated. The numerical values of these terms should also be low, but indeterminate.

APPENDIX 2

THE RELATIONSHIP BETWEEN $\rho_{i,\ i+1}$ AND E_Δ

The normalized cross-correlation coefficient was defined in Section 4.2 as:

$$\rho_{i,\ i+1} = \text{Max}\ \left[\frac{R_{i,\ i+1}(\tau)}{R_i(0)\ R_{i+1}(0)}\right] \qquad 21.$$

where $R_{i,\ i+1}(\tau) = \frac{1}{T}\int_0^T x_i(t)\ x_{i,\ i+1}(t-\tau)dt$

$$R_i(0) = \frac{1}{T}\int_0^T x_i^2(t)dt$$

$$R_{i+1}(0) = \frac{1}{T}\int_0^T x_{i+1}^2(t)dt$$

It is obvious that the three above terms are power terms; that is, they represent the average power in each case. The average power in a signal to its energy divided by the length of observation time:

$$P = \frac{E}{T}$$

The energy in a signal is simply defined as the integral of the squared signal amplitude over the observation period.

$$E = \int_0^T x^2(t)dt \qquad 22.$$

Then, $$P = \frac{1}{T}\int_0^T x^2(t)dt \qquad 23.$$

Then $R_i(0)$ is the average power contained in the signal x_i

$R_{i+1}(0)$ is the average power contained in the signal x_{i+1}

Max $R_{i,\,i+1}(\tau)$ is the average cross-power that is contained in portions of signal x_i that are coherent with signal x_{i+1}.

It can be said then that the normalized correlation coefficient can be defined as the average cross-power contained in coherent portions of two signals divided by the product of the average powers in each signal.

The value of $E\Delta$ represents the normalized energy contained in the coherent part of a signal.

$$E\Delta = \frac{\int_0^t x_i^2(t)dt}{\int_0^T x_i^2(t)dt} \qquad 24.$$

Numerator and denominator may be divided by the value T to obtain $E\Delta$ as a ratio of average powers.

$$E\Delta = \frac{\frac{1}{T}\int_0^t x_i^2(t)dt}{\frac{1}{T}\int_0^T x_i^2(t)dt} \qquad 25.$$

Then the value of $E\Delta$ may be defined as the average power contained in the first coherent return normalized by the average power returned in the complete echo series.

APPENDIX 3

THE EFFECTS OF SBR AND RECORD LENGTH OF EΔ

EΔ is the normalized ratio of the coherent energy in the echo received in a time window of fixed length to the total energy in that window. The total energy is the sum of the coherent energy and the noise and reverberant energy.

$$E\Delta = \frac{E_c}{E_T} = \frac{E_c}{E_c + E_n} \qquad 26.$$

where E_c is the coherent energy

E_n is the noise plus reverberation

EΔ may then be defined in terms of coherent power and noise power:

$$E\Delta = \frac{P_c \Delta t}{P_c \Delta t + P_n T} \qquad 27.$$

where P_c is the average coherent power in an echo pulse

Δt is the duration of the pulse

P_n is the average noise (and reverberant) power in the time window

T is the duration of the time window

$$\text{Then } E\Delta = \frac{(P_c/P_n)\Delta t}{(P_c/P_n)\Delta t + T} \qquad 28.$$

P_c/P_n is defined as signal to background ratio (SBR).

Then $E\Delta = \frac{SBR\Delta t}{SBR\Delta t + T} = \frac{SBR}{SBR + T/\Delta t}$ 29.

where $T/\Delta t$ is the ratio of window length to pulse length.

Figure 23 shows a plot of the variation of $E\Delta$ with SBR and the ratio $T/\Delta t$. It is evident that for a fixed pulse length and window length, a high signal to background is desirable. If the ratio of window length to pulse length is high, a higher SBR is required to maintain a fixed value of $E\Delta$ for a given sediment; if the $T/\Delta t$ ratio is lower, a lower SBR ratio in the received signals can be tolerated.

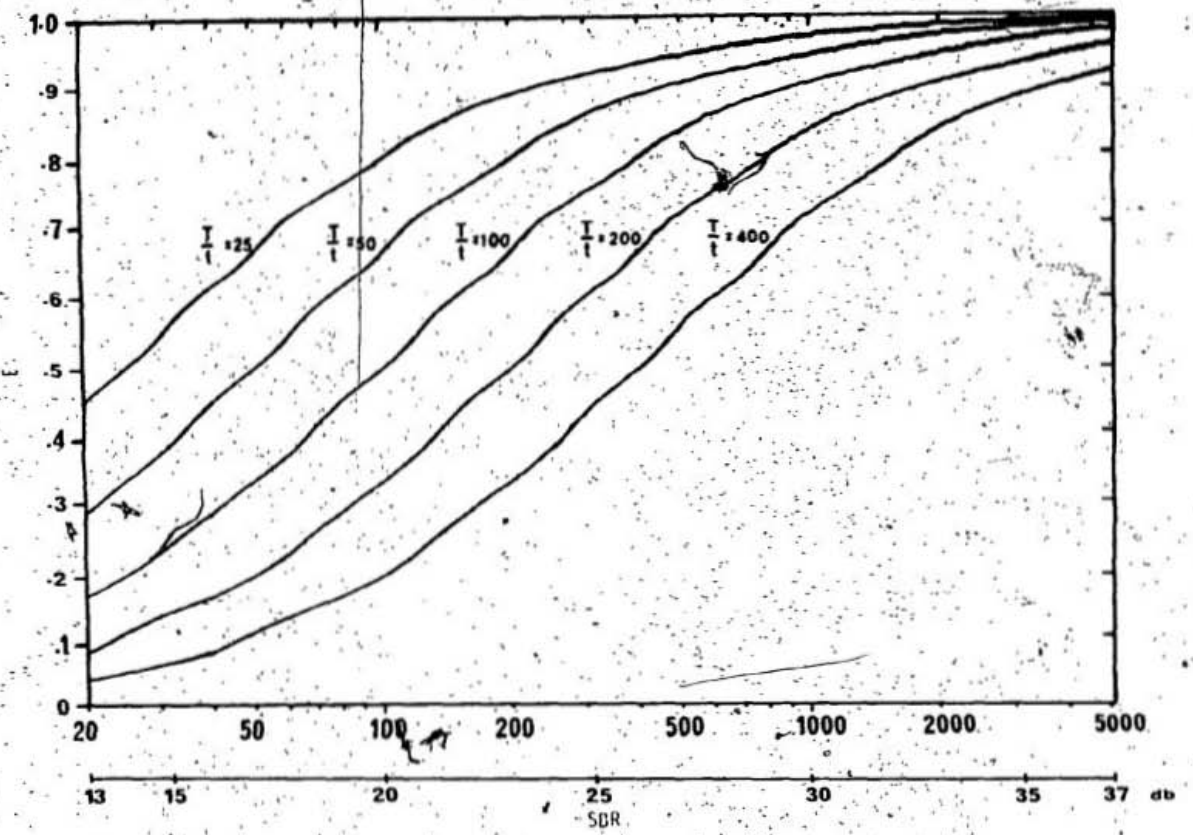

Figure 23. E_3 vs SBR as a Function of the Ratio of Pulse Length to Window Length, T/t

APPENDIX 4

THE EFFECTS OF SNR ON THE NCE FUNCTION

Since the received signals can be represented by the addition of a true signal term r(t) and a noise term n(t), the Cumulative Energy measurement obtained by squaring and integrating the return can be investigated in terms of r(t) and n(t) separately.

$$x_i(t) = r_i(t) + n_i(t) \qquad 30.$$

$$\frac{1}{E_T}\int_0^t x_i^2(t)dt = \frac{1}{E_T}\left[\int_0^t (r_i(t) + n_i(t))^2\, dt\right]$$

$$= \frac{1}{E_T}\left[\int_0^t r_i^2(t)dt + \int_0^t n_i^2(t)dt + 2\int_0^t r_i(t)n_i(t)dt\right] \qquad 31.$$

where $E_T = \int_0^T x_i^2(t)$

$$= \int_0^T r_i^2(t)dt + \int_0^T n_i^2(t)dt + \int_0^T 2r_i(t)n_i(t)dt$$

and is a normalizing constant for any one return.

The first integral in 31 is the desired cumulative energy of the returned acoustic signal. The second integral is the cumulative energy of the noise in the time window. Assuming the noise has Gaussian statistics, a mean value of noise power can be estimated from a measurement of noise made in the window prior to the first arrival. This estimate of noise power is then integrated over the time window

to obtain a mean value of noise energy which is substracted from the integrated squared return.

The third term, $\frac{1}{E_T}\int_0^t 2r_i(t)n_i(t)dt$ is more difficult to assess. It is the cross-product of two uncorrelated time series, so the instantaneous magnitude of this term is determined by the phase relations between $r_i(t)$ and $n_i(t)$. Both $r_i(t)$ and $n_i(t)$ have positive and negative values and their product may also have positive and negative values.

It is obvious that the lower bound of the cross-product term is zero; however, zero is not the expected value over a short time window, rather this term, though small since the cross terms are uncorrelated, is indeterminable.

For high signal to noise ratios (SNR), the signal term, $\frac{1}{E_T}\int_0^t r_i^2(t)dt$ will be much larger than the noise term and the cross-product term that the noise effects will be trivial. However, as the SNR ratio decreases, the noise term must be substracted from the integrated term. As the SNR ratio decreases further towards zero, the cross-product term will become significant and result is a higher variance in the accumulated normalized estimates of cumulative energy, E_Δ.

APPENDIX 5

COMPUTER PROGRAMS

Fourier Program to Compute $p_{i, i+1}$

```
  1 L       99
  4 MS      13
  7 L        0
 10 BS    4096
 13 CL       0
 16 CL       1
 19 CL       2
 22 MS      31
 25 BS    2048
 28 MS      21
 31 MS      21
 34 MS      31
 37 L        5
 40 L       10
 43 BS    4096
 46 MS      12
 49 -        0     500
 53 X>       1
 56 MS      12
 59 -        0     500
 63 BS    2048
 66 X>       1
 69 X<       2
 72 F        0       1
 76 CL       0       0      40
 81 CL       1       0      40
 86 CL       0     400    1023
 91 CL       1     400    1023
 96 F        0       1
100 X>       3
103 CR
105 CL       0       1    2047
110 $
112 X>       4
115 X<       3
118 CR       1
121 *
123 X>       3
126 X<       1
129 CR
131 CL       0       1    2047
136 $
138 *        4
141 X        3
144 :        3
```

```
147 CL      1
150 CL      2
153 Y    7703      0
157 X<      1
160 Y>      2
163 MS     11
166 A+      1
169 -       0      1
173 MS     31
176 MS     21
179 MS     31
182 MS     32     -1      1
187 #      10    158      0
192 MS     11
195 A+      2
198 -       0      1
202 A+      2
205 -       0      1
209 MS     31
212 MS     21
215 MS     31
218 MS     32      2      1
223 #       5      4      0
228 MS     31
231 MS     11
234 -       0   1408
238 Y    7701      0
242 MS     31
245 MS     21
248 MS     31
251 MS     11
254 MS     33     51
258 J      99
261 .
```

Fourier Program to Compute EΔ

```
  1 L      0
  4 CL     1
  7 CL     0
 10 MS    31
 13 MS    21
 16 MS    31
 19 L     10
 22 BS  4096
 25 MS    12
 28 F
 30 CL    0     0    83
 35 CL    0   800  2047
 40 F
 42 -     0  1000
 46 BS 2048
 49 *
 51 $
 53 X>    1
 56 -     1  2047
 60 CL    1     1  2047
 65 $     1
 68 :     1
 71 X>    1
 74 :     1    10
 78 -     1  2047
 82 CL    1     1  2047
 87 $     1
 90 A-    1
 93 *     0    -1
 97 L    13
100 -     0    64
104 IF    0    64    64
109 J    13
112 -     0  1984
116 L    23
119 -     0     1
123 IF    0    64    64
128 J    23
131 *     0    -1
135 A+    1
138 X>    1
141 MS   11
144 -     1    80
148 CL    1     1  2047
153 A+    1
```

```
156 -       Ø       1
160 MS      31
163 MS      21
166 MS      31
169 BS    4096
172 #       10      450       Ø
177
```

b

Fourier Program to Compute Running Means and Standard Deviations

```
  1 L      99
  4 MS     13
  7 L       1
 10 MS     31      .1
 14 X>      2
 17 $.
 19 X>      1
 22 -       0      50
 26 A-      1
 29 CL      0    1800    2047
 34 :       0      50
 38 MS     21
 41 *
 43 X       2
 46 *
 48 $
 50 X>      1
 53 -       0      50
 57 A-      1
 60 CL      0    1800    2047
 65 :       0      50
 69 A-      2
 72 Y    7701       0
 76 MS     21
 79 .
```

APPENDIX 6.

"OCEAN SEDIMENT PROPERTIES USING ACOUSTIC SENSING"

in the Proceedings of the Fourth International

Conference on Port and Ocean Engineering

Under Arctic Conditions

St. John's, Newfoundland, September 1977

OCEAN SEDIMENT PROPERTIES USING ACOUSTIC SENSING

R.R. MacIsaac and A.D. Dunsiger
Faculty of Engineering and Applied Science
Memorial University of Newfoundland
St. John's, Newfoundland, Canada.

FOURTH INTERNATIONAL CONFERENCE ON PORT AND OCEAN ENGINEERING UNDER ARCTIC CONDITIONS

POAC 77

SEPTEMBER 26-30, 1977. MEMORIAL UNIVERSITY OF NEWFOUNDLAND

OCEAN SEDIMENT PROPERTIES USING ACOUSTIC SENSING

R.R. MacIsaac and A.D. Dunsiger
Faculty of Engineering and Applied Science
Memorial University of Newfoundland
St. John's, Newfoundland, Canada.

INTRODUCTION

With the current interest in the exploitation of off-shore resources it is evident that a need exists for a rapid, reliable and automatic method of determining the composition and properties of the ocean floor. Such information aids in the design and siting of off-shore structures and pipe lines, provides an inventory of the mineral resources for economic development and planning and improves our understanding of the geophysical structure of the seabed.

Acoustic sources provide a rapid, non-intrusive method of remotely sensing the ocean floor. The use of a high resolution system permits the examination of small areas of the sea floor at frequent spatial intervals. Generally the echo returns require ground truthing by conventional methods such as core and grab samples, but with proper interpretation acoustic techniques can supply averaged information over large bottom swaths.

Several authors have treated the sea surface (e.g. Fortuin, 1972) and the sea bottom (e.g. Baggeroer et al. 1973) as a random filter. Adopting this approach the effects of the roughness characteristics of the ocean floor on an acoustic signal are examined. This model is used effectively by Clay and Leong (1974) in the deep oceans at seismic and echo sounding frequencies. Using shallow seismic frequencies (normally in the band from 1 kHz to 10 kHz) we examine the effects of bottom roughness on signal coherence. The results are based on acoustic data collected on the western part of the Scotian Shelf and in the eastern part of the Gulf of Maine in June 1976 aboard CSS Hudson (Figure 1).

Using a boomer-type broadband sound source at normal incidence the characteristics of a fixed aperture, the methods of filtering, and the establishment of coherence measurements on a ping to ping basis over various sediment types are presented. Further averaging of the maximum value of the time coherence function yields values which may be separated for four different sediments. The differentiation between smooth finely layered media and smooth homogeneous media is examined by means of the ratio of coherent reflected energy at the water sediment interface to the total returned energy. This is a modified application of the methods used by Dodds and reported in Simpkin et al. (1976) and is related to the cumulative energy function used by Knott et al. (1977).

1. HUNTEC DEEP TOW SEISMIC (DTS) SYSTEM

The DTS System (Hutchins et al. 1976) is a broadband boomer-type sound source. It has a maximum energy output of 600 Joules and a nominal sub-bottom penetration capability of the order of 50 m. dependent on sediment type. The source is mounted in a towed body and trailed at greater than one half the total water column depth. This results in a time window about the bottom and sub-bottom echoes which is free of surface reflections. The data was recorded at sea on analog magnetic tape. It is digitized ashore using a sampling frequency of 50 kHz with an 82 msec window corresponding to a water equivalent path of 60 m.

Due to the fixed aperture of the transmitting plate (60 cm diameter) the broadband pulse shape varies with beam angle (Figure 2(a)). The relative spectrum as a function of beam angle is shown in part (b) of the figure. In the interpretation of the data the effect of the DTS System has not been removed from the measurements. In particular, with the dependency of frequency content on beam angle, great care should be taken in the interpretation of the results in application to other systems.

The decoupling of the receiving hydrophone from the towed body is insufficient and it is subject to a vibrational response when the boomer is fired. This ringing of the receiving hydrophone is a major source of interference in the system and requires the filtering of the raw data prior to further processing. Bandpass filtering from 1 kHz to 10 kHz is accomplished after digitization using frequency domain filters. This reduces the low frequency interference and eliminates the spurious echoes from other higher frequency echo sounders operating in the near vicinity (Figure 3). Replica pulse correlation, (i.e. a filter with frequency response equal to the complex conjugate of the transmitted pulse spectrum) may also be used to reduce the effects of spurious signals. This method, however, must be used with care due to the changes in pulse spectrum with beam angle. This results in a variable filter function for echoes off the main acoustic axis of the transmitting plate. Due to the requirement of correlating with a family of replica pulses the data is, for the most part, bandpass filtered. This reduces the maximum signal to background ratio, SBR, attainable relative to replica pulse correlation, but simplifies the processing of the data.

2. SEDIMENT MODEL

2.1 The Model

Drapeau and King (1972) have associated sediment types with bottom roughness characteristics. They describe a range from flat and smooth for mud bottoms (Emerald silt and LaHave clay) to a rough hummocky surface (unsuitable for most fishing operations) for Glacial till (a mixture of mud, sand and gravel). These conditions of roughness must be considered with respect to the acoustic wavelength. The use of the broadband sound source permits the examination of roughness effects for water equivalent wavelengths from less that 20 cm to 1.5 m. As shown by Clay and Leong (1974) completely rough bottoms return acoustic energy by means of a scattering mechanism while smooth bottoms reflect the acoustic energy in a coherent fashion. Intermediate values of roughness return proportions of reflected and scattered energy.

The coherent reflected energy from a smooth bottom yields an initial echo pulse from the sediment which is closely related in shape to the transmitted pulse. The echo returns from a completely rough bottom result in a time elongation of the transmission duration with no clearly discernable initial replica pulse. Intermediate values of roughness result in echoes which contain both a reduced coherent portion

and an elongated tail referred to as reverberation. A measurement of the amount of coherent return from the ocean floor gives a measure of sediment roughness. This roughness may then be associated with a particular sediment type. In essence the classification of sediment type by means of coherence measurements is based on the supposition that hard bottoms, (e.g. till) are generally rough while soft sediments, (e.g. the muds) are generally smooth.

2.2 Sediment Types

Based on the model, four different sedimentary bottoms are analyzed in section 3. Figure 1 shows the locations of the data used in the analysis. The classification of these areas under i) Emerald silt, ii)Sambro sand, gravel, iii) LaHave clay, and iv) Glacial till is either from the surficial geology map of Drapeau and King (1972) or from a map currently in preparation by Fader et al.

3. COHERENCE MEASUREMENTS

For normal incidence the acoustic energy returned from the ocean sediment is the sum of i) the energy specularly reflected from the water-sediment interface (this is usually the first echo return), ii) the energy scattered from the interface within the illumintated area, and iii) the energy returned from scatterers within a particular layer. It is these latter two components which contribute to the elongated reverberation echo. For multilayered sediments this process repeats at each interface with the additional effects of frequency dependent absorption.

Two complementary methods of evaluating the proportion of coherent and incoherent energy are presented. The first is based on the stability of the coherent echoes with small spatial translation of the DTS system. The second method is used to estimate the coherent energy component within a single echo. In both cases ping to ping averaging, effectively spatial averaging for the transiting towed body, is used to decrease the fluctuation of the measurement.

3.1 Coherence Coefficient

For spatial translation of the sound source it is assumed that the reflected component of the echo changes slowly while the scattered component fluctuates rapidly from ping to ping. Based on this assumption it is expected that the echoes from smooth sediments would be largely coherent while those from rough sediments would fluctuate rapidly from ping to ping.

The measure of coherence used in the maximum value of the normalized cross-covariance function between the two successive echoes. Representing the echo returns by the set $\{x(t)\} = x_1(t), x_2(t), \ldots, x_i(t), x_{i+1}(t), \ldots$, this function, referred to as the coherence function, is defined by

$$\rho_{i,i+1}(\tau) = R_{i,i+1}(\tau) \; / \; [R_i(0) R_{i+1}(0)]^{\frac{1}{2}} \qquad (1)$$

where the cross-covariance function between the ith and (i+1)th echo is defined by

$$R_{i,i+1}(\tau) = \langle x_i(t) \; x_{i+1}(t-\tau) \rangle \qquad (2)$$

$\langle \cdot \cdot \rangle$ being used to denote a time average.

$$R_i(0) = \langle x_i^2(t) \rangle \qquad (3)$$

and is equal to the energy in the echo $x_i(t)$. The maximum value of the coherence

function, designated the coherence coefficient, is used as a parameter related to bottom roughness, i.e.,

$$\rho_{i,i+1} = \text{MAX}\ [\rho_{i,i+1}(\tau)] \qquad (4)$$

where $|\rho_{i,i+1}| \leq 1$. Based on the sediment model it would be expected that smooth flat bottoms would yield high values of coherence coefficient while rough bottoms, due to the random nature of the echo returns, would produce low coherence values.

The individual coherence coefficients were determined for the four sediment types of section 2.2 over a total track of 6.4 km. The running average and standard deviation of $\rho_{i,i+1}$ over 50 successive ping pairs (corresponding to approximately a 100 m track) was evaluated. Figure 4 shows a selection of the running values over approximately a 500 m track for each of the four sediment types. Selecting coherence thresholds to optimize the separation of the sediments, the resulting scatter matrix for all the analyzed data is shown in table 1. This table compares the sediment falling within the threshold range to the classification base given in section 2.2. Using this base as the reference the percentage of correct classifications is found on the diagonal of the matrix. The overall correct classification based solely on the running average of the coherence coefficient is 70%.

From the four sections shown in figure 4 it is seen that the usual descending order of coherence coefficient is silt, sand, clay and till although there are regions where these curves overlap. Since the sand is a relatively homogeneous sediment with a small grain size a very flat area of sandy bottom produces a high value for $\rho_{i,i+1}$ which approachs that for silt. In an area of silt, when an underlying region of till is included in the time window, or when there is a disruption of the stratification of the silt, the value of the coherence coefficient decreases to the value normally associated with sand. For a till bottom which is unusually flat, and contains few large angular fragments, the value of $\rho_{i,i+1}$ can increase into the region normally associated with clay.

The inclusion of the standard deviation, s.d., of the coherence coefficient adds further information. The s.d. for both silt and clay is generally less than 0.1, while that for sand or till is usually greater than this figure. The discrimination between overlapping pairs of i) silt or sand, ii) clay or sand and iii) clay or till which cannot be made on the basis of the coherence coefficient can be resolved using the s.d. relative to a 0.1 threshold. For values of s.d. < 0.1 the first 4 sediment of each of the three sets is selected, i.e., i) silt, ii) clay, iii) clay, while the opposite selection is made for a s.d. > 0.1.

3.2 Normalized Cumulative Energy (N.C.E.) Function and E_Δ.

Following the methods of Knott et al. (1977) the N.C.E. function in a window T secs is formed. This is a plot of the cumulative integral of the magnitude squared (proportional to the instantaneous power) of the echo return normalized by the total energy in the window, i.e.,

$$E(t) = (1/E_T) \int_0^t x_i^2(t)\, dt, \qquad t<T$$
$$= 1 \qquad t \geq T \qquad (5)$$

where E(t) is the N.C.E. function and E_T is the total energy in the window T.

Examples of E(t) for the four sediment types are shown in figure 5, where each curve is the average over 10 consecutive echoes.

A typical N.C.
in energy near
There is some
energy as time

The N.C.E. fur
the water-sand
smooth homoge

The N.C.E. fu
tained for sa
from a hom
tribution to t
due to a highl

Figure 5(d) sl
initial increa
reverberation

Since coherent
(this is not s
flector) then
transmitted p
flected portic
nated by E_Δ.
portion of the
is difficult t
cussed for sea

For rough bot
either large c
homogeneous o
and smooth h
coherence coef

For the smooth

smooth homoge

By automatical
block and with
values are sh
echoes is plo
multi-layered
lative to the

It is seen in
takes on an i
of its energy
with smooth s
as shown in s
efficient.
are lower be
high due to
istically ro
reverberatio
yariable.

A typical N.C.E. function for silt is seen in figure 5(a). The rapid increase in energy near the beginning of the plot is the return from the water-silt interface. There is some stratification in the silt, and a corresponding increase in returned energy as time increases.

The N.C.E. function for sand (figure 5(b)) shows an initial high intensity echo from the water-sand interface, with little internal reverberation, as is expected from a smooth homogeneous medium.

The N.C.E. function for clay is shown in figure 5(c). Similar to the results obtained for sand there is a large initial echo followed by the low level reverberation from a homogeneous sediment. The effect of a second layer is seen in the large contribution to the total energy in the latter half of the N.C.E. function. This is due to a highly stratified silt underlying the clay.

Figure 5(d) shows the N.C.E. function for glacial till. For this rough sediment, the initial increase in returned energy is immediately followed by a relatively high reverberation level due to both surface and internal scattering.

Since coherent reflections yield essentially a replica echo of the transmitted pulse (this is not strictly correct except in the case of an infinite extent perfect reflector) then by determining $E(t)$ over a time window Δt equal to the length of the transmitted pulse an estimate of the amount of coherent energy in the initial reflected portion of the echo is obtained. This value of the N.C.E. function is designated by E_Δ. E_Δ only approximates the coherent energy in the first return as the portion of the echo within Δt also contains some incoherent energy to an amount which is difficult to estimate without using replica filters. A similar problem is discussed for sea surface coherence measurements by Wijmans (1973).

For rough bottoms low values of E_Δ would be expected. For smooth bottoms E_Δ can be either large or small dependent on whether the particular sedimentary layer is homogeneous or highly stratified. The differences among rough, smooth finely layered, and smooth homogeneous sediments may be established by examining cojointly the coherence coefficient and E_Δ. For the rough sediments both $\rho_{i,i+1}$ and E_Δ are low. For the smooth finely layered sediments $\rho_{i,i+1}$ is high while E_Δ is low and for the smooth homogeneous sediments both $\rho_{i,i+1}$ and E_Δ are high.

By automatically aligning the echoes to the 10% level of the total energy in the block and with $\Delta t = 0.32$ msec, E_Δ is calculated for the four sediment types. These values are shown in figure 6 where the running mean and standard deviation over 50 echoes is plotted. It is to be noted that in calculating the E_Δ values for the multi-layered sediment of clay overlying silt the window size, T, is decreased, relative to the remaining sediments, so as to only include the first layer.

It is seen in Figure 6 that sand and clay are inseparable on the basis of E_Δ. Silt takes on an intermediate value, above that of till, which has the lowest proportion of its energy in the Δt window. Sand and clay are relatively homogeneous sediments with smooth surface profiles and are expected to show high values of E_Δ. However, as shown in section 3.1, they can be separated on the basis of their coherence coefficient. Silt is usually a highly stratified soft sediment. Hence, the E_Δ values are lower because of contributions from the layering but the coherence coefficient is high due to the coherent stratificiation of the sediment. Till, which is characteristically rough, contains many scattering sources, and the echo returns show high reverberation levels. The values of E_Δ and $\rho_{i,i+1}$ for till are both low, and are highly variable.

4. CLOSE

Using a model based on the relative roughness of marine sediments and by measuring the echo coherence we have examined two complementary methods of classification. Considering only the mean value of the coherence coefficient a 70% level of correct identificiation is attained. The combination of the mean value and the standard deviation of the coherence coefficient indicates that further separation of the classes is possible. The measurement of the normalized energy in the first echo return, E_Δ, when combined with the coherence coefficient values aids in differentiating between smooth homogeneous and smooth stratified sediments.

We have not, as yet, attempted to combine these measurements except in a descriptive way. Furthermore no account has been given to the sensitivity of the measurements to SBR although it is assured that both the coherence coefficient and E_Δ will decrease with increasing SBR.

Finally, we believe better use can be made of the bandwidth available from the acoustic source. By examining the coherence function, between successive echoes, in the frequency domain a quantitative estimate of the sediment roughness may be possible.

ACKNOWLEDGEMENTS

We would like to thank the Bedford Institute of Oceanography (Atlantic Geoscience Centre) and Huntec (70) Ltd. for sea trial time, equipment access and data support. In particular we would like to thank D.I. Ross and L.H. King of the BIO, and P.G. Simpkin, R. Hutchins and D.R. Parrott of Huntec. They have all given freely of their time and expertise in this field and have allowed us access to their extensive Seabed research programme.

The work is partially supported by a National Research Council of Canada Operating Grant. One of the authors (R.R. MacI.) is a C-CORE Fellow.

REFERENCES

Baggeroer, A.B., Knott, S.T., Hoskins, H., and Bunce, E.T., "Digital Signal Processing of Oceanic Seismic Profiler Data, 1972. Reflectivity and Sediment Classification". WHOI-73-38, Woods Hole Oceanographic Institution, June 1973, 11 pp.

Clay, C.S. and Leong, W.K., "Acoustic Estimates of the Topography and Roughness Spectrum of the Sea Floor Southwest of Iberian Pennisula." In Physics of Sound in Marine Sediments, Edited by Loyd Hampton, Plenum Press 1974. pp. 373-446.

Drapeau, G. and King, L.H., "Surficial Geology of the Yarmouth-Browns Bank Map-area." Information Canada, Ottawa, 1972, 6 pp.

Fortuin, L., "The Sea Surface as a Random Filter for Underwater Sound Waves." J. Acoust. Soc. Amer., Vol. 52, No 1(2), 1972, pp. 302-316.

Fader, G.L., King, L.H., and Maclean, B., "Surficial Geology of the Eastern Gulf of Maine and Bay of Fundy." Information Canada, Ottawa, in press.

Hutchins, R.W., McKeown, D.L., and King, L.H., "A Deep Tow High Resolution Seismic System for Continental Shelf Mapping." Geoscience Canada, Vol. 3, No. 2, May 1976, pp. 95-100.

Simpki
and Acl
1976, 5

Knott,
Marine
Seabed.
Analysi
by IEEE

Wijmans
water S
ASW Res

Table 1
at the
$\rho_T < 0.$
Values

Simpkin, P.G., Parrott, D.R., Hutchins, R., and Ross, D.I., "Seabed '75 - Objectives and Achievements.", Report BI-R-76-15, Bedford Institute of Oceanography, December 1976, 57 pp.

Knott, S.T., Hoskins, H., and LaCasce, Jr., E.O., "The Energetics of Normal-Incidence Marine Seismic Profiles and Estimation of the Acoustic Impedance Structure of the Seabed." from Conference Record of International Symposium on Computer-Aided Seismic Analysis and Discrimination - June 10-11, 1977, Falmouth, MA, U.S.A., to be published by IEEE Computer Society.

Wijmans, W., "An Experimental Study of Forward Scattering and Reflection of Underwater Sound Waves from the Rough Sea Surface." SACLANTCEN Memorandum SM-26, SACLANT ASW Research Centre, La Spezia, Italy, October 1973, 28 pp.

Table 1. Coherence Coefficient Scatter Matrix. Classification Thresholds, ρ_T, are at the following levels: a) Emerald silt, $0.725 < \rho_T < 1.0$; b) Sambro sand, $0.625 < \rho_T < 0.725$; c) LaHave Clay, $0.575 < \rho_T < 0.625$; d) Glacial till, $0.4 < \rho_T < 0.575$. Values shows are percentages.

Coherence Coefficient Classification	Reference Base (Drapeau and King and Fader et al.)			
	Silt	Sand	Clay	Till
Silt	69	30	-	-
Sand	28	48	-	-
Clay	3	22	84	20
Till	-	-	16	80
Number of Events	1820	680	480	320
Track Length(km).	3.6	1.3	.9	.6

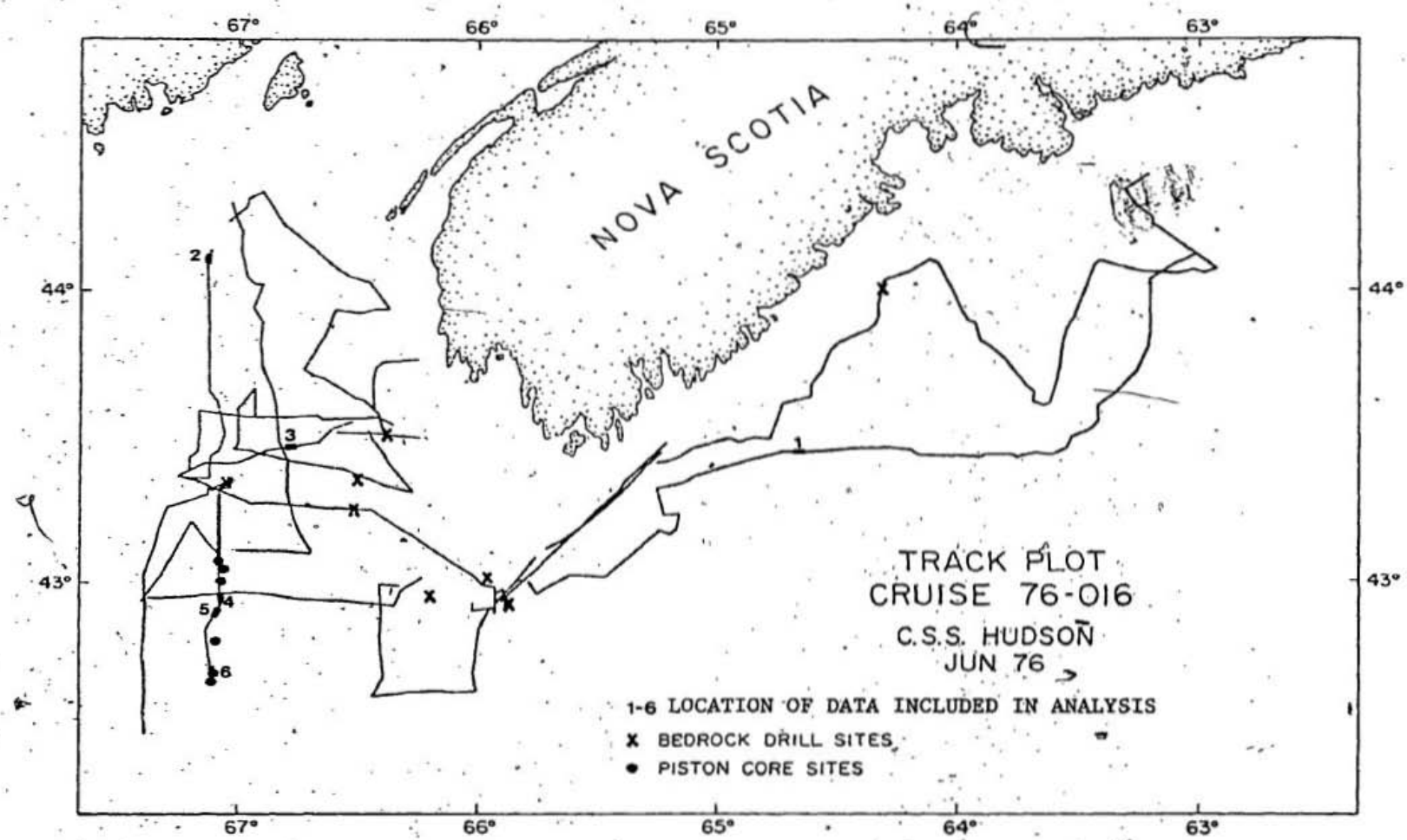

Figure 1. Locations of Acoustic Data Analysis Sites. Emerald Silt - 4,6; Sambro Sand - 2,3; LaHave Clay - 1; Glacial Till - 5

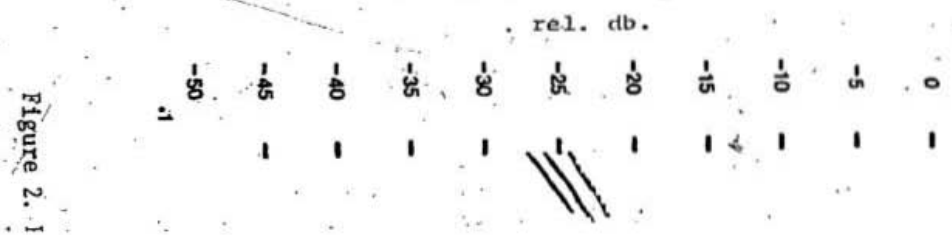

Figure 2. I

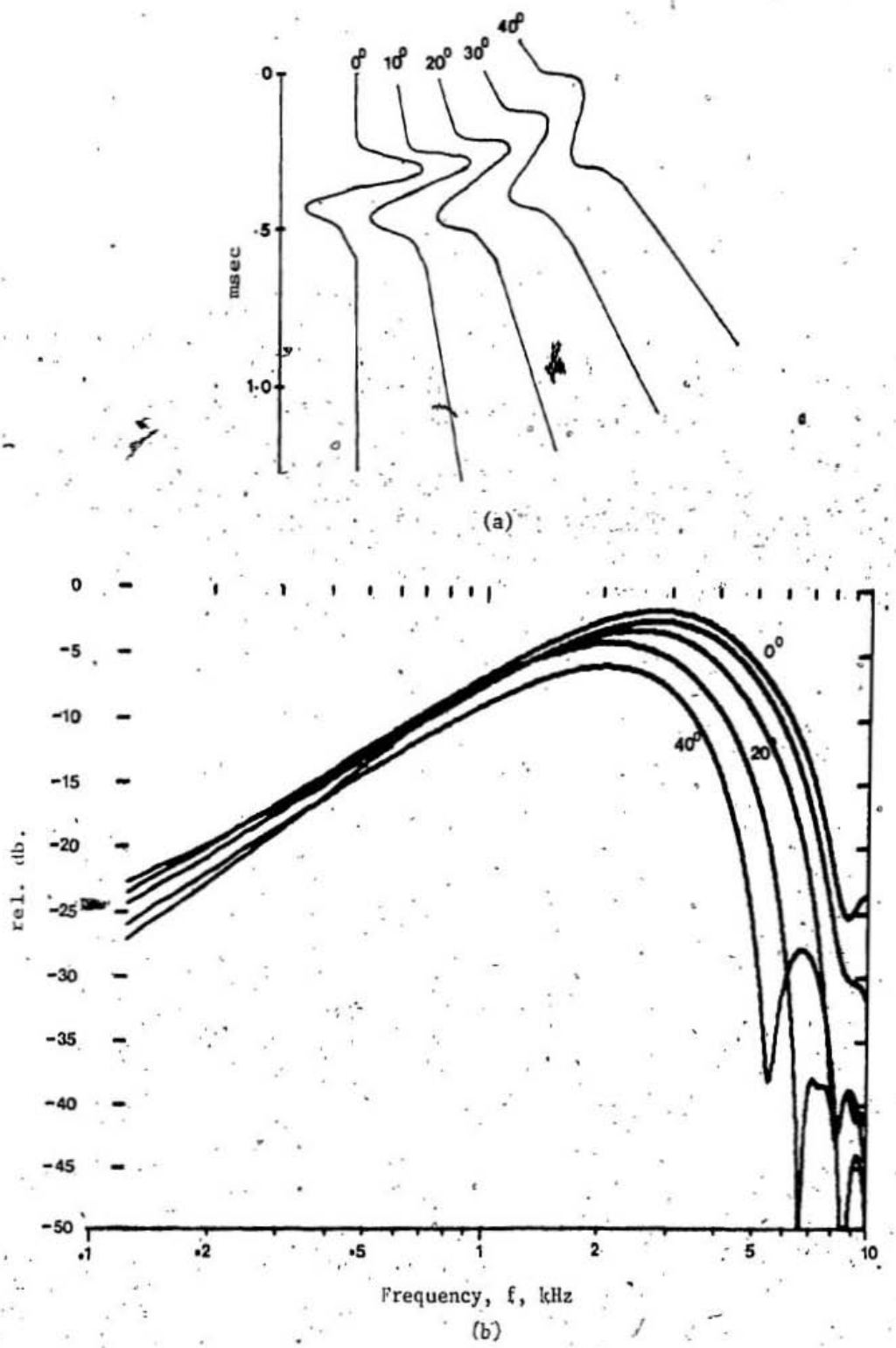

Figure 2. Pulse Signatures and Spectra as a function of Beam Angle. (a) Variation of pulse shape with angle; (b) Variation of pulse spectrum with angle.

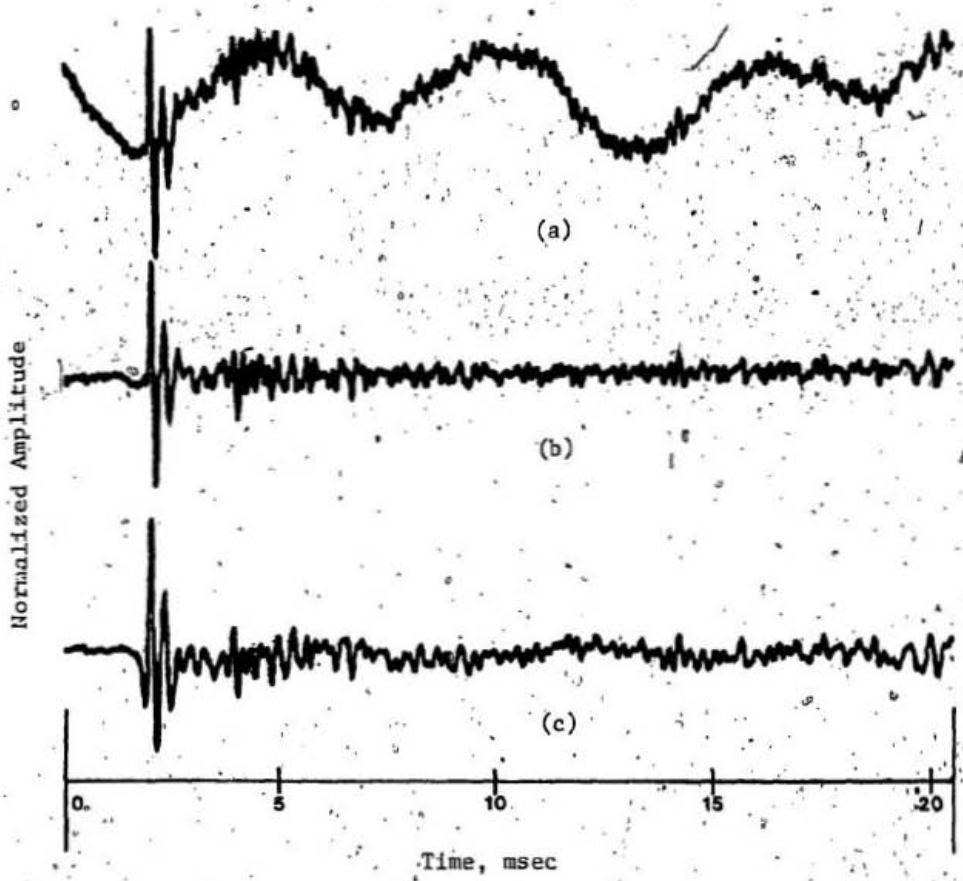

Figure 3. A Typical Acoustic Echo Return. (a) Raw, unfiltered; (b) Return in a) bandpass filtered from 1 kHz to 10 kHz. Average SBR = 19 db. Peak signal power SBR = 61 db; (c) Return in a) correlated with on-axis pulse in figure 2(a). Average SBR = 15 db. Peak signal power SBR = 57 db.

Coherence Coefficient

Standard deviation of running mean

Fi

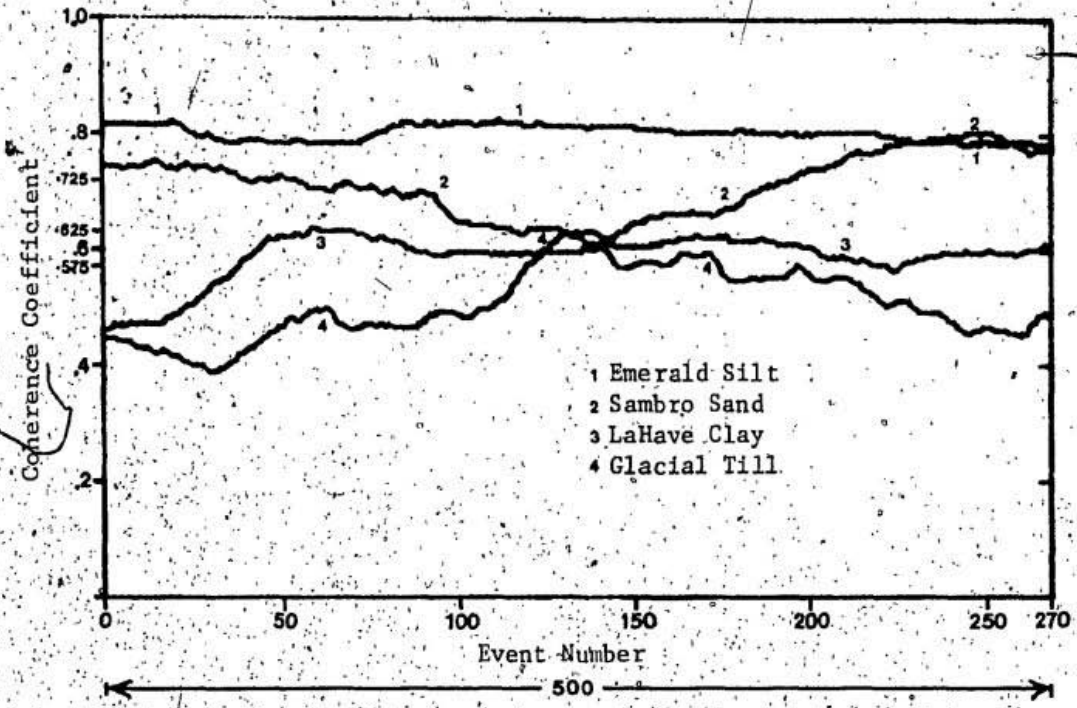

(a)

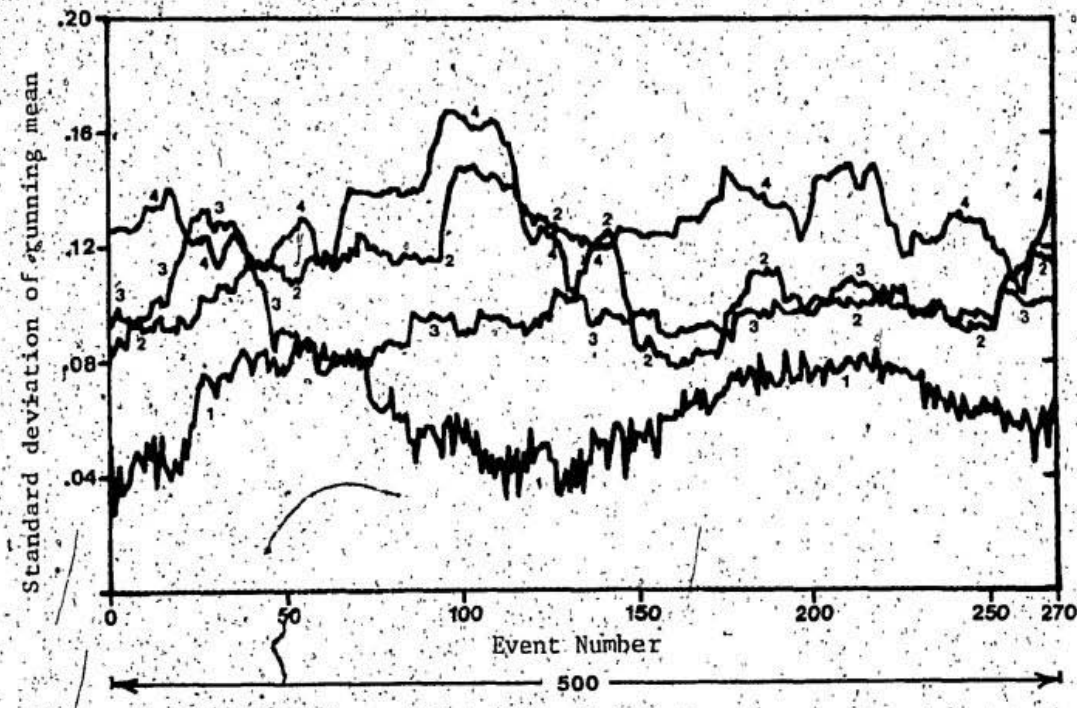

(b)

Figure 4. Coherence Coefficient, $\bar{\rho}_{i,i+1}$, vs Track Length. (a) Running mean with $\rho_{i,i+1}$, averaged over 50 ping pairs. Threshold levels are at 0.725, 0.625, 0.575, and 0.4; (b) Running Standard deviation of $\bar{\rho}_{i,i+1}$ for the same events as in (a).

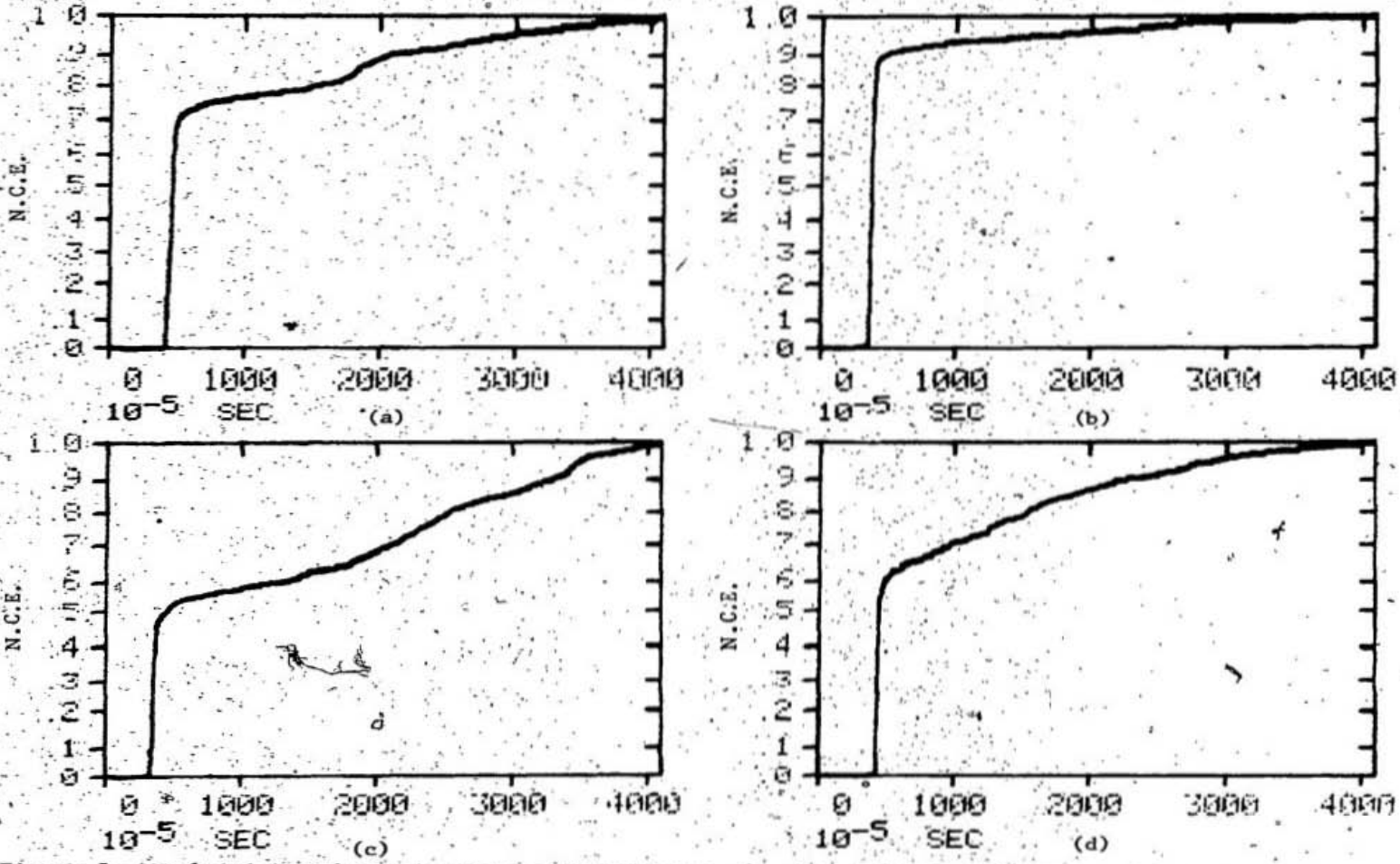

Figure 5. Normalized Cumulative Energy (N.C.E.) Functions fot (a) Emerald Silt; (b) Sambro Sand; (c) LaHave Clay; (d) Glacial Till.

s.d. of $\overline{E}_{\Delta}$

E_{Δ}

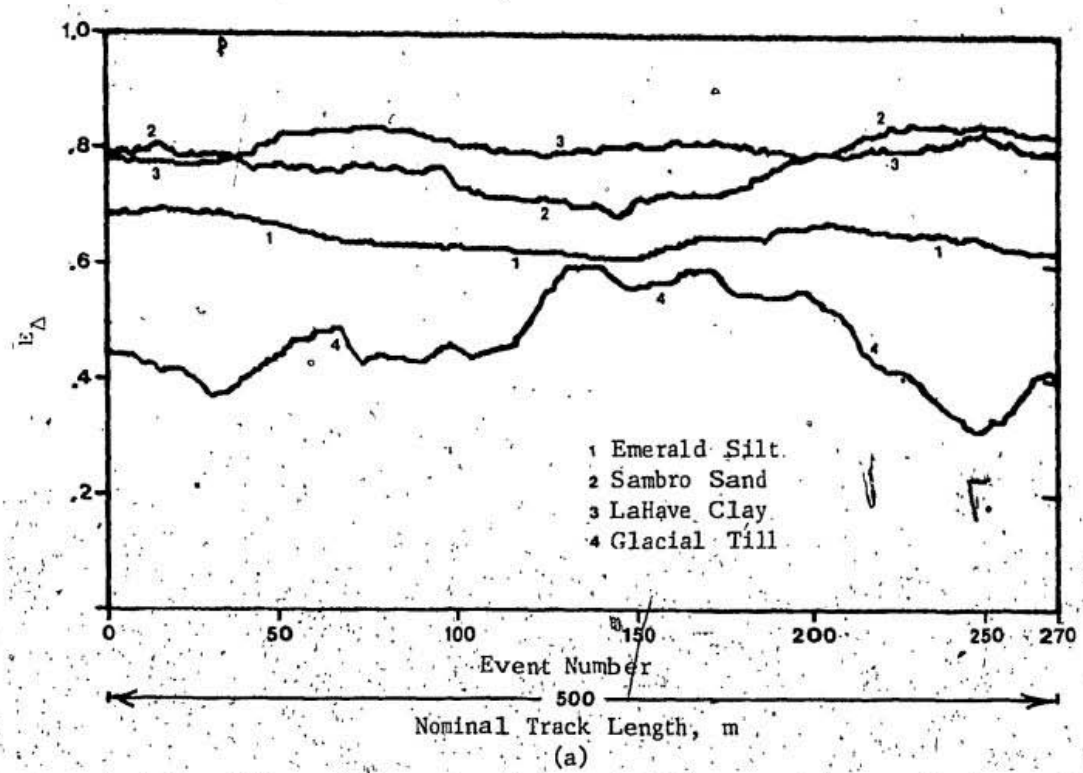

(a)

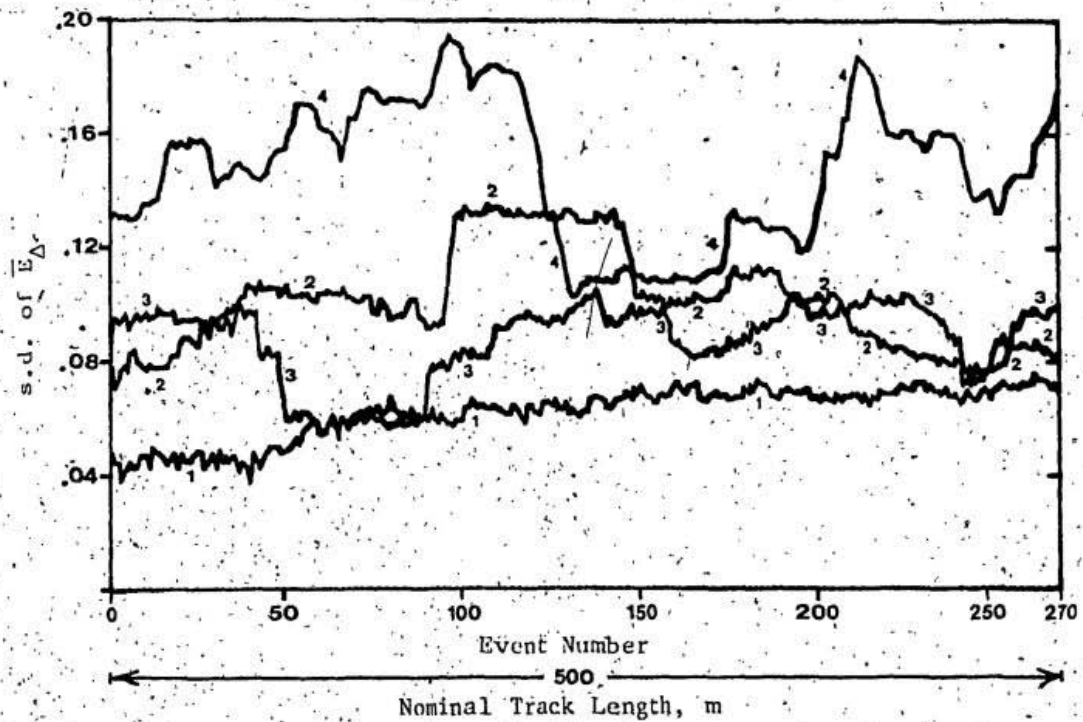

(b)

Figure 6. $\bar{E}_\Delta$ vs Track Length. (a) Running mean with E_Δ averaged over 50 pings; (b) Running standard deviation of $\bar{E}_\Delta$ for the same events as in (a).